博士論文

Doctoral Dissertation

Elucidation of electronic structure at n-GaN and electrolyte interface (n-GaN と電解液の界面における電子構造の解明)

2020 年 12 月 1 日　提出

指導教員：中野　義昭　教授

学籍番号：37-187057

Department of Electrical Engineering and Information Systems,

School of Engineering, The University of Tokyo

東京大学大学院工学系研究科電気系工学専攻

Yuki Imazeki

今関　裕貴

Abstract

Solar energy is a desired energy source due to its inexhaustibly and reducibility in CO_2 emission during energy conversion. To convert solar energy into electricity, a photovoltaic cell has been commonly installed and operated. However, we are facing with the problem of unstable energy supply such as fluctuation in time and spatially due to chaotic natural condition. To solve the problem, the solar energy should be stored and used to respond demand. Hydrogen is a desired energy storage because it can be stored for longer time than batteries. The potential in the energy storage enables us to transport the solar energy as the hydrogen to the region where amount of solar radiation is scarce. These strengths of the hydrogen as the energy storage can stabilize energy supply in time and spatially.

Water splitting photoelectrode and photocatalyst, based on the photoelectrochemical (PEC) reaction, are the desired devices for solar to hydrogen conversion. Although the narrow band gap materials are being developed for absorbing low energy photon in solar spectrum, the reported energy conversion efficiency is still far from target due to carrier recombination. To solve the problem, carrier splitting efficiency should be enhanced by optimizing the band bending in semiconductor. However, it is difficult to control the band bending at semiconductor/electrolyte due to insufficient understanding about determinants such as surface states in semiconductor, surface adsorption and redox reactions. To solve the problem, these factors should be regulated.

In this study, n-GaN(0001)/electrolyte was used as the model case of semiconductor/electrolyte interface for water splitting to clarify the determinant of the band bending due to its defined surface of +c plane, chemical stability and band edge potential that straddles the redox potentials of water oxidation and reduction reactions.

To suppress the effect of redox reaction and analyze the effect of surface adsorption, the band bending under ultra-high vacuum (UHV) and water vapor was compared. Then, the effect of redox reaction was evaluated at n-GaN/electrolyte interface.

Band bending at n-GaN/H_2O adsorption layer has been determined by X-ray photoelectron spectroscopy (XPS) from the valence band maximum (VBM), which has been calculated from Ga 3d peak using the energy difference between VBM and Ga 3d ($\Delta E_{VBM\text{-}3d}$). However, the several reported value for $\Delta E_{VBM\text{-}3d}$ caused difficulty in clarifying the determinants of the band bending. This work validates these values which have been reported previously, by analyzing the spectrum around the VBM and its distance from Ga 3d for n-GaN(0001) surface. Adopting 17.5 eV, validated value, as $\Delta E_{VBM\text{-}3d}$ suggested the origin of such band bending was Fermi level pinning to the Ga dangling bonds under UHV and the sub-surface states which cannot be compensated by H_2O under water vapor.

The band alignment at the interface between n-GaN and 1M NaOH with various treatments to define surface was investigated by observing open-circuit potential (OCP) of the GaN as a function of irradiated light intensity. For the smaller light intensity than 10^{-2} mW/cm^2, OCP value was less dependent on light intensity and it was sensitive to the surface treatment of GaN by electrochemical reducing methods, the irradiation of accelerated Ar atoms, high-energy electrons and γ-ray. The difference of pinning level among various surface treatments in same electrolyte suggested that surface states created by the treatment decided the band bending. The relationship between OCP and light intensity can be obtained without modifying the surface by photocurrent and it would be a good indicator how the surface treatment of a photoelectrode affects the photocatalytic activity.

For further discussion about the effect of surface states on the band bending, the distribution of surface states was compared with Fermi level pinning. The density of

surface states was lower than detection limit of 10^{12} cm^{-2} ev^{-1} at for as non-damaged surface. However, Fermi level pinning was observed by OCP measurement. The band bending at non-damaged n-GaN/1M NaOH was determined by the surface states although the density was lower than the criterion for Fermi level pinning at metal/semiconductor of 10^{12} cm^{-2} ev^{-1}.

Based on these results, the band bending should be determined by surface states. Therefore, the band bendings at interface between n-GaN and electrolytes other than 1M NaOH should be equal. The band bendings at n-GaN/1M NaOH, 0.2M Na_2SO_4, 1M HCl or 0.5M H_2SO_4 were evaluated as 1.1-1.2 eV under dark condition. Under irradiating photon flux of 10^{11}-10^{13} $cm^{-2}s^{-1}$, the amount of reduction in the band bending was 0.5 eV in 1M HCl and 0.2 eV in 0.5M H_2SO_4. The difference suggested the more photogenerated carriers accumulated in the vicinity of n-GaN/1M HCl interface than 0.5M H_2SO_4. This result suggested the surface recombination was suppressed by Cl^- which worked as hall scavenger.

These results suggest that surface states decide the band bending at n-GaN/electrolyte interface under dark condition without fast redox reaction. Under illumination, the band bending can be affected by redox reaction via suppressing the surface recombination. To optimize the band bending at semiconductor/electrolyte interface, the surface states distribution should be controlled and suppressing surface recombination by the hall or electron scavenger should be considered under illumination.

Table of contents

Chapter 1 Introduction

This study elucidates determinants of the band bending, which splits photogenerated carriers at semiconductor/electrolyte interface in water splitting, based on model analysis using n-GaN/electrolyte interface. General background of the photoelectrochemical (PEC) water splitting will be introduced in this chapter.

1.1 Efficient use of renewable energy

1.1.1 Solar energy

Fossil fuels have supported human society as a source of energy for heat and electricity. It has been estimated that oil and natural gas have a useful life of 50 or 51 years. With the improvement of drilling technology and the discovery of new oil and gas fields, the minable life of oil and natural gas has remained constant or increased, but there is a strong need to develop alternative energy sources. In addition, the reduction of greenhouse gas emissions, which countries have pledged to do under the Paris Agreement adopted at COP21, is also very important to stop climate change. In order to achieve these goals, the share of renewable energy sources must be increased.

Photovoltaic power generation, wind power generation, biomass power generation, and geothermal power generation are typical examples of renewable energy sources. Of these, solar power is considered to be one of the most promising energy sources. The capacity of these renewable energies is increasing rapidly year by year. Electricity from renewable energy sources accounts for about 7% of the total, and there is a need to further boost their installation.

1.1.2 Solar to hydrogen conversion

Solar power has promising potential, but in principle it has a serious drawback: fluctuating power output. During the day, the output from the solar cells is at its maximum during the day, while the demand for energy is at its minimum, resulting in an oversupply. Conversely, at night, the output from the solar cells decreases, resulting in excess energy demand. In addition, during the daytime, output fluctuations in a short period of time can cause frequency fluctuations in the AC power supply, and in the worst case, can cause large scale power outages. Fluctuations in supply are inherently unavoidable for such

renewable energies, not just solar, and must be compensated for by controlling the output of thermal power plants. Therefore, an appropriate power grid that can meet the gap between energy demand and supply must include thermal power plants along with large-scale solar power plants. Therefore, the mass introduction of solar panels alone will not be enough to solve the energy problem.

Power storage is an important technology for the large-scale introduction of renewable energy. If the fluctuating output power of renewable energy is stored in an energy storage device, stable power can be supplied from the storage device later. Currently, rechargeable batteries, such as lithium-ion batteries, are often used as energy storage. Lithium-ion batteries have the advantage of smoothing out the supply variable power in a short period of time, but they are not suitable for long-term storage because they spontaneously discharge. Hydrogen, on the other hand, does not discharge, making it a good choice for long-term storage. In addition, the energy density of hydrogen can be improved by compression. Because of these strengths, by storing energy in hydrogen, energy generated in areas with strong solar radiation can be delivered to other areas with high energy demand. Thus, the regional distribution of renewable energy on the planet can be smoothed out, and a more stable power supply can be expected.

The conversion of solar-to-hydrogen (STH) can be done in several ways. The simplest method, yet currently achieving the highest efficiency, is electrolysis with the power output from the solar cell. Water splitting techniques and solar cells using alkaline solutions and polymer electrolyte membranes (PEMs) have been developed for several decades, and the highest STH conversion efficiencies have been achieved with simple connections. On the other hand, other water splitting techniques, such as photocatalysts and photoelectrodes, are expected to produce hydrogen at lower cost, although their efficiency is still not as high as the combination of solar cells and electrolysis.

The highest value of STH currently reported is 31.7% [1]. However, this is a

measurement using a laboratory light source and does not reflect the actual environment. The highest value under actual sunlight is 24.4 % measured in Miyazaki [2]. All of these have been demonstrated using a combination of solar cells and water electrolysis cells. A multi-junction tandem cell was used for the solar cell, and the operating point was set to maximize the filling ratio. However, the cost of such multi-junction solar cells is generally very high, and considering the U.S. Department of Energy's hydrogen production benchmark of $4/kg [3], other inexpensive methods of hydrogen generation can be considered. One such method is photocatalysis. Photocatalysts consist of semiconductor powders or metal complexes dispersed in an electrolyte. When these materials absorb light, electrons and holes are generated, and the carriers are transferred to the reactive species in the electrolyte at the interface with the electrolyte, and the reaction proceeds. Photocatalysts can be obtained by the sol-gel method, which is simpler than multi-junction solar cells using metal organic chemical vapor deposition (MOVPE). Therefore, a significant reduction in the fabrication cost of the hydrogen generation system can be expected.

The cost of hydrogen production is one of the most important indicators for practical applications. Several techno-economic studies have been conducted and estimated that the hydrogen production cost in these devices could reach $0.8-4 per kg H2, meeting the U.S. Department of Energy (DOE) target of $2-4 per kg H2 [3,4]. In order to achieve these costs, relatively high STH efficiency (5-15%) and long life (5-10 years) are required. However, photocatalyst has yet to achieve the STH and lifetime values used in this techno-economic evaluation. To that end, going back to the fundamentals in reaction mechanism should be a necessary step to understand what is causing the bottleneck.

1.2 Photoelectrochemistry for solar to hydrogen conversion

1.2.1 Basics of water splitting

Before we discuss photoelectrochemical water splitting, we will discuss the basics of electrochemical water splitting. For water splitting, a potential difference of at least 1.23V is required. This 1.23 V is determined by the thermodynamics of the redox reaction. The water splitting reaction can be expressed as follows:

$$H_2O\ (l) \rightarrow H_2 + 1/2\ O_2\ \Delta H^o = 285.83\ kJ \qquad (1.1)$$

where, ΔH^o is the standard enthalpy of formation (heat of formation) in the reaction. This equation represents the heat balance of the reaction. If the enthalpy change for the water splitting reaction is positive, it means that the reaction is endothermic, while the opposite reaction, the hydrogen burning reaction, is exothermic. There is a thermodynamic limit to the maximum work that can be done by the reaction, which is called the Gibbs free energy. The Gibbs energy G^o is expressed in terms of enthalpy H^o and entropy S^o, and the change in Gibbs energy in a chemical reaction can be expressed as follows:

$$\Delta G^o = \Delta H^o - T\Delta S^o. \qquad (1.2)$$

The change in Gibbs energy when one mole of a substance in the standard state is formed from a simple substance in the standard state is called the standard Gibbs energy of formation ΔG_f^o. The Gibbs energy change of any reaction can be calculated by considering the standard Gibbs energy of formation of the substances involved in the reaction. For example, the Gibbs energy change in the water splitting reaction can be calculated from the standard Gibbs energies of formation of hydrogen (0 kJ/mol), oxygen (0 kJ/mol), and water (-237.13 kJ/mol) as follows

$$\Delta G^{o} = (\Delta G_{f(H_2)^{o}} + \Delta G_{f(O_2)^{o}}) - \Delta G_{f(H_2O)^{o}} \quad (1.3)$$

$$= (0+0) - (-237.13) = +237.13 \text{ kJ/mol}$$

Since the reaction occurs spontaneously only when ΔG is negative, an additional energy of 237.13 kJ/mol must be supplied to promote water splitting.

Electrochemical reactions, on the other hand, are chemical reactions that involve the transfer of electrons. The reaction can be broken down into a pair of half-reactions: oxidation at the anode and reduction at the cathode. The half-reaction of water splitting can be represented as follows:

$$H_2O \rightarrow 2\,H^+ + 1/2\,O_2 + 2e^-.\ (+1.23\ \text{V}\ vs.\ \text{SHE}), \quad (1.4)$$

$$2\,H^+ + 2\,e^- \rightarrow H_2. \qquad (+0.00\ \text{V}\ vs.\ \text{SHE}). \quad (1.5)$$

Half-reaction corresponds to the transfer of electrons between a substance and a metal electrode. Each half-reaction has a potential at which the reaction reaches an equilibrium state under standard conditions. This is called the normal electrode potential, and the origin of the electrode potential is defined by the normal electrode potential for the reaction shown in equation (1.5): standard hydrogen electrode (SHE). The electrons move from the negative potential to the positive potential, where their energy is higher. (More precisely, the electrons move between states of the same energy level, after which they release heat and lose energy.) In reactions on electrodes, the anode removes electrons from a substance and transfers them to another substance in a cathodic reaction at a higher equilibrium potential. Since the change in Gibbs energy needed to drive the reaction is supplied as the potential difference in electrons, the energy can be expressed as,

$$\Delta G^{o} = nF\Delta E_0. \quad (1.6)$$

where, ΔE_0 is the potential difference between the reduction and oxidation reactions; since two moles of electrons are required to produce one mole of water, the potential difference can be calculated as follows:

$$\Delta E_0 = \Delta G^o / nF \quad (1.7)$$

$$= 237.13 \text{ kJ} / (2 \times 96485 \text{ C/mol}) \sim 1.23 \text{ V}.$$

Since the water splitting reaction requires a threshold voltage of 1.23 V and the potential for the cathodic reaction is defined as 0 V vs. SHE, the electrode potential for water oxidation shown in equation (1-5) is calculated to be +1.23 V vs SHE.

1.2.2 Mechanism of photoelectrochemical water splitting

Since the first discovery of photoelectrochemical water splitting using TiO_2, known as the Honda-Fujishima effect [5], the photoelectrochemical properties of many materials have been studied. However, several conditions are required for efficient water splitting, and the number of candidate materials is limited. In this section, the conditions are described along with the reaction mechanism.

Spontaneous water splitting under light irradiation requires that the quasi-Fermi level (Gibbs energy of 1 electron/hole) of both electrons and holes should straddle the redox potentials of both hydrogen and oxygen redox evolution. Since the potential of the metal electrode is identical to the potential of the semiconductor (the quasi-Fermi level of the electron in n-type semiconductor), the maximum potential (the most negative potential) is limited by the conduction band edge potential of the n-type semiconductor. On the other hand, the energy of holes is determined by the valence band edge potential of the semiconductor. Therefore, the necessary conditions for spontaneous water splitting of PEC are expressed as follows.: conduction band edge potential is more negative than

the hydrogen generation potential (0 V vs. SHE) and valence band edge potential is more positive than the oxygen generation potential (+1.23 V vs. SHE).

When this thermodynamic requirement is satisfied, a water splitting reaction occurs. To understand the reaction mechanism, the energy band alignment of the semiconductor-electrolyte interface is important. Figure 1.1 shows the energy band alignment at the interface between the n-type semiconductor photoelectrode and the electrolyte. A similar band alignment is formed at the semiconductor-electrolyte interface for photocatalysts. In the p-type semiconductor, the band bending near the semiconductor surface is reversed. At the semiconductor-electrolyte interface, a depletion layer is formed between the semiconductor electrode and the electrolyte, resulting in a Schottky-like junction. When this junction interface is irradiated by light with energy exceeding the band gap, electron-hole pairs are excited in the semiconductor (Fig. 1.1(i)). The electrons and holes are separated according to the surface band bending (built-in potential) and transported to the interface with the electrolyte (Fig. 1.1(ii)). When quasi-Fermi level splitting between electrons and holes straddles both redox level of hydrogen and oxygen evolution, the transported electrons and holes are used for hydrogen production (reduction reaction) and oxygen production (oxidation reaction), respectively, and water electrolysis occurs to produce hydrogen (Fig. 1.1(iii)). In order to improve the energy conversion efficiency, there is a need to improve each of (i), (ii), and (iii).

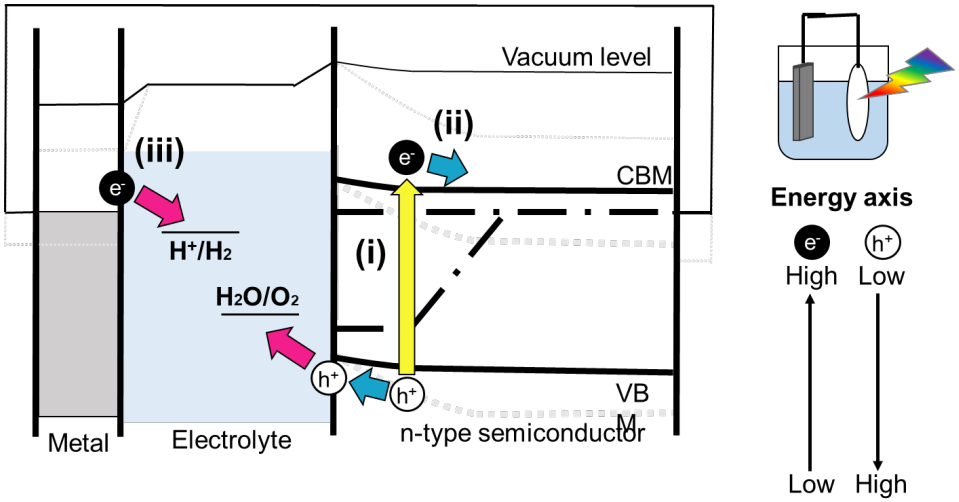

Figure 1.1 Carrier transportation and band alignment at interface of n-type semiconductor/electrolyte. (i)Photo generating electrons and hole by light absorption (ii)Splitting electrons and holes by built-in potential (band bending) (iii) Redox reaction at the interface

(i) Requirement for light absorption

The sun emits everything from X-rays to radio waves, but the strongest solar radiation is in the visible light range, and 43% of the solar energy that reaches the earth's surface is in the visible light range with wavelengths between 400 and 700 nm. If the QE (quantum efficiency) is about 100%, a photocatalyst with an absorption edge at 520 nm (band gap < 2.38 eV) is needed to achieve the target STH of 10% [6]. Therefore, in order to obtain high STH, it is important to increase the QE and to extend the wavelength of the optical absorption edge. As the Materials that can absorb light with wavelengths longer than 520 nm, Cu_2O (band gap: 2.0 eV) [7], $In_{0.9}Ni_{0.1}TaO_4$ (band gap: 2.3 eV) [8], $CaTaO_2N$ (band gap: 2.4 eV) [9], $LaMg_{1/3}Ta_{2/3}O_2N$ (band gap: 2.1 eV) [10,11] and Ta_3N_5 (nanorod) (2.1 eV),[12] have been developed. The respective QE and AQY (apparent quantum yield) are measured as 0.3 % @ 550-600 nm (QE), 0.66% @ 402 nm (QE), 3E-3 %

440±30 nm (AQY), 0.18 % @ 440±30 nm (AQY), and 2.2 % @ 320 nm (AQY). Here, QE and AQY are defined as

$$QE = \frac{number\ of\ reacted\ electrons}{number\ of\ photons\ absorbed} \tag{1.8}$$

and

$$AQY = \frac{number\ of\ reacted\ electrons}{number\ of\ incident\ photons} \tag{1.9}$$

These experimental results indicate that while the absorption length seems to be sufficient to meet the STH10% requirement, the QE and AQY are insufficient, and the photogenerated electrons and holes are annihilated inside the semiconductor.

(ii) Requirement for carrier transportation

In order to promote photoelectrochemical reactions, interfacial charge transfer is necessary for the photoexcited charge carriers to reach the redox active sites on the semiconductor surface and extract and separate the charges. Typically, in bulk semiconductors, the excitons are Mott-Wannier modes due to the large exciton radius, whereas in organic molecules and polymers, Frenkel modes are dominant [13]. After the photo-induced separation of electrons and holes that had been excitons, these carriers need to be transported from the bulk of the semiconductor to the active site on the surface to drive the catalytic reaction. The average time required for the photoexcited carriers to dissipate is called the carrier lifetime and is an indicator of how effective a semiconductor can be as a photocatalyst. However, the carrier lifetime of semiconductor photocatalysts is typically short, on the picosecond to nanosecond scale, approximately equal to the recombination time scale. [14-18] Electrons produced by light irradiation tend to fall from the conduction band to the valence band, or mid-gap states, thereby removing holes by

recombination and returning the carrier concentration to its equilibrium value. In semiconductor photocatalysts and photoelectrodes, this recombination process can occur via radiative (interband) recombination or, more commonly, via recombination through traps (defects or impurity states) in the forbidden gap. Electron-hole recombination rates on the order of picoseconds to microseconds have been reported for n-type semiconductors such as TiO_2 [19,20], WO_3[21] and a-Fe_2O_3, [22,23] as well as for many photocatalytic semiconductors. Simulations of two-dimensional particulate photocatalytic systems with high potentials reveal that QE is governed only by low charge separation efficiency and severe charge recombination in the bulk of the photocatalytic particles.[24] In order to suppress such recombination, efforts are being made to reduce the number of crystal defects in each material system. In order to enhance the carrier separation, efforts are being made to increase the band bending by changing the facet etc.

(iii) Requirement for reaction on surface

Water splitting reactions involving high activation energies or overpotentials generally suffer from low activity. In particular, multi-step proton-conjugated electron transfer reactions in oxygen evolution are kinetically slow. The cocatalyst on the semiconductor promotes photocatalytic performance by lowering the activation energy of the reaction. Nellist et al. showed that CoPi, oxygen-evolution catalyst, on α-Fe_2O_3 acts as a hole collector by operand measuring the surface potential [25]. From this result, it can be suggested that if the holes were transported to the vicinity of the catalyst, they would collect on the catalyst and produce a large overvoltage, which could accelerate the reaction. Therefore, holes should be separated from electrons by band bending.

1.3 Energy band alignment at semiconductor/electrolyte

From the discussion in the previous section, it should be possible to increase the

QE and achieve 10% STH by efficient carrier separation. Therefore, it is important to control the band bending (built-in potential) that dominates the carrier separation. This band bending is determined by the band edge potential at the semiconductor/electrolyte interface and the Fermi level in the semiconductor.

1.3.1 Band edge potential

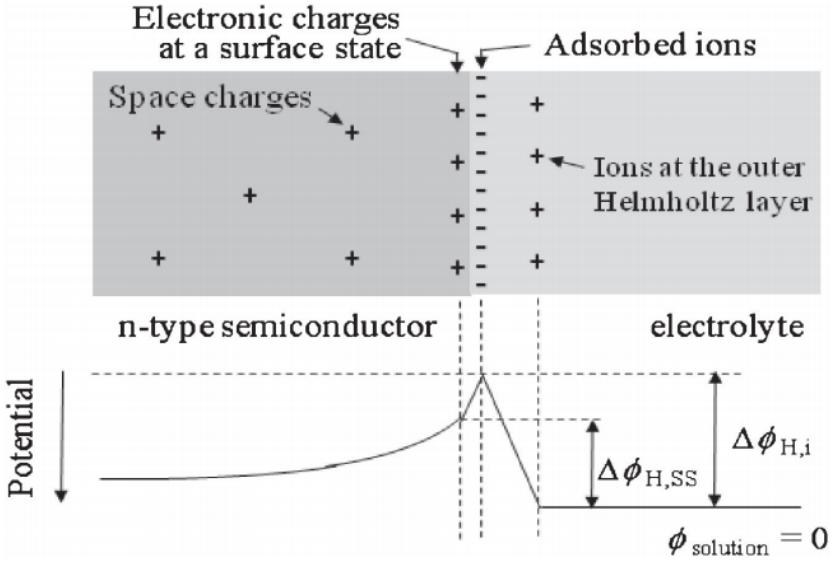

Figure 1.2 An illustration explaining how surface band energies are determined under the condition that space charges, electronic charges in a surface state, and charges of adsorbed ions are present simultaneously near the surface.[26]

Theoretically, the surface band energy of a semiconductor electrode is given by the potential difference between the Helmholtz and Gouy–Chapman layers and the electron affinity of the semiconductor (work function). When the electrolyte concentration is high (typically > 0.01 M), the contribution of the Gouy–Chapman layer can be assumed to be negligible. Adsorbed ions affect the potential difference in this Helmholtz layer. Experiments have shown that the surface band energy of most semiconductor electrodes such as GaAs, GaP, InP, and TiO2 with surface OH groups

shifts with solution pH with a slope of 0.059 V/pH at 300 K [27] and is independent of electrode potential. When there are charged surface states, the band edge potential shifts due to a steep change in potential near the surface, as shown in the figure. The band edge potential

1.3.2 Fermi level

The Fermi level is the Gibbs energy of one electron (hole) in an n(p)-type semiconductor and is an important physical quantity in describing band bending. Before discussing the junction between a semiconductor and an electrolyte, we will discuss the junction between a semiconductor and a metal.

Figure 1.3a, b shows the band alignment of a n-type semiconductor contacted to a metal. When a semiconductor and a metal are joined, charge transfer takes place between them until the Fermi level in the metal and the Fermi level in the semiconductor are aligned. If the metal's work function is larger than the semiconductor's work function, electrons from the n-type semiconductor move into the metal, and the Fermi levels are aligned. At that time, the loss of electrons near the semiconductor interface causes a positive charge, which generates an electric field. This causes the energy band, which describes the electrostatic potential, to bend. The interface thus formed (Fig. 1.3a) is called a Schottky junction, and its band bending (V_{bi}) is equal to the difference in work functions. However, if there is a high density ($<10^{13}$ cm^{-2} [28]) of electron-accepting levels (surface states) on the semiconductor surface, the electrons near the surface are trapped in the surface states even before the junction, and the band is bent. Furthermore, when bonded to a metal, if the surface states are not compensated even by charge transfer between the semiconductor and the metal, the band bending remains determined by the surface states and takes a value independent of the metal species. In this case, the Fermi

level pinning occurs because the Fermi level does not change and remains fixed. Such a junction (Fig. 1.3 b) is called a Bardeen contact, and the band bending is determined by the potential difference between the conduction band and the surface state and the carrier concentration. It is difficult to obtain an ideal Schottky contact because of the presence of crystal defects such as dangling bonds on the actual semiconductor surface.

Figure 1.4a, b shows the band alignment of a n-type semiconductor contacted to an electrolyte which contains redox pair. As in the case of metal junctions, charge transfer equilibrium is achieved by ensuring that the Fermi level in the semiconductor is aligned with the redox equilibrium potential (redox level). However, unlike metals, the band bending is not determined solely by the work function of the semiconductor and, the difference between the vacuum level and the redox level, and there is a need to consider the potential shift due to surface adsorbed ions (Fig. 1.4a). When surface states exist in high density (10^{12} cm^{-2} [29]), the band bending is determined the potential difference between the conduction band and the surface state and the carrier concentration in a similar manner to bonding with metals, regardless of the redox potential (Fig 1.4b).

Also, if the redox reaction does not proceed significantly, the charge transfer will be insufficient, and the surface states will determine the band bending. Furthermore, when there are multiple redox pairs, equilibrium is achieved between the Fermi level and the significantly more progressive reaction.

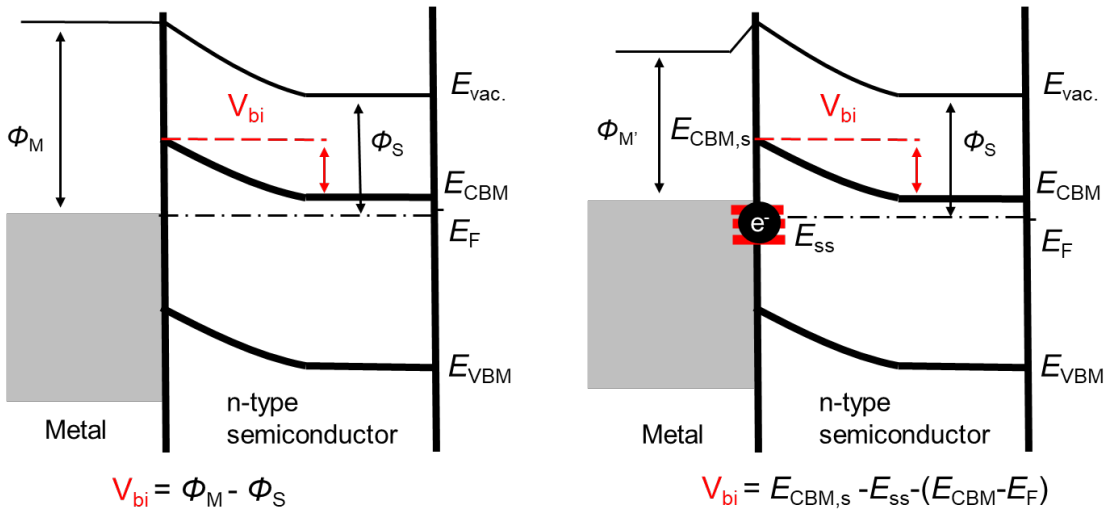

Figure 1.3 band alignment at n-type semiconductor/metal interface. (a) low density of surface states ($<10^{13}$ cm^{-2}) (b) high density of surface states ($>10^{13}$ cm^{-2}) Here, Φ_M and Φ_S are the work functions of the metal and semiconductor, respectively.

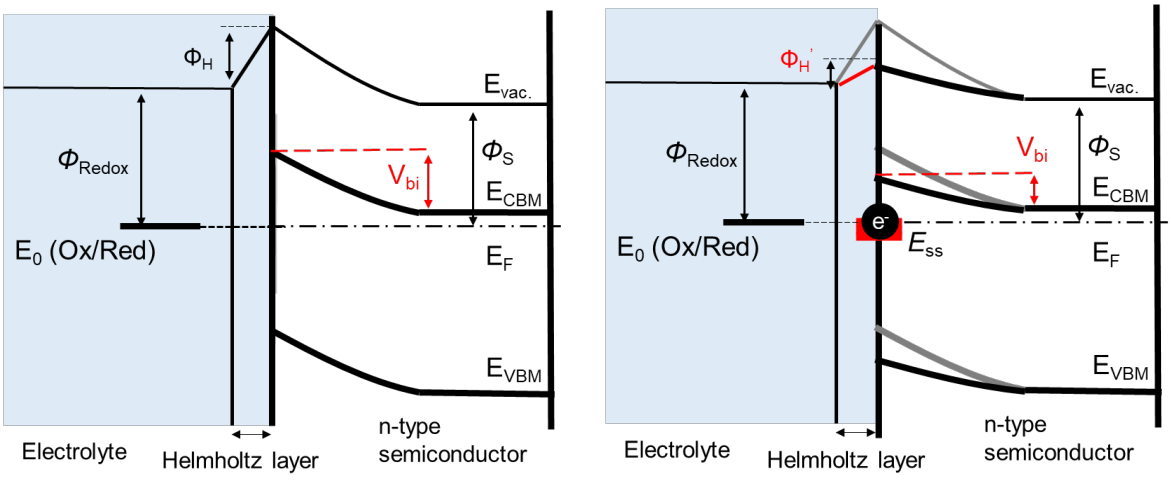

Figure 1.4 band alignment at n-type semiconductor/electrolyte contains redox pair. (a) low density of surface states ($<10^{12}$ cm^{-2}) (b) high density of surface states ($>10^{12}$ cm^{-2}) Here, Φ_{Redox} and Φ_S are the difference between vacuum level and redox level, and functions of the metal and semiconductor, respectively.

1.4 n-GaN for photoelectrochemical application

Si-doped n-type GaN is one candidate for well-defined photoanodic materials for water splitting due to its chemical stability, [30-32] relatively longer diffusion length of carriers, [33,34] and proper band edge positions. [30,35-39]. GaN is a wurtzite and has +c, -c, m, and a planes. Among these, the growth technology for the +c plane is the most mature. In addition, the crystallinity of n-GaN is higher than that of p-GaN. By using n-GaN, very high external quantum efficiency was reported in a photoelectrochemical cell, and it was over 40 % in UV region (< 360 nm) using monochromatic light [40]. Owing to these advantages, n-GaN has been used for clarifying the mechanism of carrier transport through electrochemical measurement. [36,41-43] Winnerl et al. investigated the electrochemical properties of n-GaN etched in HCl and passivated by oxidation.20 Their results indicate the possibility that surface states due to Ga dangling bonds on the n-GaN (0001) caused Fermi level pinning. However, Chen and Kuo,[44] and Sato et al. [45] have reported that the Ga dangling bonds are theoretically compensated with the dissociative adsorption of H_2O onto the GaN surface. To confirm whether or not the Ga dangling bonds cause the pinning in the presence of H_2O molecules, the evidence for the origin of pinning should be obtained experimentally.

In addition to the surface states, it is suggested that redox reactions may affect the band alignment. In 1.0 mol/L KOH aqueous solution, a clear generation of hydrogen from the counter electrode due to n-GaN photoelectrochemical reaction was observed when +1.0 V counter electrode bias was applied to the working electrode.[46] In 1.0 mol /L NaCl, the overpotential for water reduction in neutral water electrolyte was higher than that in acidic 1.0 mol/L HCl and basic 1.0 mol/L KOH.[47] These situations were similar when acidic, neutral, and basic were 0.5 mol/L Na_2SO_4, 0.5 mol/L H_2SO_4, and 1.0 mol/L NaOH (III-nitride photoelectrodes, respectively.

The electrolyte dependence was also evaluated and it was summarized that the

NaOH aqueous electrolyte is relatively good except in the case of non-oxygen evolution reactions such as HCl aqueous electrolyte.[48] The overpotential evaluated from the comparison between the flat band potential obtained from the Mott-Schottky plot and the turn-on voltage of the photocurrent was found to be larger in the case of H_2SO_4 acidic aqueous solution than in the case of NaOH basic aqueous solution. This may be due to the difference in photovoltage generated in n-GaN and slower reaction rate in oxidation of water (H_2O) molecule in HCl than OH^- in NaOH. Therefore, the effect of electrolytes on the band bending, which determines carrier splitting, and photovoltage shoule be investigated.

1.5 Overview

In this dissertation entitled “Elucidation of Electronic Structure at n-GaN and Electrolyte interface”, n-GaN (0001)/electrolyte was used as the model case of semiconductor/electrolyte interface for water splitting to clarify the effect of adsorption, surface states and redox reaction on the band bending. To suppress the effect of redox reaction and analyze the effect of surface adsorption, the band bending under ultra-high vacuum (UHV) and water vapor was compared. Then, the effect of surface states and redox reaction was evaluated at n-GaN/electrolyte interface.

In chapter 2, the effect of surface adsorption on band bending will be discussed by comparison between the band bending under ultra-high vacuum (UHV) and water vapor.

In chapter 3, method to evaluate band bending at semiconductor/electrolyte will be introduced.

In chapter 4, the effect of surface state on band bending will be discussed by introduced evaluation method with n-GaN contains abundant surface states.

In chapter 5, the effect of redox reaction on band bending will be discussed by introduced evaluation method with n-GaN/various electrolytes system.
In chapter 6, conclusion of this research will be given.

REFERENCE

[1] T.N.D. Tibbits, P. Beutel, M. Grave, C. Karcher, E. Oliva, G. Siefer, A. Wekkeli, M. Schachtner, F. Dimroth, A.W. Bett, R. Krause, M. Piccin, N. Blanc, M. Muñoz-Rico, C. Arena, E. Guiot, C. Charles-Alfred, C. Drazek, F. Janin, L. Farrugia, B. Hoarau, J. Wasselin, A. Tauzin, T. Signamarcheix, T. Hannappel, K. Schwarzburg, A. Dobrich, New Efficiency Frontiers With Wafer-Bonded Multi-Junction Solar Cells, 29th Eur. PV Sol. Energy Conf. (2014) 4.

[2] NREL, available online: http://www.nrel.gov/pv/national-center-for-photovoltaics.html, (2016).

[3] B.A. Pinaud, J.D. Benck, L.C. Seitz, A.J. Forman, Z. Chen, T.G. Deutsch, B.D. James, K.N. Baum, G.N. Baum, S. Ardo, H. Wang, E. Miller, T.F. Jaramillo, Technical and economic feasibility of centralized facilities for solar hydrogen production via photocatalysis and photoelectrochemistry, Energy Environ. Sci. 6 (2013) 1983–2002.

[4] C. a. Rodriguez, M. a. Modestino, D. Psaltis, C. Moser, Design and cost considerations for practical solar-hydrogen generators, Energy Environ. Sci. 7 (2014) 3828–3835.

[5] A. Fujishima, K. Honda, Electrochemical Photolysis of Water at a Semiconductor Electrode, Nature. 238 (1972) 37–38.

[6] Q. Wang, and K. Domen, Particulate Photocatalysts for Light-Driven Water Splitting:

Mechanisms, Challenges, and Design Strategies, Chem. Rev. 2020, 120, 919−985

[7] Hara, M.; Kondo, T.; Komoda, M.; Ikeda, S.; Kondo, J. N.; Domen, K.; Hara, M.; Shinohara, K.; Tanaka, A., Cu2O as a Photocatalyst for Overall Water Splitting under Visible Light, Irradiation. Chem. Commun. 1998, 1998, 357−358.

[8] Zou, Z.; Ye, J.; Sayama, K.; Arakawa, H. Direct Splitting of Water under Visible Light Irradiation with an Oxide Semiconductor Photocatalyst. Nature 2001, 414, 625−627.

[9] Xu, J.; Pan, C.; Takata, T.; Domen, K. Photocatalytic Overall Water Splitting on the Perovskite-Type Transition Metal Oxynitride CaTaO2N under Visible Light Irradiation. Chem. Commun. 2015, 51,7191−7194.

[10] Pan, C.; Takata, T.; Nakabayashi, M.; Matsumoto, T.; Shibata,N.; Ikuhara, Y.; Domen, K. A Complex Perovskite-Type Oxynitride:The First Photocatalyst for Water Splitting Operable at up to 600 nm.Angew. Chem., Int. Ed. 2015, 54, 2955−2959.

[11] Pan, C.; Takata, T.; Domen, K. Overall Water Splitting on the Transition-Metal Oxynitride Photocatalyst LaMg1/3Ta2/3O2N over a Large Portion of the Visible-Light Spectrum. Chem. - Eur. J. 2016, 22,1854−1862.

[12] Wang, Z.; Inoue, Y.; Hisatomi, T.; Ishikawa, R.; Wang, Q.; Takata, T.; Chen, S.; Shibata, N.; Ikuhara, Y.; Domen, K. Overall Water Splitting by Ta3N5 Nanorod Single Crystals Grown on the Edges of KTaO3 Particles. Nat. Catal. 2018, 1, 756−763.

[13] Takanabe, K. Solar Energy for Fuels; Springer International Publishing, 2015; pp 73−104.

[14] Pendlebury, S. R.; Wang, X.; Le Formal, F.; Cornuz, M.; Kafizas, A.; Tilley, S. D.; Gratzel, M.; Durrant, J. R. Ultrafast Charge ¨ Carrier Recombination and Trapping in Hematite Photoanodes under Applied Bias. J. Am. Chem. Soc. 2014, 136, 9854−9857.

[15] Ravensbergen, J.; Abdi, F. F.; van Santen, J. H.; Frese, R. N.; Dam, B.; van de Krol, R.; Kennis, J. T. M. Unraveling the Carrier Dynamics of BiVO4: A Femtosecond to Microsecond Transient Absorption Study. J. Phys. Chem. C 2014, 118, 27793–27800.

[16] Yamakata, A.; Vequizo, J. J. M.; Kawaguchi, M. Behavior and Energy State of Photogenerated Charge Carriers in Single-Crystalline and Polycrystalline Powder SrTiO3 Studied by Time-Resolved Absorption Spectroscopy in the Visible to Mid-Infrared Region. J. Phys. Chem. C 2015, 119, 1880–1885.

[17] Godin, R.; Kafizas, A.; Durrant, J. R. Electron Transfer Dynamics in Fuel Producing Photosystems. Curr. Opin. Electrochem. 2017, 2, 136–143.

[18] Li, X.; Yu, J.; Jaroniec, M.; Chen, X. Cocatalysts for Selective Photoreduction of CO2 into Solar Fuels. Chem. Rev. 2019, 119, 3962–4179.

[19] N. Serpone, D. Lawless, R. Khairutdinov and E. Pelizzetti, Subnanosecond Relaxation Dynamics in TiO2 Colloidal Sols (Particle Sizes Rp = 1.0-13.4 nm). Relevance to Heterogeneous Photocatalysis, J. Phys. Chem., 1995, 99, 16655–16661.

[20] A. J. Cowan, J. W. Tang, W. H. Leng, J. R. Durrant and D. R. Klug, Water Splitting by Nanocrystalline TiO2 in a Complete Photoelectrochemical Cell Exhibits Efficiencies Limited by Charge Recombination, J. Phys. Chem. C, 2010, 114, 4208–4214.

[21] F. M. Pesci, A. J. Cowan, B. D. Alexander, J. R. Durrant and D. R. Klug, Charge Carrier Dynamics on Mesoporous WO3 during Water Splitting, J. Phys. Chem. Lett., 2011, 2, 1900–1903.

[22] S. Pendlebury, M. Barroso, A. J. Cowan, K. Sivula, J. Tang, M. Gratzel, D. R. Klug and J. R. Durrant, Dynamics of photogenerated holes in nanocrystalline α-Fe2O3

electrodes for water oxidation probed by transient absorption spectroscopy, Chem. Commun., 2011, 47, 716–718.

[23] N. J. Cherepy, D. B. Liston, J. A. Lovejoy, H. M. Deng and J. Z. Zhang, Ultrafast Studies of Photoexcited Electron Dynamics in γ- and α-Fe2O3 Semiconductor Nanoparticles, J. Phys. Chem. B, 1998, 102, 770–776.

[24]Garcia-Esparza, A. T.; Takanabe, K. A Simplified Theoretical Guideline for Overall Water Splitting Using Photocatalyst Particles. J. Mater. Chem. A 2016, 4, 2894–2908

[25] Nellist, M.R., Laskowski, F.A.L., Qiu, J. et al. Potential-sensing electrochemical atomic force microscopy for in operando analysis of water-splitting catalysts and interfaces. Nat Energy 3, 46–52 (2018).

[26] Y. Nakato, A New Method for Estimating Surface Band Energies of a Semiconductor Electrode in Contact with an Electrolyte Solution, Chemistry Letters 2013 42:2, 135-136

[27] H. Gerischer, inPhysical Chemistry, ed. by H. Eyring, D. Henderson, W. Jost, Academic Press, New York, 1970, Vol. 9A, Chap. 5, pp. 463–542.

[28] J. Bardeen, Surface States and Rectification at a Metal Semi-Conductor Contact, Phys. Rev. 71, 717 (1947).

[29] A. J. Bard, A. B. Bocarsly, F. R. F. Fan, E. G. Walton, and M. S. Wrighton, The concept of Fermi level pinning at semiconductor/liquid junctions. Consequences for energy conversion efficiency and selection of useful solution redox couples in solar devices, J. Am. Chem. Soc. 1980, 102, 11, 3671–3677

[30] Kibria, M. G.; Mi, Z. Artificial photosynthesis using metal/nonmetal-nitride semiconductors: current status, prospects, and challenges. *J. Mater. Chem. A* **2016,** *4,* 2801-2820.

[31] Alotaibi, B.; Nguyen, H. P. T.; Zhao, S.; Kibria, M. G.; Fan, S.; Mi, Z. Highly Stable Photoelectrochemical Water Splitting and Hydrogen Generation Using a Double-Band InGaN/GaN Core/Shell Nanowire Photoanode. *Nano Lett.* **2013,** *13,* 4356-4361.

[32] Jung, H. S.; Hong, Y. J.; Li, Y.; Cho, J.; Kim, Y. J.; Yi, G. C. Photocatalysis Using GaN Nanowires. *ACS Nano* **2008,** *2,* 637-642.

[33] Yamakata, A.; Yoshida, M.; Kubota, J.; Osawa, M.; Domen, K. Potential-Dependent Recombination Kinetics of Photogenerated Electrons in n- and p-Type GaN Photoelectrodes Studied by Time-Resolved IR Absorption Spectroscopy. *J. Am. Chem. Soc.* **2011,** *133,* 11351-11357.

[34] Jiang, C.; Moniz, S. J. A.; Wang, A.; Zhang, T.; Tang, J. Photoelectrochemical devices for solar water splitting – materials and challenges. *Chem. Soc. Rev.* **2017,** *46,* 4645-4660.

[35] Howgate, J.; Schoell, S. J.; Hoeb, M.; Steins, W.; Baur, B.; Hertrich, S.; Nickel, B.; Sharp, I. D.; Stutzmann, M.; Eickhoff, M. Photocatalytic Cleavage of Self-Assembled Organic Monolayers by UV-Induced Charge Transfer from GaN Substrates. *Adv. Mater.* **2010,** *22,* 2632-2636.

[36] Wang, D.; Pierre, A.; Kibria, M. G.; Cui, K.; Han, X.; Bevan, K. H.; Guo, H.; Paradis, S.; Hakima, A. R.; Mi, Z. Wafer-Level Photocatalytic Water Splitting on GaN Nanowire Arrays Grown by Molecular Beam Epitaxy. *Nano Lett.* **2011,** *11,* 2353-2357.

[37] Yotsuhashi, S.; Deguchi, M.; Zenitani, Y.; Hinogami, R.; Hashiba, H.; Yamada, Y.; Ohkawa, K. Photo-induced CO_2 Reduction with GaN Electrode in Aqueous System. *Appl. Phys. Express* **2011,** *4,* 117101.

[38] Schäfer, S.; Wyrzgol, A.; Caterino, R.; Jentys, A.; Schoell, S. J.; Hävecker, M.; Knop-Gericke, A.; Lercher, J. A.; Sharp I. D.; Stutzmann, M. Platinum Nanoparticles on

Gallium Nitride Surfaces: Effect of Semiconductor Doping on Nanoparticle Reactivity. *J. Am. Chem. Soc.* **2012,** *134*, 12528-12535.

[39] Kibria, M. G.; Nguyen, H. P. T.; Cui, K.; Zhao, S.; Liu, D.; Guo, H.; Trudeau, M. L.; Paradis, S.; Hakima, A. R.; Mi, Z. One-Step Overall Water Splitting under Visible Light Using Multiband InGaN/GaN Nanowire Heterostructures. *ACS Nano* **2013,** *7,* 7886-7893.

[40] Iwaki, Y., Ono, M., Yamaguchi, K., Kusakabe, K., Fujii, K. and Ohkawa, K. (2008), Nitride photocatalyst to generate hydrogen gas from water. Phys. Status Solidi (c), 5: 2349-2351

[41] Sachsenhauser, M.; Sharp, I. D.; Stutzmann, M.; Garrido, J. A. Surface State Mediated Electron Transfer Across the N-Type SiC/Electrolyte Interface. *J. Phys. Chem. C* **2016,** *120,* 6524-6533.

[42] Winnerl, A.; Garrido, J. A.; Stutzmann, M. GaN surface states investigated by electrochemical studies. *Appl. Phys. Lett.* **2017,** *110,* 101602.

[43] Winnerl, A.; Pereira, R. N.; Stutzmann, M. Kinetics of optically excited charge carriers at the GaN surface: Influence of growth technique, doping and polarity. *J. Appl. Phys.* **2015,** *118,* 155704.

[44] Chen, Y. W.; Kuo, J. L. Density Functional Study of the First Wetting Layer on the GaN (0001) Surface. *J. Phys. Chem. C* **2013,** *117,* 8774-8783.

[45] Sato, M.; Imazeki, Y.; Fujii, K.; Nakano, Y.; Sugiyama, M. First-principles modeling of GaN(0001)/water interface: Effect of surface charging. *J. Chem. Phys.* **2019,** *150,* 154703.

[46] (16) K. Fujii, T. Karasawa and K. Ohkawa, Hydrogen gas generation by splitting aqueous water using n-type GaN photoelectrode with anodic oxidation, Jpn. J. Appl. Phys., 44 (2005), p. L543

[47] K. Fujii and K. Ohkawa, Hydrogen generation from aqueous water using n-GaN by photoassisted electrolysis, Phys. Status Solidi C, 3 (2006), pp. 2270-2273

[48] K. Koike, A. Nakamura, M. Sugiyama, Y. Nakano and K. Fujii, Surface stability of n-type GaN depending on carrier concentration and electrolytes under photoelectrochemical reactions Phys. Status Solidi C, 11 (2014), pp. 821-823

Chapter 2 Band bending at n-GaN/H_2O interface

To improve the performance of semiconductor photoelectrodes for water splitting, the amount of band bending in the depletion layer of a semiconductor should be accurately ascertained, since it determines the splitting efficiency of photogenerated carriers. Band bending has been determined by X-ray photoelectron spectroscopy (XPS) from the valence band maximum (VBM), which has been calculated from Ga 3d peak using the energy difference between VBM and Ga 3d ($\Delta E_{\mathrm{VBM\text{-}3d}}$). This work validates several values for $\Delta E_{\mathrm{VBM\text{-}3d}}$ which have been reported previously, by analyzing the spectrum around the VBM and its distance from Ga 3d for n-GaN(0001) surface under both ultra-high vacuum (UHV) and ambient H_2O. $\Delta E_{\mathrm{VBM\text{-}3d}}$ is estimated to be between 17.36 eV and 17.55 eV. By adopting 17.5 eV as $\Delta E_{\mathrm{VBM\text{-}3d}}$, the amounts of band-bending were 0.5 eV under UHV and 0.1 eV under a relative humidity of 46% respectively. For the latter condition, surface photo voltage of 20 meV was observed upon Xe lamp irradiation, confirming the existence of band bending even with H_2O adsorption on the surface. The origin of such band bending seems to be Fermi level pinning to the sub-surface states which cannot be compensated by H_2O.

2.1 Introduction

Efforts have been made to improve STH in hydrogen production using photoelectrochemical reactions [1-6]. For further efficiency improvement, the cause of pinning [7,8] needs to be clarified in order to control the band bending.

n-GaN is a promising material for elucidating the carrier transport mechanism in photoelectrochemical reactions [15,19-21] due to its chemical stability [9-11], long carrier diffusion length [12,13], and suitable band edge location [9,14-18]. Winnerl et al. investigated the electrochemical properties of n-GaN etched in hydrochloric acid[20] .

Their results suggest that the surface state caused by Ga dangling bonds on n-GaN(0001) may be responsible for the Fermi level pinning. However, Chen and Kuo, [22] and Sato et al [23] reported that Ga dangling bonds are theoretically compensated by the dissociative adsorption of H2O on the GaN surface. In order to confirm whether Ga dangling bonds cause pinning in the presence of H2O molecules, it is necessary to obtain experimental evidence for the origin of pinning.

As this experimental approach to elucidate the relation between band bending and the origin of the pinning, X-ray photoelectron spectroscopy (XPS) is an effective experimental approach. Bermudez et al. investigated the band bending of GaN (0001) in the vicinity of the pristine and H_2O dosed surface of GaN under UHV conditions.[24] They reported a reduction in band bending by ~0.14 eV with the removal of the surface states upon H_2O adsorption, resulting in a residual band bending of ~0.52 eV. The H_2O coverage was estimated to be 0.46 ML. The residual band bending was therefore attributed to bulk defects. Lorenz et al. reported that the band bending for GaN (0001) in UHV was reduced by 0.5 eV with the H_2O coverage of 0.8 ML [25,26], resulting in a flat-band condition. Zhang and Ptasinska used ambient pressure X-ray photoelectron spectroscopy (AP-XPS) to clarify the correspondence between the surface chemistry and the band structure for the GaN (0001) surface, which mimics in situ conditions as a photoelectrode.[27] They reported a reduction in band bending by 0.2 eV under an ambient pressure of 0.1 mbar H_2O at room temperature, and a band bending of ~0.4 eV was reported to exist under this ambient H_2O vapor. Such variation in the reported amount of band bending with H_2O adsorption on the GaN (0001) surface emphasizes the necessity of further experimental investigation, so that we can discuss the correspondence between theoretical prediction and experimental evidence.

Furthermore, there exists a significant drawback in the estimation of GaN band bending using binding energies obtained by XPS. In those previous reports using XPS,

the energy difference between the VBM and Ga 3d ($\Delta E_{VBM\text{-}3d}$) in the bulk of GaN was assumed to be 17.76 ± 0.03 eV.[28,29] However, Bermudez pointed out the problem that the VBM estimated by subtracting this value from the Ga 3d was not consistent with the direct evaluation by linear extrapolation.[30] The value 17.76 ± 0.03 eV was evaluated as the $\Delta E_{VBM\text{-}3d}$ by fitting valence band spectra from a surface sensitive method, XPS (with ~16 Å as an information depth), with the valence band density of state obtained by theoretical calculation.[28] Recently, by a similar fitting method, the value 17.25 and 17.29 eV were evaluated as the $\Delta E_{VBM\text{-}3d}$ for GaN.[31] They mentioned the difference from 17.76 ± 0.03 eV was possibly caused by uncertainty in spectrum broadening or extra surface state signals in the band edge. In addition, the value of the $\Delta E_{VBM\text{-}3d}$ in GaN is evaluated as 17.5 eV by soft X-ray emission (SXE) [32], a bulk sensitive method with an information depth of ~500 Å. [33-35] Although the $\Delta E_{VBM\text{-}3d}$ value of 17.76 ± 0.03 eV has been widely used, it needs critical validation because of the aforementioned variation in proposed values.

In this study, we examined the validity of these values as the $\Delta E_{VBM\text{-}3d}$ for GaN by comparing the VBM obtained by using different evaluation methods: linear extrapolation of the valence band spectrum and subtracting $\Delta E_{VBM\text{-}3d}$ from Ga 3d using the XPS spectra for n-GaN (0001) surface under both ultra-high vacuum (UHV) and ambient H_2O. In addition, surface photovoltage (SPV) under Xe lamp irradiation was measured and used for validation. On the basis of the present results, we accurately determined the band bending at the GaN surface and its shift under ambient H_2O vapor. Furthermore, we compared our results with the values calculated from the data reported in other literature, using the validated value of $\Delta E_{VBM\text{-}3d}$.

2.2 Method

2.2.1 Sample preparation and experiment

The experiments were performed at the AP-XPS endstation [36,37] at SPring-8 BL07LSU.[38] The photon energy and flux of incident X-rays were 735 eV and 1.2 × 10^{15} s^{-1} cm^{-2}, respectively. Binding energy was calibrated by fitting XPS spectrum near Fermi edge in Pd (111) by Fermi-Dirac function. The sample was n-GaN with a Ga-polar (0001) surface (thickness of n-GaN: 2.5 μm), grown on a Si substrate by metal organic vapor phase epitaxy (MOVPE). The carrier density evaluated by Hall effect measurement was 4 × 10^{18} cm^{-3} at room temperature. The donor density evaluated by Mott-Schottky plot was 9 × 10^{18} cm^{-3}. The clean surface of n-GaN was prepared by cycles of 0.5 keV nitrogen ion bombardment followed by annealing at 1100 K in N_2 (1.0 × 10^{-6} mbar). The sample temperature was measured by a K-type (chromel-alumel) thermocouple sandwiched between the GaN (0001) surface and the tantalum foil fixed to the sample holder. After cleaning, the (1 × 1) surface was confirmed by low energy electron diffraction (LEED) (see Figure A.1 in the Appendix A. On the clean GaN (0001) surface, no carbon was detected in C 1s XPS spectra and the atomic ratio of oxygen to gallium was at ca. 10%. Base pressure of analysis chamber was 4.1 × 10^{-10} mbar before the experiment. The n-GaN (0001) surface was exposed to ambient pressure H_2O vapor after the XPS measurements in UHV. The H_2O was outgassed by freeze–pump–thaw cycles. The adsorbed states of H_2O on solid surfaces at ambient conditions were changed as a function of relative humidity.[39] For AP-XPS measurements in this study, the relative humidity was ~46% (2 mbar H_2O pressure and 270 K). The temperature of the sample was kept constant by cooling it with a water chiller (Julabo FP50-HE). The band bending was calculated by using the peak position of Ga 3d XPS spectra. SPV was evaluated as the difference of the peak location with and without Xe lamp irradiation as light source

for carrier photogeneration. The flux density of the Xe lamp for carrier generation (which has higher energy than GaN band gap, 3.4 eV) was 1.3×10^{16} s^{-1} cm^{-2} because it was focused by using a lens.

2.2.2 Evaluation method for band bending

Conventionally, the amount of band bending near a GaN crystal surface has been evaluated from the energy position of the VBM determined by linear extrapolation of the edge to the baseline. However, the results have contained notable errors because the spectral feature of VBM is overlapped with that of the surface-state. To make an accurate evaluation, we adopted the following equation (eq. (2.1)) that does not contain the value of VBM for analyzing the amount of band bending at the GaN surface. [24,27] (see Figure 1 for reference):

$$Band\ bending + E_{\mathrm{Ga\ 3d\ s}} = \Delta E_{\mathrm{F-CBM}} + \mathrm{Band\ gap} + \Delta E_{\mathrm{VBM-3d}}, \quad (2.1)$$

where $E_{\mathrm{Ga\ 3d\ s}}$ is the binding energy of Ga 3d at the surface and $\Delta E_{\mathrm{F-CBM}}$ is the difference between the Fermi level and the conduction band minimum. $E_{Ga\ 3d\ s}$ is acquired as the peak location of Ga 3d in the photoelectron spectrum by XPS. $\Delta E_{\mathrm{F-CBM}}$ is calculated by equation (2.2) following Boltzmann distribution:

$$\Delta E_{\mathrm{F-CBM}} = \mathrm{k}T\ln\left(\frac{n}{N_{\mathrm{c}}}\right), \quad (2.2)$$

where k is Boltzmann factor, T is temperature, n is carrier concentration and N_c is effective density of state for the conduction band. N_{c} is obtained by the following equation (2.3):

$$N_c = 2\left(\frac{2\pi \mathrm{m}^{*}\mathrm{k}T}{\mathrm{h}^2}\right)^{\frac{3}{2}}, \quad (2.3)$$

where m^* is effective mass of an electron in the conduction band of GaN and h is Planck's constant. The value of m^* is given by $0.20\,m_e$ with the mass of electron in vacuum, m_e.[40] Therefore, ΔE_{F-CBM} was 0.02 V for both at 280 K under UHV and at 270 K under ambient H_2O vapor. For the value of the band gap for wurtzite GaN, 3.4 eV [41] was used.

$\Delta E_{VBM\text{-}3d}$ in equation (1) is the constant of wurtzite GaN. The value of 17.76 ± 0.03 eV has been used for this constant in previous reports.[24,27] Recently, the values of 17.25 and 17.29 eV were reported as $\Delta E_{VBM\text{-}3d}$.[31] All the values were evaluated as the $\Delta E_{VBM\text{-}3d}$ by the fitting of valence band spectra by XPS with Al Kα excitation, a surface sensitive measurement due to a probing depth of ~16 Å.[28] The problem is that the valence band spectrum near the surface is extended in the direction of the conduction band due to the surface states, leading to an underestimation of the energy difference $E_{VBM\ s}$ between the VBM and E_F to be $E_{VBM\ ss}$ (see in Figure 1). As a result, $\Delta E_{VBM\text{-}3d}$ was overestimated as $\Delta E_{VBM\ ss\text{-}3d\ s}$. Alternatively, $\Delta E_{VBM\text{-}3d}$ was evaluated as 17.5 eV for n-GaN (0001) [32] by bulk sensitive SXE with its probing depth of ~500 Å. [33-35] In this case, the effect of surface state on VBM can be eliminated. The value of $\Delta E_{VBM\text{-}3d}$ is essential for an accurate evaluation of band bending and it is to be validated through further analysis.

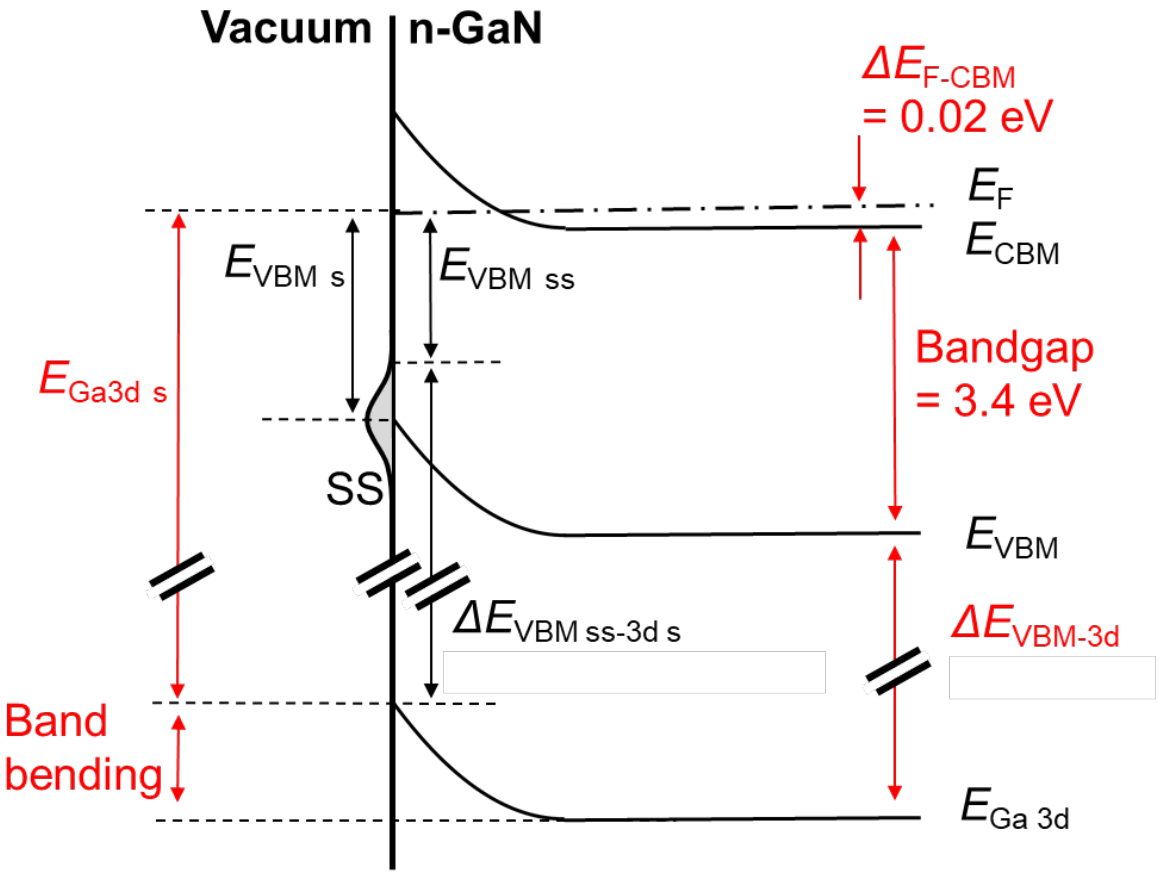

Figure 2.1 Evaluation of the band bending in the vicinity of GaN surface. E_F, E_{CBM}, E_{VBM}, and $E_{Ga\ 3d}$ are Fermi level, energy of conduction band minimum, valence band maximum, and Ga 3d, respectively. SS means surface states. The $\Delta E_{VBM\text{-}3d}$ has been widely adopted as 17.76 ± 0.03 eV, but we found that 17.5 eV obtained by SXE for n-GaN (0001) [32] leads to more consistent evaluation of the band bending for GaN. The length of depletion layer in the vicinity of the GaN/vacuum interface was calculated as ~8 nm from the band bending of 0.5 eV under UHV.

2.3 Results and discussion

2.3.1 Position of valence band maximum

To examine the validity of these values for $\Delta E_{\text{VBM-3d}}$, the VBM position evaluated by the linear extrapolation of the valence band spectrum to the baseline was compared with the VBM obtained by subtracting $\Delta E_{\text{VBM-3d}}$ from the peak energy of Ga 3d obtained by XPS. The binding energy of the VBM by linear extrapolation has the possibility of underestimation due to surface states, whereas the VBM evaluated by the subtraction should be correct if $\Delta E_{\text{VBM-3d}}$ is the constant for a bulk GaN. The VBM spectra under UHV and after exposure to H_2O vapor are shown in Figure 2 a, b. By linear extrapolation, the VBM under UHV was estimated as 3.07 ± 0.23 eV (Figure 2 c). In order for this value to match the value of VBM by subtracting $\Delta E_{\text{VBM-3d}}$ from 20.394 ± 0.004 eV obtained as Ga 3d peak energy (Figure 3a), $\Delta E_{\text{VBM-3d}}$ should be 17.32 ± 0.23 eV. The value 17.76 ± 0.03 eV, which has been used as $\Delta E_{\text{VBM-3d}}$, is out of this range. The assumption that $\Delta E_{\text{VBM-3d}}$ = 17.76 ± 0.03 eV leads to the VBM at 2.63 ± 0.03 eV, which is 0.44 ± 0.26 eV closer to the Fermi level than the VBM obtained by extrapolation. In principle, subtraction of $\Delta E_{\text{VBM-3d}}$ from Ga 3d peak energy should yield a VBM position which is more distant from the Fermi level than the VBM obtained by the extrapolation, because the linear extrapolation should underestimate the binding energy of the VBM due to the effect of surface states on the valence band spectrum (Figure 1). Bermudez pointed out the same problem in his review:[9] subtracting the value, 17.76 ± 0.03 eV, from Ga 3d peak energy yielded the VBM binding energy of 2.4 eV, which is smaller than the value by linear extrapolation, 2.89 eV, reported by Kočan et al.[42] Although the reason for this discrepancy was not mentioned in the review, we believe that the problem was the use of 17.76 ± 0.03 eV as the constant. By subtracting 17.25 eV, 17.29 eV and 17.5 eV as the $\Delta E_{\text{VBM-3d}}$ from the position of Ga 3d in UHV, 20.394 ± 0.004 eV, the VBM was estimated as 3.14 eV,

3.10 eV and 2.9 eV, respectively. These values are closer to the value of VBM by linear extrapolation, 3.07 ± 0.23 eV, and the differences are in an error range (Figure 2c).

Similarly, under ambient H_2O vapor, the VBM was obtained as 3.43 ± 0.23 eV by linear extrapolation (Figure 2d). Subtracting this value from the 20.796 ± 0.003 eV obtained as Ga 3d peak energy (Figure 3b) yields $\Delta E_{\mathrm{VBM\text{-}3d}}$ as 17.36 ± 0.23 eV. On the other hand, by subtracting 17.25 eV, 17.29 eV, 17.5 eV and 17.76 ± 0.03 eV from 20.796 ± 0.003 eV, the VBM values of 3.55 eV, 3.51 eV, 3.3 eV and 3.04 ± 0.03 eV are obtained, respectively. The $\Delta E_{\mathrm{VBM\text{-}3d}}$ 17.25 eV, 17.29 eV and 17.5 eV led to VBM which are consistent with the value 17.36 ± 0.23 eV obtained by linear extrapolation, while 17.76 ± 0.03 eV yielded the inconsistent VBM, considering the possibility of underestimating VBM by linear extrapolation due to the surface states (Figure 2d). We therefore believe that 17.25 eV, 17.29 eV and 17.5 eV are acceptable values as $\Delta E_{\mathrm{VBM\text{-}3d}}$.

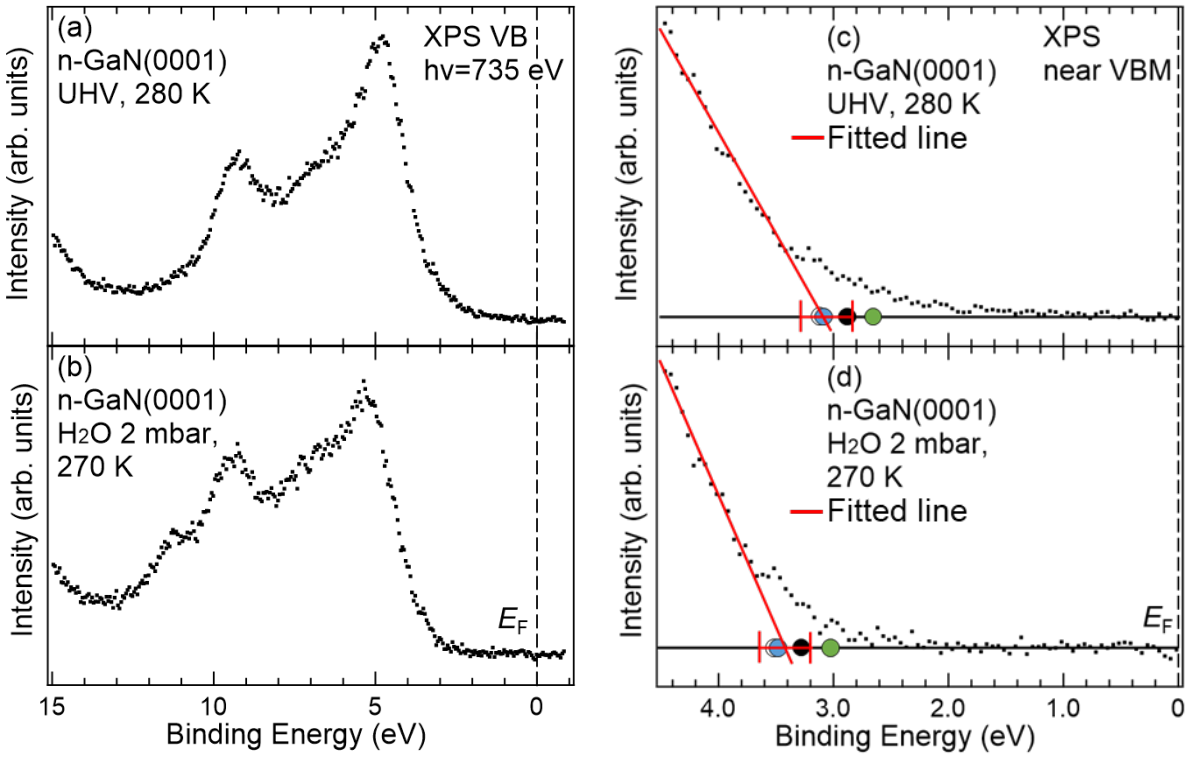

Figure 2.2 XPS spectrum for the valence band on n-GaN (0001) surface under UHV condition at 280 K (a) and under 2 mbar ambient H_2O vapor at 270 K (b). The incident photon energy was 735 eV. The enlarged view of the valence band spectrum under UHV is shown as (c). The VBM was evaluated as 3.07 ± 0.23 eV under UHV (the cross point with a red error bar) below the Fermi level by the linear extrapolation with least square fitting. The VBM evaluated by subtracting $\Delta E_{\text{VBM-3d}}$ from the energy of Ga 3d peak were 3.14 eV (the white circle), 3.10 eV (the black circle), 2.9 eV (the blue circle) and 2.63 ± 0.03 eV (the green circle) based on $\Delta E_{\text{VBM-3d}}$=17.25 eV, 17.29 eV, 17.5 eV and 17.76 ± 0.03 eV, respectively. The enlarged view of the valence band spectrum under ambient H_2O vapor is shown as (d). The VBM evaluated by the linear extrapolation was 3.43 ± 0.23 eV (the cross point with red error bar). The VBM evaluated by subtracting $\Delta E_{\text{VBM-3d}}$ from the energy of Ga 3d peak were 3.55 eV (the white circle), 3.51 eV (the blue circle), 3.3 eV (the black circle) and 3.04 ± 0.03 eV (the green circle) based on $\Delta E_{\text{VBM-3d}}$=17.25 eV, 17.29 eV, 17.5 eV and 17.76 ± 0.03 eV, respectively.

2.3.2 Band bending reduction under H_2O vapor

For further discussion about the validity of these values, the band bending was evaluated. As shown in Figure 3a, the peak position of Ga 3d in UHV was evaluated as 20.394 ± 0.004 eV by fitting the Ga 3d spectrum. Therefore, the upward band bending evaluated by Eq. (1) was 0.28 eV, 0.32 eV and 0.5 eV based on $\Delta E_{\mathrm{VBM\text{-}3d}}$=17.25 eV, 17.29 eV, and 17.5 eV, respectively. After n-GaN was exposed to H_2O vapor, the Ga 3d peak was shifted to 20.796 ± 0.003 eV (Figure 3b), indicating a reduction in band bending by 0.402 eV. Similar amount of change in the band bending was also observed in N 1s XPS spectra between UHV and ambient H_2O vapor (see Figure A2a, b in the Appendix A). The upward band bending evaluated by Eq. (1) was –0.13 eV, –0.09 eV and 0.1 eV based on $\Delta E_{\mathrm{VBM\text{-}3d}}$=17.25 eV, 17.29 eV and 17.5 eV, respectively. The negative values might suggest a complete disappearance of the depletion layer in the vicinity of GaN surface, but negative band bending with substantial amplitude does not seem realistic since there is no structure on the surface with H_2O adsorption to accumulate such a large amount of negative charge.

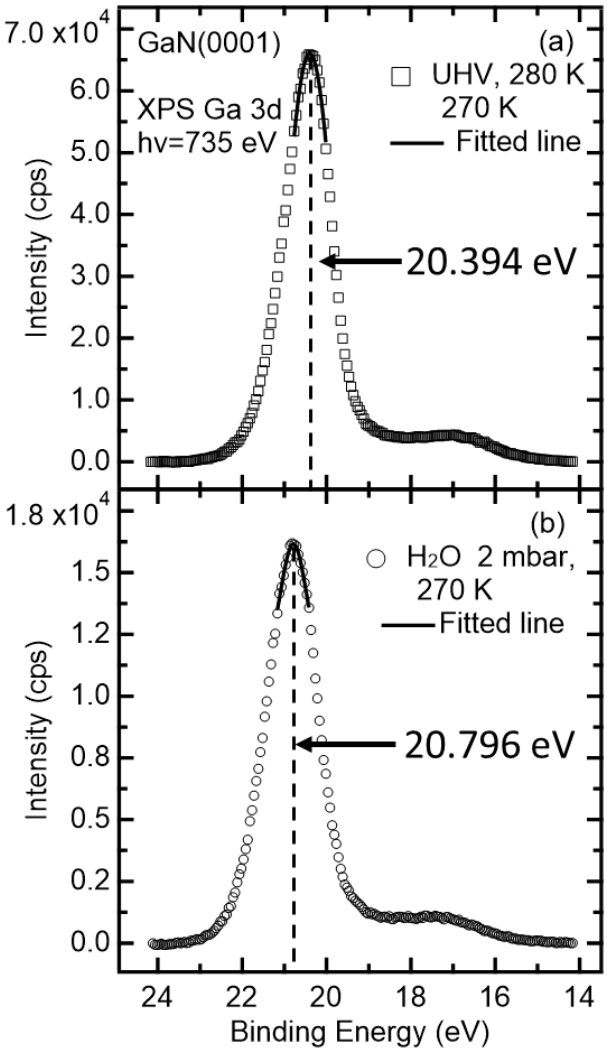

Figure 2.3 XPS spectra for Ga 3d on the n-GaN (0001) surface under (a) UHV at 280 K (the black circles) and under (b) 2 mbar ambient H_2O vapor at 270 K (the black squares). These peaks were normalized for comparison. The incident photon energy was 735 eV. The lines are the result of fitting to find out the peak location. The $E_{Ga\ 3d\ s}$, the peak location of Ga 3d, was evaluated as 20.394 ± 0.004 eV under UHV and 20.796 ± 0.003 eV under 2 mbar ambient H_2O vapor, respectively.

2.3.3 Surface photovoltage under H_2O vapor

To obtain further evidence for validating the values of $\Delta E_{VBM\text{-}3d}$, SPV under ambient 2 mbar H_2O vapor was evaluated by the shift of the peak location of Ga 3d under Xe lamp irradiation (Figure 4a, b). SPV, or the reduction in upward band bending under illumination, is caused by the accumulation of photogenerated carriers in the depletion layer of GaN. Figure 4b is the enlarged view around the peak in Figure 4a. In Figure 4b, the peak location of Ga 3d before Xe lamp irradiation is set at zero. Under Xe lamp irradiation, the relative shift of the peak location was +20 meV in binding energy scale. The same amount of peak shift was also observed in N 1s (see Figure A3a, b in the Appendix A). The shift by SPV cannot be observed in the case of negative band bending. To allow this amplitude of SPV, the upward bending of GaN should be equal to or larger than 20 meV under ambient 2 mbar H_2O vapor without Xe lamp irradiation. Therefore, the negative band bending –0.13 eV and –0.09 eV based on $\Delta E_{VBM\text{-}3d}$=17.25 eV and 17.29 eV are not consistent with the SPV effect. To obtain the positive band bending equal to or larger than 20 meV, $\Delta E_{VBM\text{-}3d}$ should be equal to or larger than 17.36 eV based on Eq. (2.1).

2.3.4 Recommended value of $\Delta E_{VBM\text{-}3d}$ and reconsidered band bending

As described in 3.2, to obtain the VBM consistently by both the linear extrapolation of the VBM spectrum and the subtraction of $\Delta E_{VBM\text{-}3d}$ from the Ga 3d peak energy, $\Delta E_{VBM\text{-}3d}$ should be equal to or smaller than 17.32 ± 0.23 eV. On the other hand, as described in 3.3 and 3.4, the observed value of SPV and the band bending analysis under ambient 2 mbar H_2O vapor suggested that $\Delta E_{VBM\text{-}3d}$ should be equal to or larger than 17.36 eV. As such, the genuine value of $\Delta E_{VBM\text{-}3d}$ should be between 17.36 eV and 17.55

eV. The value obtained by SXE, $\Delta E_{\mathrm{VBM\text{-}3d}}$=17.5 eV fits in this range although error range for SXE is not clear, and we will hence adopt this value for discussing the band bending at the n-GaN/H_2O interface.

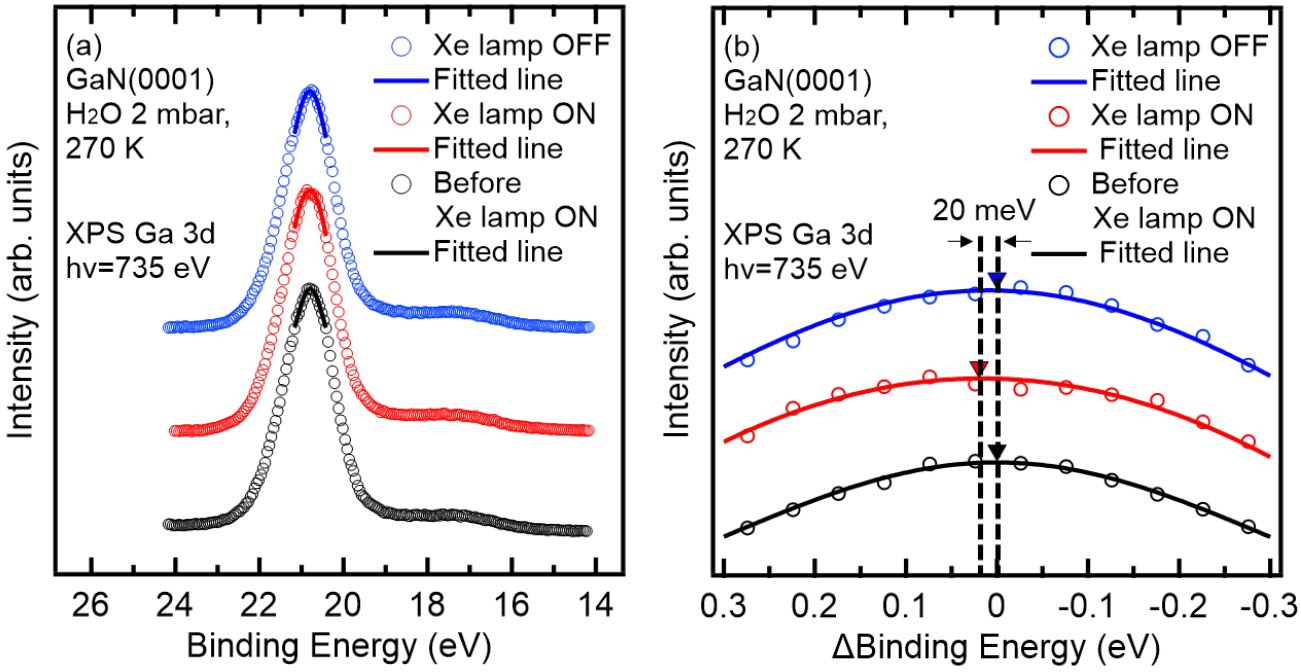

Figure 2.4 (a) (a) XPS spectra for Ga 3d on the n-GaN (0001) surface under 2 mbar ambient H_2O vapor at 270 K before Xe lamp irradiation (the black dots and line denoted by "Before Xe lamp ON"), with irradiation ("Xe lamp ON": the red dots and line) and after shutting off Xe lamp ("Xe lamp OFF": the blue dots and line). Dots and lines are experimental data and results of peak fitting, respectively. The energy and flux of X-rays for XPS were 735 eV and 1.2×10^{15} s^{-1} cm^{-2}. The photon flux density (which has higher energy than GaN band gap, 3.4 eV) of the Xe lamp for carrier generation was 1.3×10^{16} s^{-1} cm^{-2}. (b) The enlarged view around the maximum intensity, with the peak locations indicated by the triangles. The peak location before Xe lamp irradiation is set to zero in the binding energy axis. The peak location is shifted by +20 meV under Xe lamp irradiation in binding energy scale. After shutting off the Xe lamp, the peak location approached zero.

As shown in Figure 3a, the peak position of Ga 3d in UHV was evaluated as 20.394 ± 0.004 eV by fitting the Ga 3d spectrum. Adopting 17.5 eV as $\Delta E_{\mathrm{VBM\text{-}3d}}$ in Eq. (1), the upward band bending was evaluated as 0.5 eV (Figure 5). If the amount of band bending is re-calculated using both $\Delta E_{\mathrm{VBM\text{-}3d}}$ = 17.5 eV and the peak location of Ga 3d reported in the literature, a similar amplitude of band bending was obtained: 0.4 eV for the data by Gutt et al. [25] and 0.4 eV for the data by Bermudez et al. [24] (Table 1). The band bending in UHV should be governed by Fermi level pinning at the surface states on GaN (0001). The pinning level was 2.9 eV above the VBM position. The pinning state was considered to be the unoccupied Ga dangling bonds, in reference to theoretical analysis.[43]

After n-GaN was exposed to H_2O vapor, the Ga 3d peak was shifted to 20.796 ± 0.003 eV (Figure 3b). Correspondingly, the upward band bending was reduced to 0.1 eV after exposure to H_2O vapor. As we discussed in our previous report [44], the band bending is reduced by the adsorption of water molecules on the GaN surface because the dissociative adsorption of water molecule compensates for the surface states originating from the Ga dangling bonds. The dissociative adsorption was confirmed by the increase of OH group in O 1s (see Figure A4a, b in the Appendix A). However, band bending still remained after exposure to H_2O vapor.

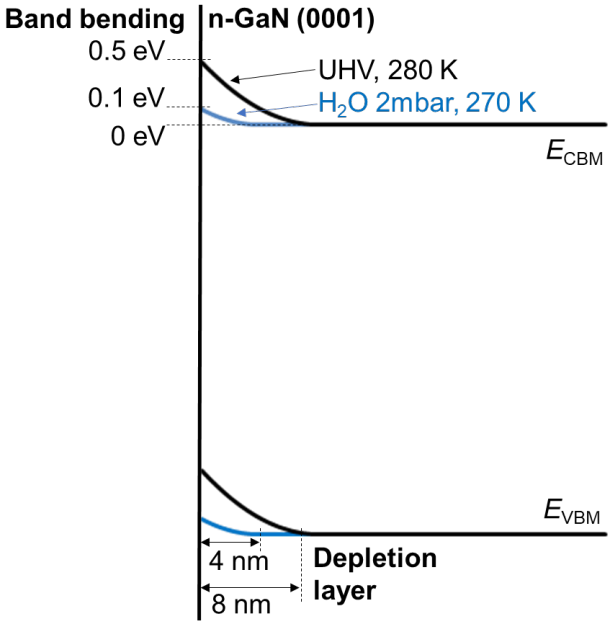

Figure 2.5 The band diagram under UHV at 280 K (black) and under 2 mbar ambient H_2O vapor at 270 K (blue). The band bending was evaluated as 0.5 eV under UHV and 0.1 eV under ambient H_2O vapor by adopting 17.5 eV as $\Delta E_{VBM\text{-}3d}$ in Eq. (1). The band bending was caused by Fermi level pinning at the surface states above the VBM around 2.9 eV under UHV and 3.3 eV, respectively. Based on the band bending, the lengths of depletion layer were calculated as 8 nm under UHV and 4 nm under ambient H_2O vapor, respectively.

To examine the consistency of our result, band bending after exposure to H_2O vapor was compared with the previous reports. In Table. 1, the band bending (BB) values are listed for this study and the previous results by Bermudez et al. [24], Lorenz et al. [26], Zhang and Ptasinska.[27] The values marked by * are the original values in the reports, which are positioned corresponding to the evaluation methods. The BB values under UHV by linear extrapolation were based on the VBM evaluated by the present authors using the spectra in the reports. [24, 26, 27] The authors' estimation of VBM for the spectrum by Lorenz et al. differed from the original value by 0.5 eV and both values are listed in the table. The other BB values under UHV were calculated using the data in the reports based on both Eq. (1) and $\Delta E_{VBM\text{-}3d}$ (either the conventionally used 17.76 ±

0.03 eV or 17.5 eV as our recommendation). The BB values after exposure to H_2O vapor were offset from the values under UHV by the reported shift in Ga 3d peak locations from UHV to H_2O ambient.

The upward band bending in the report of Bermudez et al. was calculated as 0.3 eV with 0.46± 0.03 ML of H_2O adsorption after water vapor exposure of 1 Langmuir.[24] Lorenz et al. reported that the upward band bending was completely flattened after water adsorption following water vapor exposure of 20 Langmuir [26], on the basis of their assumption that the band bending under UHV was 0.4 eV, which had been evaluated by Gutt et al. based on the VBM position (2.9 eV *vs*. E_F) obtained by the linear extrapolation. [25] However, our linear extrapolation using the spectrum under UHV condition reported by Lorenz et al. suggests that the VBM was smaller than 2.9 eV, leading to the band bending under UHV being larger than 0.4 eV. To eliminate such ambiguity associated with linear extrapolation of the VBM, we evaluated the band bending using both the Ga 3d peak location under UHV, which was obtained by ultraviolet photoelectron spectroscopy using *He* I and *He* II excitations as well as x-ray source, and Eq.1 with $\Delta E_{\text{VBM-3d}}$ = 17.5 eV; the band bending under UHV calculated as 0.7 eV. Lorenz et al. reported that the band bending was shifted by 0.5 eV after water adsorption. Therefore, we consider the band bending in the experiment by Lorenz et al. to have actually been 0.2 eV after water adsorption. In the report of Zhang and Ptasinska, the band bending was calculated as −0.1 eV under relative humidity of 1%.[27] In their report, the $\Delta E_{\text{F}-\text{CBM}}$ was described as 0.6 eV, which is larger than the value for unintentionally doped GaN in other reports (~ 0.1 eV). If we apply both $\Delta E_{\text{VBM-3d}}$ = 17.5 eV and $\Delta E_{\text{F}-\text{CBM}}$~0.1 eV to their results, the band bending under ambient H_2O would be ~0.7 eV.

Our measurement and the reexamination of the reported values mentioned above suggest that the band bending of GaN after compensation of Ga dangling bonds is 0.1–0.3 eV regardless of the growth method of GaN (MOVPE or molecular beam epitaxy) or the

surface preparation of GaN. The result by Zhang and Ptasinska deviates from this range but is subject to the ambiguity of $\Delta E_{\mathrm{F-CBM}}$. The carrier concentration in their GaN was calculated as ~ 1×10^8 cm^{-3} by Eq. (2.2) based on their $\Delta E_{\mathrm{F-CBM}}$ of 0.6 eV. Carrier concentration in n-type semiconductor is also evaluated by the following equation (2.4):

$$n = \frac{1}{\mathrm{q}\rho\mu_{\mathrm{n}}}, \tag{2.4}$$

where ρ is resistivity and μ_{n} is electron mobility. According to Eq. (2.4), the carrier concentration in their sample should be larger than 1×10^{16} cm^{-3} based on the resistivity (< 0.5 Ohm cm) and typical value of the electron mobility of ~ 1×10^3 cm^2 V^{-1} s^{-1} at 300 K.[45] The carrier concentration which was obtained by Eq. (2.2) was contrary to the inequality obtained by Eq. (2.4). Therefore, the value of $\Delta E_{\mathrm{F-CBM}}$ in their evaluation should be reconsidered to evaluate the band bending.

It has been suggested that band bending should decrease as the amount of H_2O vapor exposure increases due to the compensation of the Ga dangling bonds. However, the residual band bending under ambient H_2O was evidenced in both this study and the preceding reports [24,26,27] (with the reconsideration of band bending), and the amplitude of the bending seems to be insensitive to the amount of H_2O vapor exposure. The Ga dangling bonds which caused the Fermi level pinning under UHV should be fully compensated after water vapor exposure. Therefore, the upward band bending of 0.1 eV was considered to be caused by Fermi level pinning at the sub-surface states in GaN, which are not compensated by dissociative adsorption of water molecules on the surface. The pinning level was 0.1 eV below the CBM, and the origin of pinning was considered to be a nitrogen vacancy (V_N) [46,47] or a complex defect related with an oxygen substituting for nitrogen (O_N) decorated along dislocation. [48,49] Fernández-Garrido et al. and Koleske et al. reported nitrogen is lost more quickly than Ga by annealing at temperatures above ~800 °C. [50,51] In our study, the V_N should be formed by the

annealing process and the presence is consistent with N-to-Ga atomic ratio of 78% which was obtained by XPS. B-C. Chung, and M. Gershenzon reported the O_N was formed by the incorporation of H_2O into N-site in GaN grown by MOVPE.[52] In our study, O_N should be formed by the incorporation of H_2O into V_N and the presence was suggested by the Ga-O bond observed at the O 1s by XPS. Therefore, it is probable that complex defects related to V_N or O_N pinned the Fermi level even under ambient H_2O in our experiment.

Table 2.1 Band bending (BB) for GaN (0001) under UHV and after exposure to H_2O vapor shown with the evaluation method. The original values of BB in previous reports are indicated by "*1"

corresponding to their evaluation methods. $\Delta E_{\mathrm{F-CBM}}$ is the reported value for the difference between the conduction band minimum and the Fermi level. The amount of adsorption was defined as a monolayer (ML). Bermudez et al. used the different definition of 1 ML from Lorenz et al. The coverage in Lorenz et al. was converted by using the definition of 1 ML which was adopted by Bermudez et al. and indicated as "*2".

	Evaluation method (**The value of $\Delta E_{\mathrm{VBM\text{-}3d}}$**)	**BB under UHV /eV**	**BB after exposure to H_2O vapor /eV [# of ads. layer]**	**$\Delta E_{\mathrm{F-CBM}}$ /eV**
This study	Linear extrapolation	0.35 ± 0.23	0.04 ± 0.32	-0.02
	Eq. 1 (17.76 ± 0.03 eV)	0.79 ± 0.03	0.38 ± 0.03	
	Eq. 1 (17. 5 eV)	0.5	0.1	
	Eq. 1 (17. 29 eV)	0.32	-0.09	
	Eq. 1 (17. 25 eV)	0.28	-0.13	
			[-]	
Bermudez et al. [24]	Linear extrapolation	0.4	0.3	0.07
	Eq. 1 (17.76 ± 0.03 eV)	0.66 ± 0.03*[1]	0.52 ± 0.03*[1]	
	Eq. 1 (17. 5 eV)	0.4	0.3	
			[0.46 ML]	
Lorenz et al. [26]	Linear extrapolation	0.4*[1]	–0.1	0.1
	{revised by the author}	{0.9}	{0.4}	
	Eq. 1 (17.76 ± 0.03 eV)	0.96 ± 0.03	0.46 ± 0.03	
	Eq. 1 (17. 5 eV)	0.7	0.2	
			[~0.8 ML*[2]]	
Zhang and Ptasinska [27]	Linear extrapolation	0.2	0	0.6
	Eq. 1 (17.76 ± 0.03 eV)	0.6 ± 0.03*[1]	0.4 ± 0.03*[1]	
	Eq. 1 (17. 5 eV)	0.3	0.1	
			[-]	

In this study, the effect of SPV by X-ray for XPS on the band bending was neglected. The surface photovoltage caused by the accumulation of photogenerated

carriers under X-ray irradiation decreases band bending. If we remove the effect of reduction in the band bending due to SPV by X-ray for XPS, the band bending under ambient H_2O will be larger than 0.1 eV. Therefore, the effect of SPV by X-ray for XPS on the band bending does not make any difference in the conclusion that the Fermi level was pinned at sub-surface states.

2.4 Conclusion

Band bending for GaN (0001) was investigated under UHV and ambient H_2O. The energy difference $\Delta E_{VBM\text{-}3d}$ for GaN should be between 17.36 and 17.55 eV. $\Delta E_{VBM\text{-}3d}$ = 17.5 eV, which was evaluated by bulk sensitive SXE, is recommended instead of the conventionally used 17.76 eV. With this constant, the band bending was estimated to be 0.5 eV under UHV and 0.1 eV under a relative humidity of 46%. For the latter condition, a SPV of 20 meV was observed upon Xe-lamp irradiation with a photon flux density (above a photon energy of 3.4 eV) of 1.3×10^{16} s^{-1} cm^{-2}. By re-evaluating the band bending for the previous reports using $\Delta E_{VBM\text{-}3d}$ = 17.5 eV and reported Ga 3d peak locations, it appears that the band bending for GaN (0001) after passivation of Ga dangling bonds is 0.1–0.3 eV regardless of the growth method of GaN (MOVPE or molecular beam epitaxy) or the surface preparation of GaN. Upon H_2O adsorption, Ga dangling bonds on the GaN surface are considered to be passivated with the dissociative absorption of H_2O, but sub-surface states in the vicinity of GaN (0001) surface, such as V_N or a complex defect related to O_N decorated along dislocation, may still pin the Fermi level.

REFERENCES

[1] Cheng, W. H.; Richter, M. H.; May, M. M.; Ohlmann, J.; Lackner, D.; Dimroth, F.; Hannappel, T.; Atwater, H. A.; Lewerenz, H.J. Monolithic Photoelectrochemical Device for Direct Water Splitting with 19% Efficiency. *ACS Energy Lett*. **2018,** *3,* 1795-1800.

[2] Verlage, E.; Hu, S.; Liu, R.; Jones, R. J. R.; Sun, K.; Xiang, C.; Lewis, N. S.; Atwater, H. A. A monolithically integrated, intrinsically safe, 10% efficient, solar-driven water-splitting system based on active, stable earth-abundant electrocatalysts in conjunction with tandem III–V light absorbers protected by amorphous TiO_2 films. *Energy Environ. Sci*. **2015,** *8,* 3166-3172.

[3] Pihosh, Y.; Turkevych, I.; Mawatari, K.; Uemura, J.; Kazoe, Y.; Kosar, S.; Makita, K.; Sugaya, T.; Matsui, T.; Fujita, D. et al. Photocatalytic generation of hydrogen by core-shell WO_3/$BiVO_4$ nanorods with ultimate water splitting efficiency. *Sci. Rep*. **2015,** *5,* 11141.

[4] Kim, J. H.; Jang, J. W.; Jo, Y. H.; Abdi, F. F.; Lee, Y. H.; Van de Krol, R.; Lee, J. S. Hetero-type dual photoanodes for unbiased solar water splitting with extended light harvesting, *Nat. Commun*. **2016,** *7,* 13380.

[5] Liu, J.; Liu, Y.; Liu, N.; Han, Y.; Zhang, X.; Huang, H.; Lifshitz, Y.; Lee, S. T.; Zhong, J.; Kang, Z. Metal-free efficient photocatalyst for stable visible water splitting via a two-electron pathway. *Science* **2015,** *347,* 970-974.

[6] Wang, Q.; Hisatomi, T.; Suzuki, Y.; Pan, Z.; Seo, J.; Katayama, M.; Minegishi, T.; Nishiyama, H.; Takata, T.; Seki, K. et al. Particulate Photocatalyst Sheets Based on Carbon Conductor Layer for Efficient Z-Scheme Pure-Water Splitting at Ambient Pressure. *J. Am. Chem. Soc*. **2017,** *139,* 1675-1683.

[7] Bard, A. J.; Bocarsly, A. B.; Fan, F. R. F.; Walton, E. G.; Wrighton, M. S.; The concept of Fermi level pinning at semiconductor/liquid junctions. Consequences for

energy conversion efficiency and selection of useful solution redox couples in solar devices. *J. Am. Chem. Soc.* **1980,** *102,* 3671-3677.

[8] Gerischer, H. The role of semiconductor structure and surface properties in photoelectrochemical processes. *J. Electroanal. Chem.* **1983,** *150,* 553-569.

[9] Kibria, M. G.; Mi, Z. Artificial photosynthesis using metal/nonmetal-nitride semiconductors: current status, prospects, and challenges. *J. Mater. Chem. A* **2016,** *4,* 2801-2820.

[10] Alotaibi, B.; Nguyen, H. P. T.; Zhao, S.; Kibria, M. G.; Fan, S.; Mi, Z. Highly Stable Photoelectrochemical Water Splitting and Hydrogen Generation Using a Double-Band InGaN/GaN Core/Shell Nanowire Photoanode. *Nano Lett.* **2013,** *13,* 4356-4361.

[11] Jung, H. S.; Hong, Y. J.; Li, Y.; Cho, J.; Kim, Y. J.; Yi, G. C. Photocatalysis Using GaN Nanowires. *ACS Nano* **2008,** *2,* 637-642.

[12] Yamakata, A.; Yoshida, M.; Kubota, J.; Osawa, M.; Domen, K. Potential-Dependent Recombination Kinetics of Photogenerated Electrons in n- and p-Type GaN Photoelectrodes Studied by Time-Resolved IR Absorption Spectroscopy. *J. Am. Chem. Soc.* **2011,** *133,* 11351-11357.

[13] Jiang, C.; Moniz, S. J. A.; Wang, A.; Zhang, T.; Tang, J. Photoelectrochemical devices for solar water splitting – materials and challenges. *Chem. Soc. Rev.* **2017,** *46,* 4645-4660.

[14] Howgate, J.; Schoell, S. J.; Hoeb, M.; Steins, W.; Baur, B.; Hertrich, S.; Nickel, B.; Sharp, I. D.; Stutzmann, M.; Eickhoff, M. Photocatalytic Cleavage of Self-Assembled Organic Monolayers by UV‐Induced Charge Transfer from GaN Substrates. *Adv. Mater.* **2010,** *22,* 2632-2636.

[15] Wang, D.; Pierre, A.; Kibria, M. G.; Cui, K.; Han, X.; Bevan, K. H.; Guo, H.; Paradis, S.; Hakima, A. R.; Mi, Z. Wafer-Level Photocatalytic Water Splitting on GaN Nanowire Arrays Grown by Molecular Beam Epitaxy. *Nano Lett.* **2011,** *11,* 2353-2357.

[16] Yotsuhashi, S.; Deguchi, M.; Zenitani, Y.; Hinogami, R.; Hashiba, H.; Yamada, Y.; Ohkawa, K. Photo-induced CO_2 Reduction with GaN Electrode in Aqueous System. *Appl. Phys. Express* **2011,** *4,* 117101.

[17] Schäfer, S.; Wyrzgol, A.; Caterino, R.; Jentys, A.; Schoell, S. J.; Hävecker, M.; Knop-Gericke, A.; Lercher, J. A.; Sharp I. D.; Stutzmann, M. Platinum Nanoparticles on Gallium Nitride Surfaces: Effect of Semiconductor Doping on Nanoparticle Reactivity. *J. Am. Chem. Soc.* **2012,** *134*, 12528-12535.

[18] Kibria, M. G.; Nguyen, H. P. T.; Cui, K.; Zhao, S.; Liu, D.; Guo, H.; Trudeau, M. L.; Paradis, S.; Hakima, A. R.; Mi, Z. One-Step Overall Water Splitting under Visible Light Using Multiband InGaN/GaN Nanowire Heterostructures. *ACS Nano* **2013,** *7,* 7886-7893.

[19] Sachsenhauser, M.; Sharp, I. D.; Stutzmann, M.; Garrido, J. A. Surface State Mediated Electron Transfer Across the N-Type SiC/Electrolyte Interface. *J. Phys. Chem. C* **2016,** *120,* 6524-6533.

[20] Winnerl, A.; Garrido, J. A.; Stutzmann, M. GaN surface states investigated by electrochemical studies. *Appl. Phys. Lett.* **2017,** *110,* 101602.

[21] Winnerl, A.; Pereira, R. N.; Stutzmann, M. Kinetics of optically excited charge carriers at the GaN surface: Influence of growth technique, doping and polarity. *J. Appl. Phys.* **2015,** *118,* 155704.

[22] Chen, Y. W.; Kuo, J. L. Density Functional Study of the First Wetting Layer on the GaN (0001) Surface. *J. Phys. Chem. C* **2013,** *117,* 8774-8783.

[23] Sato, M.; Imazeki, Y.; Fujii, K.; Nakano, Y.; Sugiyama, M. First-principles modeling of GaN (0001)/water interface: Effect of surface charging. *J. Chem. Phys.* **2019,** *150,* 154703.

[24] Bermudez, V.M.; Long, J.P. Chemisorption of H_2O on GaN (0001). *Surface Science* **2000,** *450,* 98-105.

[25] Gutt, R.; Lorenz, P.; Tonisch, K.; Himmerlich, M. Electronic structure of GaN (0001)-2 × 2 thin films grown by PAMBE. *phys. stat. sol. (RRL)* **2008,** *2,* 212-214.

[26] Lorenz, P.; Gutt, R.; Haensel, T.; Himmerlich, M.; Schaefer, J. A.; Krischok, S. Interaction of GaN (0001) - 2 × 2 surfaces with H_2O. *phys. stat. sol. (c)* **2010,** *7,* 169-172.

[27] Zhang, X.; Ptasinska, S. Electronic and chemical structure of the H_2O/GaN (0001) interface under ambient conditions. *Sci. Rep.* **2016,** *6,* 24848.

[28] Waldrop, J.R.; Grant, R.W. Measurement of AlN/GaN (0001) heterojunction band offsets by x - ray photoemission spectroscopy. *Appl. Phys. Lett.* **1996,** *68,* 2879.

[29] Bloom, S.; Harbek, G.; Meier, E.; Ortenburge, I. B. Band Structure and Reflectivity of GaN. *phys. stat. sol. (b)* **1974,** *66,* 161-168.

[30] Bermudez, V.M. The fundamental surface science of wurtzite gallium nitride. *Surface Science Reports* **2017,** *72,* 147-315.

[31] Huang, Z.; Wu, Y.; Zhao, Y.; Shi, L.; Huang, R.; Li, F.; Liu, T.; Xu, L.; Gao, H.; Zhou, Y. et al. Accurate surface band bending determination on Ga-polar n-type GaN films by fitting x-ray valence band photoemission spectrum. *AIP Advances* **2019,** *9,* 115106.

[32] Magnuson, M.; Mattesini, M.; Höglund, C.; Birch, J.; Hultman, L. Electronic structure of GaN and Ga investigated by soft x-ray spectroscopy and first-principles methods. *Phys. Rev. B* **2010,** *81,* 085125.

[33] Katsikini, M.; Paloura, E. C.; Fieber-Erdmann, M.; Kalomiros, J.; Moustakas, T. D.; Amano, H.; Akasaki, I. N *K*-edge x-ray-absorption study of heteroepitaxial GaN films. *Phys. Rev. B* **1997,** *56,* 13380.

[34] Tröger, L.; Arvanitis, D.; Rabus, H.; Wenzel, L.; Baberschke, K. Comparative study of fluorescence- and electron-yield detection on $YB_2Cu_3O_{7-\delta}$ at the O *K* edge through x-ray absorption. *Phys. Rev. B* **1990,** *41,* 7297.

[35] Tröger, L.; Yokoyama, T.; Arvanitis, D.; Lederer, T.; Tischer, M.; Baberschke, K. Determination of bond lengths, atomic mean-square relative displacements, and local thermal expansion by means of soft-x-ray photoabsorption. *Phys. Rev. B* **1994,** *49,* 888.

[36] Koitaya, T.; Yamamoto, S.; Shiozawa, Y.; Takeuchi, K.; Liu, R.-Y.; Mukai, K.; Yoshimoto, S.; Akikubo, K.; Matsuda, I.; Yoshinobu, J. Real-time observation of reaction processes of CO_2 on Cu(997) by ambient-pressure X-ray photoelectron spectroscopy. *Top. Catal.* **2016,** *59,* 526-531.

[37] Koitaya, T.; Yamamoto, S.; Matsuda, I.; Yoshinobu, J. Surface Chemistry of Carbon Dioxide on Copper Model Catalysts Studied by Ambient-Pressure X-ray Photoelectron Spectroscopy. *J. E-journal Surf. Sci. Nanotechnol.* **2019,** *17,* 169-178.

[38] Yamamoto, S.; Senba, Y.; Tanaka, T.; Ohashi, H.; Hirono, T.; Kimura, H.; Fujisawa, M.; Miyawaki, J.; Harasawa, A.; Seike T. et al. New soft X-ray beamline BL07LSU at SPring-8. *J. Synchrotron Rad.* **2014,** *21,* 352-365.

[39] Yamamoto, S.; Kendelewicz, T.; Newberg, J. T.; Ketteler, G.; Starr, D. E.; Mysak, E. R.; Andersson, K. J.; Ogasawara, H.; Bluhm, H.; Salmeron, M. et al. Water Adsorption on α-Fe_2O_3(0001) at near Ambient Conditions. *J. Phys. Chem. C* **2010,** *114,* 2256-2266.

[40] Rinke, P.; Winkelnkemper, M.; Qteish, A.; Bimberg, D.; Neugebauer, J.; Scheffler, M. Consistent set of band parameters for the group-III nitrides AlN, GaN, and InN. *Phys. Rev. B* **2008,** *77,* 075202.

[41] Strite, S.; Morkoç, H. GaN, AlN, and InN: A review. *J. Vac. Sci. Technol. B* **1992,** *10,* 1237-1266.

[42] Kočan, M.; Rizzi, A.; Lüth, H.; Keller, S.; Mishra, U.K. Surface Potential at as-Grown GaN(0001) MBE Layers. *phys. stat. sol. (b)* **2002,** *234,* 773-777.

[43] Van de Walle, C. G.; Segev, D. Microscopic origins of surface states on nitride surfaces. *J. Appl. Phys.* **2007,** *101,* 081704.

[44] Sato, M.; Imazeki, Y.; Takeda, T.; Kobayashi, M.; Yamamoto, S.; Matsuda, I.; Yoshinobu, J.; Nakano, Y.; Sugiyama, M. Atomistic-Level Description of GaN/Water Interface by a Combined Spectroscopic and First-Principles Computational Approach. *J. Phys. Chem. C* **2020,** *124,* 12466-12475.

[45] Chin, V. W. L.; T. Tansley, L.; Osotchan¸ T. Electron mobilities in gallium, indium, and aluminum nitrides. *J. Appl. Phys.* **1994,** *75,* 7365.

[46] Fang, Z-Q.; Look, D. C.; Kim, W.; Fan, Z.; Botchkarev, A.; Morkoc¸ H. Deep centers in n-GaN grown by reactive molecular beam epitaxy. *Appl. Phys. Lett.* **1998,** *72,* 2277-2279.

[47] Lyons, J. L.; Van de Walle, C.G. Computationally predicted energies and properties of defects in GaN. *npj Comput. Mater.* **2017,** *3,* 12.

[48] Soh, C. B.; Chua, S. J.; Lim, H. F.; Chi, D. Z.; Tripathy, S.; Liu, W. Assignment of deep levels causing yellow luminescence in GaN. *J. Appl. Phys.* **2004,** *96,* 1341-1347.

[49] Polenta, L.; Castaldini, A.; Cavallini A. Defect characterization in GaN: Possible influence of dislocations in the yellow-band features. *J. Appl. Phys.* **2007,** *102,* 063702.

[50] Koleske, D.D.; Wickenden, A.E.; Henry, R.L.; DeSisto, W.J.; Gorman, R.J. Growth model for GaN with comparison to structural, optical, and electrical properties. *J. Appl. Phys.* **1998,** *84,* 1998-2010.

[51] Fernández-Garrido, S.; Koblmüller, G.; Calleja, E.; Speck, J.S. In situ GaN decomposition analysis by quadrupole mass spectrometry and reflection high-energy electron diffraction. *J. Appl. Phys.* **2008,** *104,* 033541.

[52] Chung, B-C.; Gershenzon, M. The influence of oxygen on the electrical and optical properties of GaN crystals grown by metalorganic vapor phase epitaxy. *J. Appl. Phys.* **1992,** *72,* 651-659.

Chapter 3 Evaluation method for band bending at n-GaN/electrolyte interface

The band alignment at the interface between an electrolyte and n-GaN photoanode was investigated by observing open-circuit potential (OCP) of the GaN as a function of irradiated Xe-lamp intensity. The OCP drifted to negative values almost linearly with respect to the logarithm of light intensity, similarly to the behavior of open-circuit voltage in solar cells. For the smaller light intensity than 10^{-2} mW/cm2, OCP value was less dependent on light intensity and it was sensitive to both the surface treatment of GaN and the surface damage which was introduced intentionally prior to the photoelectrochemical analysis by the irradiation of accelerated Ar atoms, high-energy electrons, and γ-ray. The relationship between OCP and light intensity can be obtained without modifying the surface by photocurrent and it would be a good indicator how the surface treatment of a photoelectrode affects the photocatalytic activity.

3.1 Introduction

For semiconductor photoelectrochemistry to split water upon sunlight irradiation, alignment of semiconductor band edges with respect to redox potentials for the evolution of hydrogen and oxygen from water is of crucial importance.[1] Two essential factors are involved in the alignment: 1) the position of semiconductor band edges with respect to the standard electrode potential and 2) the band bending inside the depletion region of the semiconductor adjacent to an electrolyte.[2] Both of these are related to the atomistic nature at the semiconductor/electrolyte interface: the former is affected by the electrical double layer at the interface[3] and the latter is determined by the energy level of mid-gap states originating from the chemical bonds of the semiconductor exposed to the electrolyte.[4] These may be affected by a lot of factors such as pH of the electrolyte,[5]

the existence of an oxidized layer[6] and/or atomistic disorder on the semiconductor surface, and crystal defects inside the semiconductor. Due to such complexity, it is not straightforward to characterize the band alignment at the interface.

Mott-Schottky plot by measuring the capacitance of the depletion layer at the surface vicinity of a semiconductor photoelectrode under the externally-applied DC bias is widely used for analyzing the position of semiconductor band edges with respect to the standard electrode potential.[7] If we obtained Mott-Schottky plot under light irradiation, we would be able to know how band edges are aligned at the semiconductor/electrolyte interface corresponding to the operation environment as a photocatalyst. For a photoanode, however, photocurrent under a reverse bias can lead to surface corrosion, and the analysis of the band alignment simultaneously damages the surface. [8,9] We here propose a non-destructive method for clarifying such band alignment at the semiconductor/electrolyte interface: measurement of circuit potential (OCP) under light irradiation. Under open-circuit condition, almost no anodic current exists even under light irradiation and the surface can be almost free from corrosion. From a viewpoint of physics, OCP of a semiconductor photoanode corresponds to the quasi-Fermi level of electrons. OCP should move to the negative direction with increased light intensity incident on its surface. For an ideal situation like a Schottky junction between a metal and a semiconductor, the relationship between OCP and the logarithm of light intensity will follow a linear relationship owing to the accumulation of photo-generated carriers inside the semiconductor and the resultant reduction of band bending, approaching a situation with nearly flat band under a sufficiently-large light intensity.[10] Defects in a semiconductor facilitates the recombination of photo-generated carriers and will prevent such a drift of OCP to the negative direction. Furthermore, the metal/semiconductor interface tends to be accompanied by a lot of mid-gap states and lock the quasi-Fermi level at the energy of interfacial states regardless of the intensity of irradiated light: a

phenomenon known as Fermi-level pinning. For the interface between an electrolyte and a semiconductor photoelectrode, we can expect a similar behavior of the quasi-Fermi level, i.e., OCP, with respect to the intensity of irradiated light. In other words, the relationship between OCP and light intensity will provide us an insight on how ideal a semiconductor photoelectrode is, or how the defects in both bulk semiconductor and the electrolyte/semiconductor interface affect the accumulation of photo-generated carriers and the resultant energy of the quasi-Fermi level.

As a proof of concept for such analysis of OCP under light irradiation, we have chosen n-type GaN photoanode because epitaxial GaN layer has relatively high crystal quality and is stable in electrolytes for photoelectrochemical experiments. [11-14] Starting from such ideal photoelectrode, we tried to damage it by the irradiation of high-energy particles such as Ar atoms, electrons and photons (γ-ray). Through the observation of OCP behavior under light irradiation for such intentionally damaged GaN photoelectrodes, we aimed at clarifying the sensitivity of OCP on the defects and interfacial non-idealities of semiconductor photoelectrodes.

3.2 Method

3.2.1 Sample preparation and experiment

N-type GaN epitaxial layers were prepared on sapphire substrates by metalorganic vapor-phase epitaxy (MOVPE). The layers were doped by Si at a carrier density of 1.6×10^{17} cm^{-3}. Some GaN layers were bombarded with high-energy particles to introduce damages. For the irradiation of Ar atoms, Ar^{+} ions are accelerated at 1 kV and then introduced to a conductive aperture. The ions are neutralized and irradiated to the surface of GaN in vacuum at room temperature for 3 min. For the irradiation of high-energy electrons, they were accelerated at 1 MV and irradiated to the surface of GaN with 10^{15}

cm^{-2} dose in the atmosphere at room temperature. For the irradiation of γ-ray, they were emitted from ^{60}Co and irradiated to the surface of GaN with 1 MGy (for SiO_2) in N_2 ambient at room temperature. These particles are expected to generate different defects in the GaN layer. The beam of Ar atoms is attenuated in the surface vicinity of GaN and it will generate defects on the surface. In contrast, high-energy electrons and γ-ray will penetrate to the depth of GaN layer due to relatively weak interaction with the atoms composing the layer. Especially, γ-ray will generate defects almost uniformly in the GaN bulk rather than electrons.

3.2.2 Evaluation method for band bending

As-grown GaN layers and those irradiated with Ar atoms, electrons and γ-ray were processed into photoelectrodes using epoxy-resin. A photoelectrode was put in a pH=14

electrolyte with NaOH. Before the OCP measurement, the surface of the as-grown GaN electrode was reduced in an electrolyte by applying cathodic current with static potential mode at -1.6 V vs. Ag/AgCl or with cyclic voltammetry mode from -1.5 V to 0 V vs. Ag/AgCl. The surface of the damaged GaN surface was reduced in an electrolyte by cathodic current with static potential mode at -1.6V vs. Ag/AgCl. The light from a Xe lamp was irradiated onto the surface of the photoelectrode. The intensity was adjusted from 10^{-5} to 10^{2} mW/cm^2 using neutral density filters. Under the light irradiation, OCP of the photoelectrode was measured with respect to an Ag/AgCl reference electrode, which potential is +0.2 V with respect to Normal Hydrogen Electrode (NHE).

3.3 Results and discussion

3.3.1 OCP behavior with varied light intensity for an GaN photoelectrode

As shown in Fig. 3.1, there is almost no hysteresis in the behavior of OCP versus the light intensity irradiated on the surface of GaN photoelectrode, indicating that the surface of the electrode hardly changed during the analysis. This is the merit of analyzing OCP with no photocurrent, as expected. OCP with respect to an Ag/AgCl reference electrode moved to the negative direction almost linearly with the logarithm of light intensity above a light intensity 10^{-2} mW/cm^2, until it reached flat-band potential (FBP) at a light intensity of 10^{2} mW/cm^2. Here, the FBP value of -1.4 V was obtained from the Mott-Schottky plot under dark in a different experiment. Below an intensity of 10^{-2} mW/cm^2, OCP stayed at approximately 0.9 eV below FBP. Such a behavior is similar to so-called "Fermi-level pinning." This tendency indicates that the quantum states would exist at ca. 0.9 eV below the conduction band edge and these states pinned the quasi-Fermi level of GaN in the weak light intensity regime. The origin of such mid-gap pinning states would be an oxidized layer on the surface of GaN and/or the dangling bonds on the GaN surface facing to the molecules in an electrolyte. It is clear that the quasi-Fermi level of electrons exceeded the redox potential of H_2 evolution, i.e., water splitting becomes possible, when the light intensity exceeded ca. 1 mW/cm^2. Figure 3.2 depicts the change of band lineup at the electrolyte/n-GaN interface under light irradiation. If irradiated light is weaker than a threshold, most of the photo-generated carriers will recombine via the mid-gap states in the surface vicinity and carriers will not accumulate in spite of the increased light intensity. Therefore, the independence of OCP from light intensity would indicate the existence of non-negligible interfacial states.

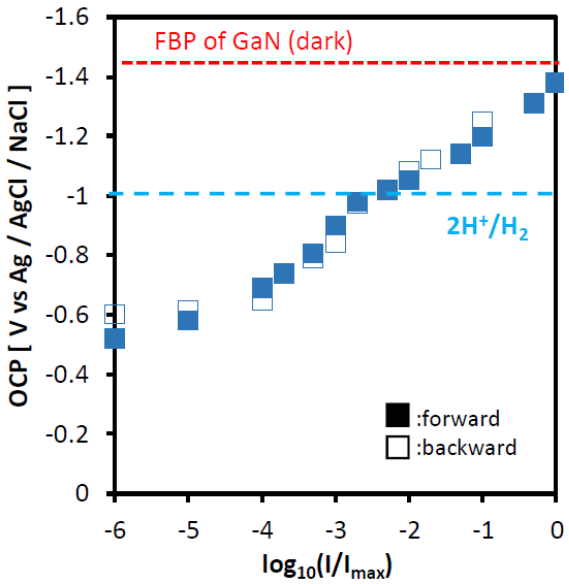

Figure 3.1 Open-circuit potential (OCP) of n-type GaN photoanode as a function of the light intensity of a Xe lamp with *I*max=0.1 W/cm² in a NaOH solution with pH=14. The light intensity was varied in the ascending direction (filled symbols) and then it was changed to the descending direction (open symbols). The standard electrode potential of the reaction $2H^+ + 2e^- = H_2$ (1) at this pH and the flat-band potential of the n-type GaN electrode under dark condition are shown as references.

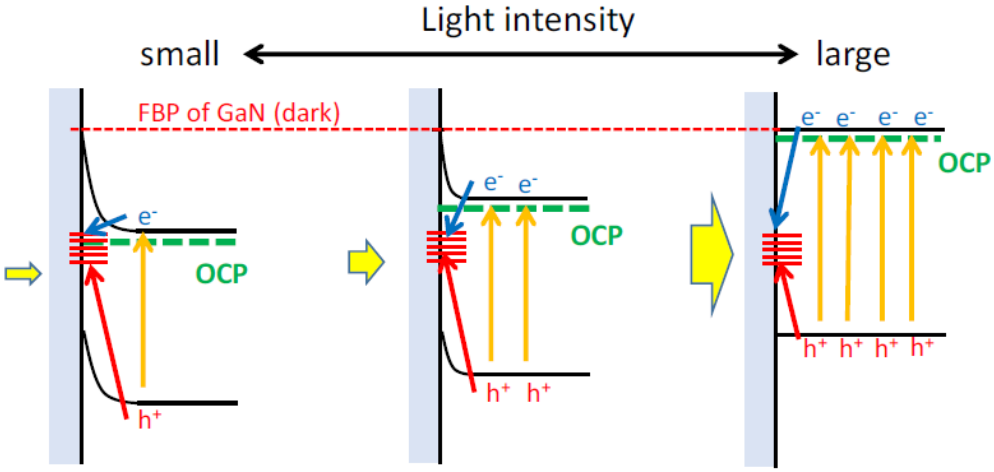

Figure 3.2 Supposed band lineup of n-type GaN photoanode under small, medium, and large light intensity. The lines at the semiconductor/electrolyte interface indicates the quantum states originating from the imperfection such as the surface dangling bonds and the defects of GaN. Arrows to the lines indicate the recombination of photogenerated carriers.

3.3.2 OCP behavior for the GaN photoelectrode with the damaged surface

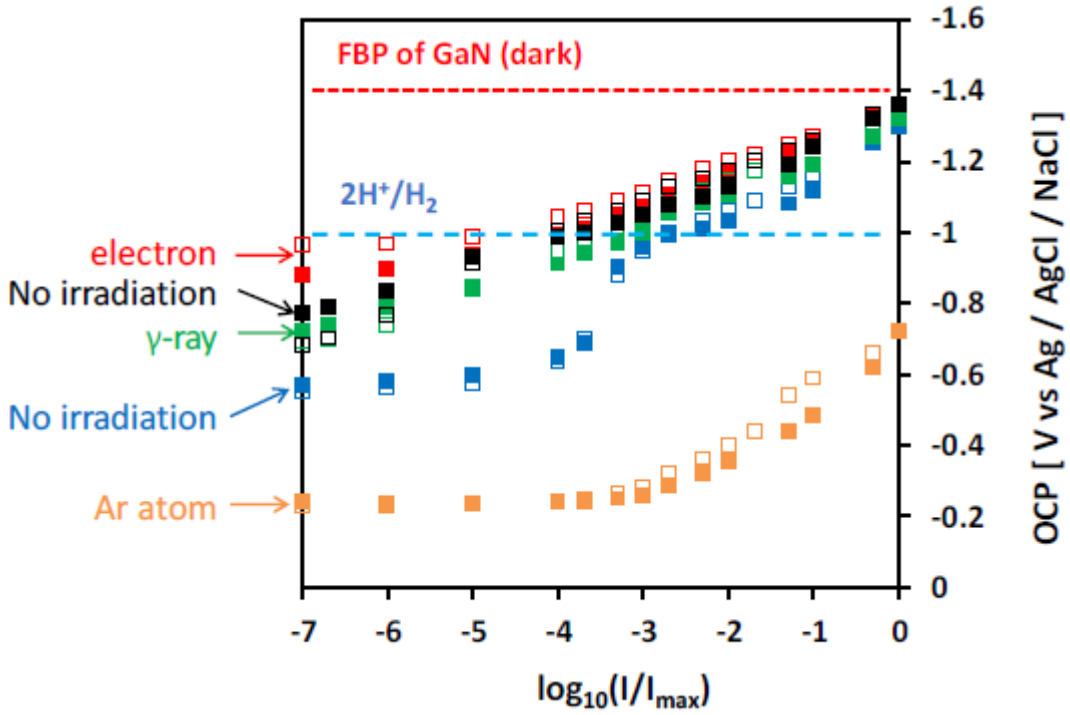

Figure 3.3 Open-circuit potential (OCP) versus light intensity plot for a variety of n-type GaN irradiated with high-energy particles: electrons, γ-ray and Ar atoms. The correspondence between such treatment for damaging GaN and each data series is indicated at the left-hand side of the plot. There are two data series for the GaN without irradiation. The different behavior, especially the difference in OCP value at the lowest light intensity, is attributed to the initial treatment of GaN surface in the electrolyte prior to light irradiation.

In order to investigate the impact of defect states in GaN on the OCP dependence of light intensity, the surface of the n-GaN electrodes was damaged with high-energy electrons, γ-ray and accelerated Ar atoms. Such treatments changed the value of OCP as shown in Figure 3.3. There are two data series for the GaN without irradiation. The different behavior, especially the difference in OCP value at the lowest light intensity, is attributed to the initial treatment of GaN surface in the electrolyte prior to light irradiation.

The behavior of OCP seems to be very sensitive to the existence of an oxidized layer and/or roughness on the surface of GaN and even a small difference in the initial surface reduction procedure would result in different surfaces of GaN. The impact of the irradiation with either high-energy electrons or γ-ray is within such a variation of the OCP behavior associated with the initial surface treatment. These irradiation treatments would generate defects in the bulk of GaN layer rather than the surface and it might be said that the bulk defects are less affective on photocatalytic activities than the surface defects. Light intensity larger than ca. 0.1 mW/cm^2 makes the OCP behavior almost similar, indicating that such a subtle difference both on the surface and in the bulk of the GaN becomes almost invisible under strong-enough light irradiation. In contrast, irradiation with accelerated Ar atoms resulted in the dramatic change in the behavior of OCP. The value under small light intensity is shifted to the positive direction and OCP is locked to that value up to a larger light intensity (ca. 0.1 mW/cm^2). This tendency indicates the existence of high-density defect states which were introduced to the GaN surface by the bombardment of high-energy and heavy Ar atoms, and the energy of these defect states are closer to the middle of the bandgap of GaN than the states associated with the oxidized layer on the GaN photoelectrode. As a result of such severe surface damage, it became difficult for the quasi-Fermi level of electrons to exceed the redox potential of hydrogen evolution, i.e., water splitting was impossible, even under strong light irradiation.

3.4 Conclusion

The dependence of OCP of a semiconductor photoelectrode on the irradiated light intensity gives us an insight on how the defects, especially those on the surface of a semiconductor, affect the photocatalytic activity. The quantum states at the electrolyte/semiconductor interface seems to be very impactful on the increase of quasi-Fermi-level splitting with light intensity, which is the driving force of photoelectrochemical reactions. A good surface modification for boosting photocatalytic activity, such as the introduction of co-catalyst and surface coating, should never lock the OCP at a certain value with an increase in light intensity. The proposed method of observing OCP under light irradiation is a concise and effective method for screening good photoelectrodes with appropriate surface modification.

REFERENCES

[1] Z. Chen, H. N. Dinh and E. Miller, Photoelectrochemical Water Splitting Standards, Experimental Methods, and Protocols, p3, Springer-Verlag, New York (2013).

[2] Abdi FF, Han L, Smets AH, Zeman M, Dam B, van de Krol R. Efficient solar water splitting by enhanced charge separation in a bismuth vanadate-silicon tandem photoelectrode. Nat Commun. 2013;4:2195.

[3] Y. Nakato, A New Method for Estimating Surface Band Energies of a Semiconductor Electrode in Contact with an Electrolyte Solution, Chem. Lett., **42**, 135 (2013).

[4] H. Gerischer, Charge transfer processes at semiconductor-electrolyte interfaces in connection with problems of catalysis, Surface Science, Volume 18, Issue 1, 1969, Pages 97-122.

[5] K. Fujii and K. Ohkawa, Photoelectrochemical Properties of p-Type GaN in Comparison with n-Type GaN, Jpn.J.Appl.Phys., **44**, L909 (2005).

[6] J. N. Chazalviel and T. B. Truong, A quantitative study of Fermi level pinning at a semiconductor-electrolyte interface, Journal of Electroanalytical Chemistry and Interfacial Electrochemistry, J. Electroanal. Chem., **114** 299 (1980).

[7] K. Fujii and K. Ohkawa, Bias-Assisted H2 Gas Generation in HCl and KOH Solutions Using n-Type GaN Photoelectrode J. EIectroehem. soc**.**, **153(3)**, A468 (2006).

[8] P. Allongue, H. Cachet, M. Froment, R. Tenne, On the kinetics of charge transfer between an illuminated CdSe electrode and polysulphide electrolyte, Journal of Electroanalytical Chemistry and Interfacial Electrochemistry, Volume 269, Issue 2, 1989, Pages 295-304.

[9] K. Fujii, and K. Ohkawa, Hydrogen generation from aqueous water using n-GaN by photoassisted electrolysis, Phys. stat. sol. (c), **3**, 2270 (2006).

[10] M. J. Kerr and A. Cuevas, Generalized analysis of quasi-steady-state and transient decay open circuit voltage measurements, J. Appl. Phys., **91(1)**, 399 (2002).

[11] I. M. Huygens, K. Strubbe and W. P. Gomes, Electrochemistry and Photoetching of n-GaN , J. Electrochem. Soc., **147**, 1797 (2000).

[12] L. H. Peng, C. W. Chuang, J. K. Ho, C. N. Huang and C. Y. Chen, Deep ultraviolet enhanced wet chemical etching of gallium nitride, Appl. Phys. Lett.,**72**, 939 (1998).

[13] C. H. Ko, Y. K. Su, S. J. Chang, W. H. Lan, J. Webb, M. C. Tu and Y. T. Cherng, Photo-enhanced chemical wet etching of GaN, Mater. Sci. & Eng. B, **96**, 43 (2002).

[14] J. A. Grenko, C. L. Reynolds, R. Schlesser, K. Bachmann, Z. Rietmeier, R. F. Davis and Z. Sitar, Selective Etching of GaN from AlGaN/GaN and AlN/GaN

Structures, MRS Internet J. Nitride Semicond., **9**, 5 (2004).

Chapter 4 Surface states and band bending at n-GaN/1M NaOH interface

To clarify the effect of surface states on the band alignment at a semiconductor/electrolyte interface, light-induced drift of open-circuit potential (OCP) for an n-GaN was analyzed under photoanode operation in NaOH (pH=14). Below the threshold, OCP seemed affected by carrier recombination via the defect states in the surface vicinity of GaN. When the surface of n-GaN was treated with Ar plasma, the impact of the defect states became more dominant and OCP almost stayed at the dark value for a wide range of photon flux, and the OCP hardly exceeded the redox potential for hydrogen evolution even under strong light irradiation. Based on the analysis, the surface state derived from $V_{Ga}O_N$ is considered to be the origin of the Fermi level pinning at n-GaN/1M NaOH interface. Furthermore, although theoretical calculation in previous reports have quantitatively shown that a surface states density of 10^{13} cm^{-2} is required for complete Fermi level pinning to occur , our measurement revealed that the Fermi level is pinned at the surface state with a density of less than 10^{12} cm^{-2}. Light-induced drift in OCP will provide us the band alignment at the semiconductor/electrolyte interface on photoelectrochemistry.

4.1 Introduction

After the development of the first photoelectrochemical water splitting [1], the modification of semiconductor surfaces using electrocatalysts [2,3] and protective layers [4,5] is now being carried out to increase the efficiency and the lifetime.To optimize their materials and structures toward the highest efficiency and the longest life time, both the mechanism and kinetics of carrier transport at the interface between a semiconductor and an electrolyte should be understood.

Some reports suggested that the surface state, stemming from dangling bonds or adsorbed molecules on the surface of a semiconductor, mediated the interfacial carrier transport.[6-11] Also, other reports suggested that surface states function as recombination centers or traps[12-17] for photo-generated carriers. Surface states influence on band alignment by Fermi level pinning:[18-20] Fermi level is fixed at the energy level of surface states regardless of the free energy in the medium adjacent to a semiconductor, such as a metal or an electrolyte. The pinning is caused by capturing electrons at high density surface states. Since the pinning affects the band bending, it has a significant impact on the interfacial charge transfer and the progress of water splitting reaction. However, experimental evaluation on the impact of surface states is still difficult. One of methods for evaluation is impedance spectroscopy.[21-25] Although this technique clarifies the surface states distribution and the band edge potential, equivalent circuit model includes some uncertainty especially for the semiconductor/electrolyte interface. Also, the technique can be utilized under illumination.[23-25] However, applied bias voltage should be restricted to protect the surface of photoelectrodes from photocorrosion during measurement.[25] In addition, it is uncertain whether the Fermi level is pinned at the surface states evaluated by Impedance spectroscopy only. Recently, operand X-ray photoelectron spectroscopy has been used.[26-28] Lichterman et al. reported the band alignment at TiO_2/KOH interface using this technique.[28] However, the result was easily affected by the evaporation of the thin-film electrolyte on the semiconductor surface and by the limited conductivity of the electrolyte due to bubbles formed by electrochemical reaction.

In this work, the band alignment at semiconductor/electrolyte interface was evaluated by open-circuit potential (OCP) measurement under illumination [29] and impedance analysis to evaluate the effect of surface states. In Section 3, we discussed the behavior of OCP in n-GaN. Under dark and weak illumination, OCP, which corresponds

with the quasi-Fermi level, in n-GaN is pinned at the surface state, whereas under strong illumination, the quasi-Fermi level is free from pinning due to filling of surface states with photogenerated carriers. When defects were introduced into n-GaN by Ar atom, higher light intensity was required due to the release from pinning. This difference in light intensity is thought to be due to the difference in the density of the pinning surface states. To clarify presence of the pinning surface states, in this section, we will compare the pinning observed by this OCP with the density of surface states evaluated by impedance spectroscopy. We will further discuss the origin of the surface states, and obtain insight into the determinants of band bending. .In section 2, we clarified that Ga dangling bonds on the GaN surface are considered to be passivated with the dissociative absorption of H_2O, but sub-surface states in the vicinity of GaN(0001) surface, such as V_N or a complex defect related to O_N decorated along dislocation, may still pin the Fermi level. There is a need to clarify whether Fermi level pinning due to the sub-surface states occur in the electrolyte as well.

We try to clarify it, the impact of surface states on the band alignment will be investigated by OCP measurement under illumination and impedance spectroscopy on n-GaN with and without Ar plasma exposure.

4.2 Method

4.2.1 Sample preparation

In this research, the photoanode was (0001) n-GaN layer on a Si substrate grown by metal organic chemical vapor phase epitaxy (MOVPE), provided by NuFlare Technology. The carrier concentration of the undamaged n-GaN was approximately 4×10^{18} cm^{-3} as estimated by hall measurement. Before electrochemical measurement, to remove organic compounds on the surface, the electrode was cleaned with ultrasound in

acetone and isopropanol for 2 min, respectively. Then, it was rinsed in ultra-pure water and dried with nitrogen blow. The ohmic contact was formed on the surface of n-GaN with indium. The contact was covered with epoxy resin so that there is no electrical contact between the indium contact and an electrolyte.

In order to increase the density of surface state intentionally, the undamaged n-GaN chip was exposed to Ar plasma for 1.5 min. The capacitive coupled plasma of Ar was excited at 75 W input power and 2.0 Pa pressure. Therefore, unlike the Ar fast atom beam used for defect introduction in Section 3, no acceleration is performed, and the defects should be more concentrated near the surface.

4.2.2 Evaluation method for surface defect states

The GaN photoelectrodes were analyzed in the experimental system shown in Fig. 4.1. Each sample was fixed on an electrochemical cell made of UV-transparent quartz glass. The photoelectrode was contacted with 1 M NaOH solution (pH = 14) via a circular hole (6 mm in diameter) opened on the wall of the cell. Before the measurement, the cell was purged by 0.11 MPa Ar gas to remove the dissolved gas. All measurements were done in three-electrodes configuration with a potentiostat. A platinum wire and an Hg/HgO/1 M NaOH electrode (+0.11 V vs. standard hydrogen electrode (SHE) at 290 K) were used as counter and reference electrode, respectively.

To measure light intensity dependence of OCP, 325 nm He-Cd laser was used as a light source. The laser light was TEM multimode and the beam diameter ($1/e^2$) was 1.78 mm. The photon energy (3.82 eV) is enough to induce the intra-band transition of carriers (3.42 eV in bandgap for GaN). Laser spot size was optically expanded to 6.0 mm in diameter to cover the hole entirely. A blackout curtain was employed to define the dark

condition. The irradiated light intensity was varied from 2.9×10^{-5} to 1.6×10^{2} mW/cm^2 with ND filters. The corresponding photon flux ranged from 10^{9} to 10^{16} s^{-1} cm^{-2}.

Using this setup, light intensity dependence of OCP was measured for the n-GaN photoelectrodes in 1 M NaOH solution. Laser light at each setpoint intensity was irradiated and the value of OCP jumped from a value under the dark condition to a value under illumination. Since the OCP value showed a slight drift after the onset of light irradiation, the value after stabilization was used as the value corresponding to the light intensity. To examine the variation of OCP by physical or chemical surface modification after illumination, the light-intensity dependence of OCP was measured with both increasing and decreasing light intensity.

Impedance measurement was also conducted to obtain Mott-Schottky plot under the dark condition after the OCP measurement. DC bias voltage in impedance measurement was increased from -0.2 V to +1.1 V *vs*. reversible hydrogen electrode (RHE). At each DC bias voltages, impedance was measured by applying a small AC signal with frequencies from 2.0×10^{4} and 1.0×10^{2} Hz.

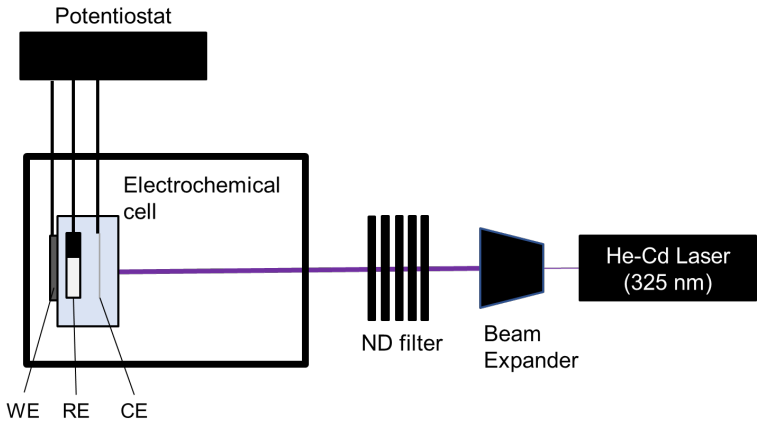

Figure 4.1 An experimental setup. The electrochemical cell was enclosed in a blackout curtain. A n-GaN working electrode (WE) was faced to 1 M NaOH solution through a window on the cell. An Hg/HgO/1 M NaOH reference (RE) and a platinum counter (CE) electrode were put on the electrolyte

in the atmosphere. Laser was irradiated to n-GaN surface through a hole in the curtain. The laser beam was expanded and attenuated outside the curtain.

4.3 Results and discussion

4.3.1 Band edge potential of n-GaN photoelectrode

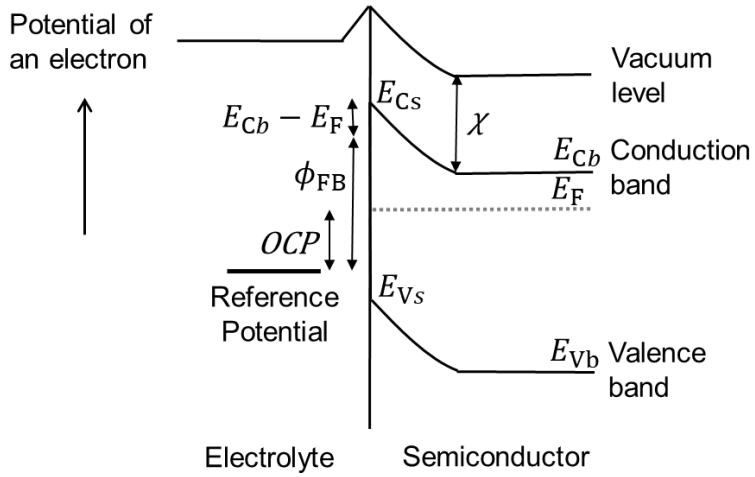

Figure 4.2 Band alignment at the surface of n-type semiconductor contacted with electrolyte. ϕ_{FB} is the flat-band potential, E_{Cs} is the conduction band edge potential at the surface, E_{Vs} is the valence band edge potential at the surface, E_{Cb} is the conduction band edge potential in the bulk, E_{Vb} is the valence band edge in the bulk, χ is electron affinity of semiconductor and E_F is the Fermi level. Band edge potential at the surface can be estimated from the flat-band potential and the potential difference between the Fermi level and the conduction band edge in the bulk. The Fermi level can be evaluated as OCP.

Fig. 4.2 summarizes the band alignment under the dark condition, which will be elucidated through electrochemical analysis for the n-GaN photoelectrode. The conduction-band-edge potential, E_{Cs}, was evaluated by Mott-Schottky plot as the inverse square of the capacitance in the surface depletion region of n-GaN, C_{int}, as a function of applied bias in Fig. 4.3a, b. Flat-band potential, ϕ_{FB}, was estimated by fitting linear region with the following relationship,[30]

$$\frac{1}{C_{int}^2} = \frac{2}{\mathrm{e}\epsilon\epsilon_0 N_\mathrm{D}}\left(\phi - \phi_\mathrm{FB} - \frac{kT}{\mathrm{e}}\right), \tag{4.1}$$

where, e is the elemental charge, ϵ is the relative permittivity of 10.4 [31], ϵ_0 is the permittivity of vacuum, N_D is the donor density, ϕ is the applied potential, k is the Boltzmann constant and T is the absolute temperature.

To obtain C_{int}, the experimental data has been fitted using the equivalent circuit models in Fig. 4.3(c) presented in the literatures [6,32]. The experimental data is represented by symbols and the lines show fits according to the Eq. (4.1). For an ideal semiconductor/electrolyte system, a linear dependence of the inverse square of the interface capacitance on the applied bias potential is expected [30]. For n-GaN without Ar plasma treatment, such a linear dependence is observed between –0.2 V and +1.1 V vs. RHE. From this linear dependence, the flat band potential is evaluated as -0.64 V vs. RHE. This value is in good agreement with previous reports [33]. The fitting according to the M-S equation evaluates the donor density N_D as 3.1×10^{19} cm^{-3}. This value deviates from the carrier concentration evaluated by Hall measurement, 4×10^{18} cm^{-3}. Such a difference has been reported and discussed in previous studies. ref. This difference affects the conduction band edge potential evaluated by the relationship,

$$E_\mathrm{Cs} = \phi_\mathrm{FB} - \frac{\mathrm{k}T}{\mathrm{e}}\ln\left(\frac{\mathrm{N_C^*}}{n}\right) \tag{4.2}$$

where, E_{Cs} is the potential of conduction band edge at the surface, $\mathrm{N_C^*}$ is the effective density of states in the conduction band and n is the net carrier concentration. Even if all donors are activated and the carrier concentration is 3.1×10^{19} cm^{-3}, the difference is insignificant, approximately 50 meV, as calculated by Eq. (4.2). The band edge potential at the surface of n-GaN without Ar plasma treatment was evaluated as -0.62 V vs. RHE with $\mathrm{N_C^*}$ calculated as 2.13×10^{18} cm^{-3} from effective mass for the

electron of 0.20 m_0 [32], where m_0 is the rest mass of the electron. Using this value and the bandgap of GaN (3.42 eV), the valence-band-edge potential E_{Vs} at the surface of an undamaged n-GaN photoelectrode is deduced to be + 2.80 V vs. RHE. Also, the vacuum level at the surface is -4.7 V vs. RHE, with the electron affinity of 4.1 eV [38].

To obtain, C_{int} (Z_{CPE}), the experimental data is fitted using the equivalent circuit models (Fig. 4.3c) presented in a previous work [6,32]. The experimental data is represented by symbols and the lines show fits according to the Mott-Schottky equation. For an ideal semiconductor/electrolyte system, a linear dependence of the inverse square of the interface capacitance on the applied bias potential is expected [30].

For n-GaN without Ar plasma treatment, a linear dependence is observed between –0.2 V and +1.1 V vs. RHE. From this linear dependence, the flat band potential is evaluated as -0.64 V vs. RHE. This value is in good agreement with previous reports [33]. Furthermore, the fitting according to the Mott-Schottky equation evaluates the donor density N_D as 3.1×10^{19} cm^{-3}. For n-GaN with Ar plasma treatment, a significant deviation of the capacitance values from the linear behavior is observed for potentials between +0.4 V and +0.7 V vs. RHE. Linear behavior was observed between -0.2 V and +0.4 V, and between +0.7 V and +1.1 V. This behavior is discussed in Fig. 4.4. When the Fermi level reaches the energy levels of the surface states, the electrons begin to occupy the empty surface states. The Fermi level is pinned at these traps. As a result, a horizontal M-S plot is observed because the capacitance of the depletion layer is independent of the potential change. The linear M-S gradient is again observed when the surface states are completely filled. Here, the charges of the acceptor-like and donor-like surface states are denoted as Q_A and Q_D, and the capacitances as C_A and C_D, respectively. The potential used to occupy all acceptor-like surface states is $-Q_A/C_A$, resulting in a shift from U_{fb} to U_{fb}'. Similarly, the potential used to completely deplete all donor-like surface state is $+Q_D/C_D$, resulting in a shift from U_{fb} to U_{fb}''.

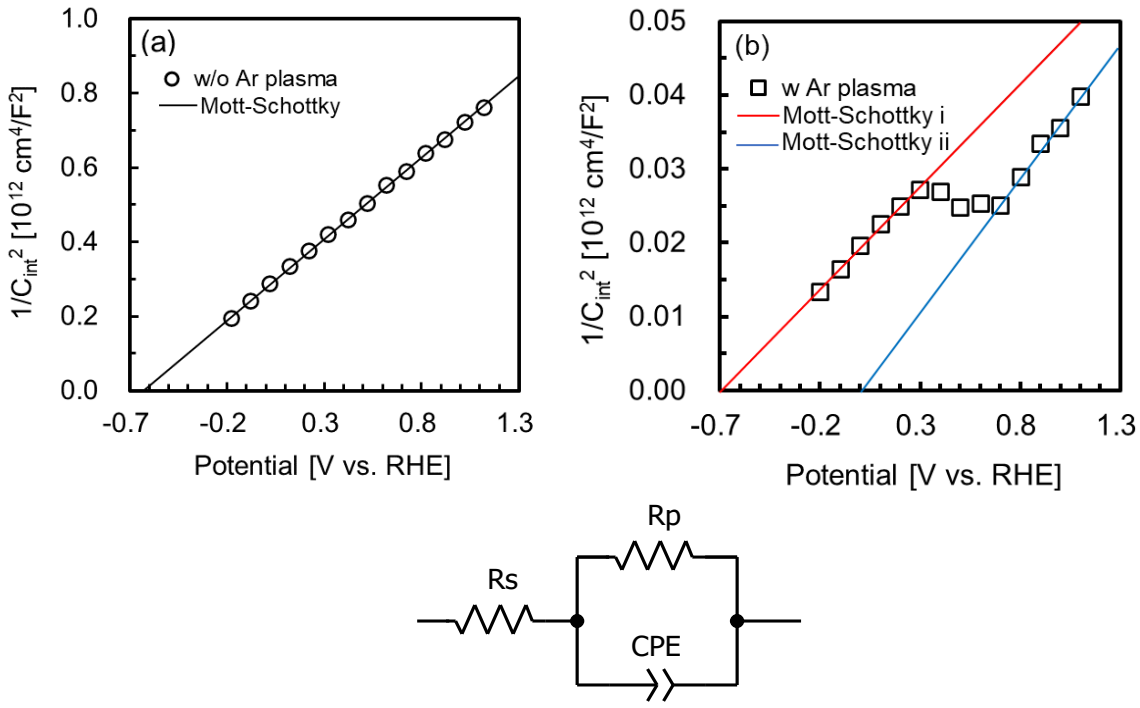

Figure 4.3 Mott-Schottky plot for an n-GaN photoelectrode (a) without and (b) with Ar plasma treatment. The capacitance was obtained from fitting impedance data at each DC bias with the equivalent circuit shown in (c). CPE and R_p are constant-phase element and resistance in the semiconductor/electrolyte interface, respectively. R_s is the series resistance including the contribution of both the electrolyte and the semiconductor. If the exponent α is whithin a slight deviation from ideality ($1.0 \geq \alpha > 0.9$), the CPE parameter Q can be interpreted as an approximation of the interface capacity C_{int}. The fitting was done in frequency range between 2.0×10^4 and 1.0×10^2 Hz. The solid line was analyzed by the M-S equation in Equation (4.1). The red and blue lines in (b) are without and with activated donor-like surface states, respectively.

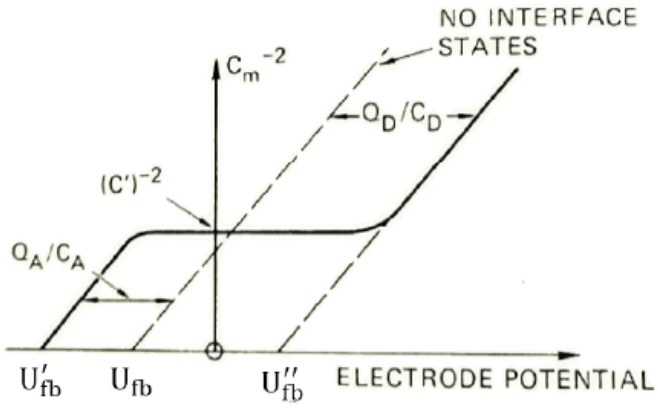

Figure 4.4 A Mott-Schottky plot of the semiconductor influenced by the charging and discharging of the surface states. [34,35]

Therefore, there is a need to clarify the Fermi level in Ar plasma treated n-GaN in order to evaluate its flat band potential. Since the Fermi level corresponds to OCP and the value was +0.8 V vs. RHE under dark condition, the blue line in Fig. 4.3(b) was analyzed by eq. (4.1). As a result, the flat band potential was 0.00 V, and the donor density was 3.8 × 10^{20} cm^{-3}. The donor density of n-GaN is increased by Ar plasma treatment due to the creation of nitrogen vacancy-related shallow donors in the near-surface region [36,37]. When the acceptor-like surface state is inactivated, the flat band potential becomes -0.69 V vs. RHE, which is close to the potential of n-GaN without Ar plasma treatment.
, which was evaluated Therefore, the conduction band edge potential was evaluated as -0.67 V vs. RHE and 0.00 V vs. RHE without and with activated acceptor-like surface states, respectively.

4.3.2 Surface states distribution

To determine the energy distribution of the surface states, the potential dependence of the interfacial capacitance can be used, as demonstrated by Sachsenhauser et al. [6] The capacitance evaluated by impedance measurement can be divided into the capacitance in the space charge region and the capacitance originating from the surface

state. Since the capacitance in the space charge region, C_{SCR}, depends on the thickness of the depletion region, it satisfies the following equation (4.3):

$$C_{SCR} = \sqrt{\frac{e\epsilon\epsilon_0 N_D}{2\left(\phi - \phi_{FB} - \frac{kT}{e}\right)}} \tag{4.3}$$

The capacitance of the surface state, C_{ss}, also depends on the accumulation of carriers in the surface states. This accumulation occurs when the Fermi level and the level of the surface state are aligned. Therefore, the capacitance derived from the surface states reaches its maximum when the Fermi level is aligned with the potential of the surface states.

Because the capacitive contribution of the surface state is frequency dependent, [39,40] it should be considered as a frequency-dependent constant phase element (CPE), Z_{CPE}, which is given by

$$Z_{CPE} = \frac{1}{Q}(i\omega)^{-\alpha} \tag{4.4}$$

where Q and α are the CPE parameters. If the exponent α is within a slight deviation from ideality ($1.0 \geq \alpha > 0.9$), the CPE parameter Q can be interpreted as an approximation of the interface capacity C_{int} .[39] As mentioned in section 4.3.1, we considered the equivalent circuit in Fig. 4.3 (c). In our measurement, since the value of α was between 1 and over 0.9 under all DC bias, therefore, Z_{CPE} was interpreted as an approximation of the interface capacitance C_{int}. Therefore, an equivalent circuit with CPE in Fig. 4.3(c) was replaced by the capacitance, C_{int}, was used for the impedance fitting.

The potential dependences of C_{int} in n-GaN with and without Ar plasma treatment are shown in Fig. 4.5a and b, respectively. Since $C_{\mathrm{int}} = C_{SCR} + C_{SS}$, C_{SS}, can be evaluated by subtracting the value of C_{SCR} calculated using eq. (4.3) and from C_{int}. For n-GaN without Ar plasma treatment, calculated value of C_{SCR} agrees with C_{int}, indicating that C_{SS} is negligible. However, for n-GaN with Ar plasma treatment, above 0.3V, there is a

discrepancy between the experimental value of C_{int} and the calculated value of C_{SCR}, indicating the presence of surface states in the bandgap of the GaN electrodes. When the Fermi level of GaN is aligned with the energy of the surface states, charge transfer occurs, and the effective surface state capacitance, C_{SS}, must be considered as well as the capacitance of the space charge region C_{SCR}.

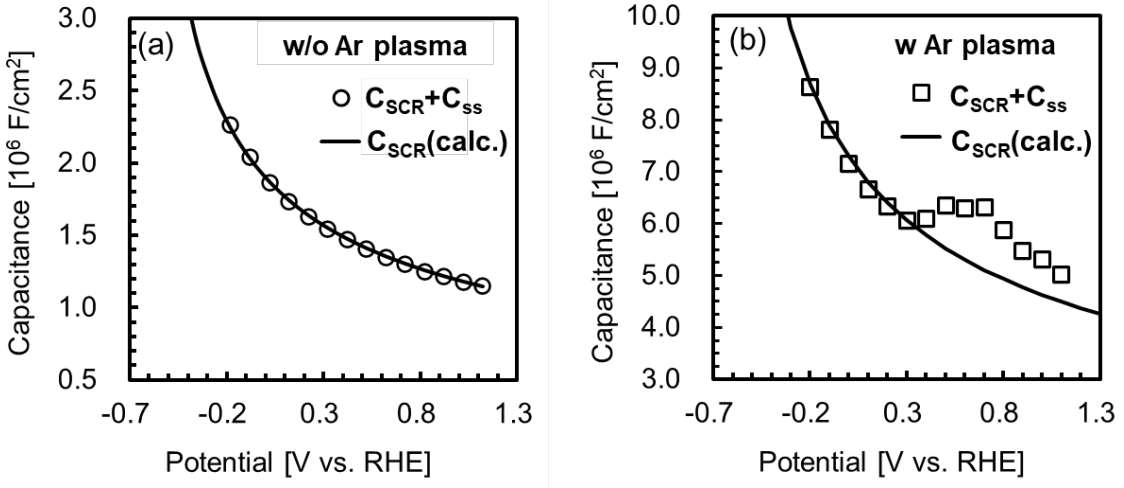

Figure 4.5 Interface capacitance, $C_{\text{int}} = C_{\text{SCR}} + C\text{ss}$, plotted with respect to the applied potential to a GaN electrode (a)without and (b) with Ar plasma treatment, respectively. The solid line is calculated C_{SCR} by eq. (4.3) with dope density, N_D, and flat band potential, ϕ_{FB}, obtained by Mott-Schottky plot (Figure. 4.4). The N_D and ϕ_{FB} were 3.1×10^{19} cm^{-3} and -0.64 V vs. RHE without Ar plasma treatment, and 4.9×10^{20} cm^{-3} and -0.69 V vs. RHE with Ar plasma treatment, respectively.

The effective density of surface states, N_{ss}, is estimated by

$$N_{ss} = \frac{C_{SS}}{e} \tag{4.5}$$

The N_{SS} values for n-GaN without and with Ar plasma treatment in 1M NaOH is shown in Figure 4.6. For the Ar plasma treated sample alone, the presence of surface states was confirmed above +0.3 V vs. RHE. The N_{SS} peak value for the surface treated

with Ar plasma was 7.4×10^{12} eV^{-1} cm^{-2}, at around 0.7 V vs. RHE. Since the band edge potential of Ar plasma treated n-GaN is 0.00 eV vs. RHE with potential shift by charged acceptor-like surface states, the surface states seem to exist at about 0.7 V from the conduction band edge. Comparing the position of this surface states with previous studies, the origin is considered to be the 2–/– level of the $V_{Ga}O_N$ complex [41]. This is consistent with the decrease in nitrogen and increase in oxygen after Ar plasma irradiation, as evidenced by XPS spectra (Appendix.B.1).

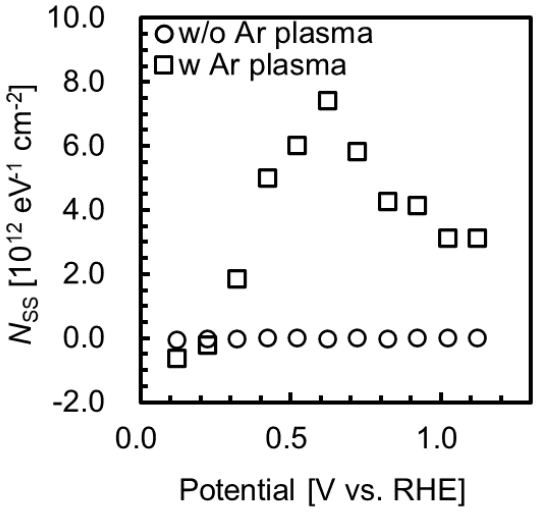

Figure 4.6 Surface states density N_{SS}, which was estimated by eq.(4.5), on GaN(0001) with (squares) and without Ar plasma treatment (circles). For n-GaN with Ar plasma treatment, the surface states above 0.3 V vs. RHE was observed.

4.3.3 Fermi level pinning observed by OCP measurement

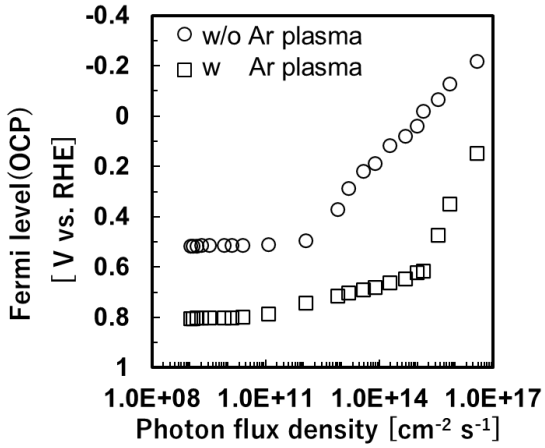

Figure 4.7 Open-Circuit potential (OCP) plotted with respect to logarithm of light intensity. The values for n-GaN with and without Ar plasma are shown as circles and squares.

(i) n-GaN without Ar plasma treatment

Since the electric contact is in equilibrium with n-GaN, OCP of n-GaN in NaOH electrolyte corresponds to E_F in Fig. 4.2 under the dark condition. The value shifted to the negative direction with increasing illumination intensity. The value of OCP is plotted in Fig. 4.7 with respect to the logarithm of illumination intensity.

For n-GaN without Ar plasma treatment, OCP was +0.51 V vs. RHE under the dark condition. The band alignment under the dark condition is deduced as in Fig. 4.8a and the band bending was 1.2 V. With increasing photon flux, OCP approached to the flat-band potential and band bending was reduced accordingly. Under the photon flux of 3.7×10^{16} s^{-1} cm^{-2}, OCP was -0.22 V vs. RHE and the band alignment is deduced as Fig. 4.8b, where the band bending became 0.8 V. Here, it is assumed that the band edge potential under illumination stays at the position under the dark condition.

Under a photon flux of $1.2 \times 10^{12}\ s^{-1}\ cm^{-2}$, the value of OCP seems to be affected significantly by the surface states as will be discussed below (section 4.3.3 (iii)). This pinning position was 1.1 V below conduction band edge. Above a photon flux of $1.2 \times 10^{12}\ s^{-1}\ cm^{-2}$, the behavior of OCP is considered to be almost free from the impact of the surface states and the accumulation of photocarriers in the depletion region of n-GaN seems to be responsible for the reduction of band bending. The linear relationship between OCP and the logarithm of light intensity is often observed for open-circuit voltage in photovoltaic cells.

(ii) n-GaN with Ar plasma treatment

For the GaN photoelectrode exposed to Ar plasma, OCP was +0.80 V *vs*. RHE, unlike the situation for the undamaged GaN under the dark condition. The band alignment under the dark condition is deduced as in Fig. 4.8c. As described in Figure 4.4, the flat band potential of Ar plasma treated n-GaN shifts to the positive direction due to activated acceptor-like surface states.Therefore, there was a difference between -0.65 V vs. RHE (without activated acceptor-like surface states) and +0.00 V (with activated acceptor-like surface states). The potential drop due to surface states and band bending were 0.67 V and 0.80 V, respectively. With increasing photon flux, OCP shifted from +0.8 to +0.6 V *vs*. RHE in a very gradual manner in the photon flux range from $10^9\ s^{-1}\ cm^{-2}$ to $10^{15}\ s^{-1}\ cm^{-2}$. This gradual shift of OCP might be caused by the pinning of Fermi level at the energy level of surface states with high density which were introduced by the exposure to Ar plasma. The origin of surface states is considered to be the 2–/– level of the $V_{Ga}O_N$ complex [41]. Surface states originating from the defects may pin the Fermi level. Above a photon flux of $10^{15}\ s^{-1}\ cm^{-2}$, OCP shifted drastically from +0.4 to +0.15 V *vs*. RHE with the increase in photon flux. In this range, the surface states due to the defects seems to be filled with photo-generated electrons and the Fermi level was free from pinning. However,

the OCP hardly exceeded the redox potential for hydrogen evolution (0 V vs. RHE) even under strong light irradiation. Under the photon flux of 3.7×10^{16} s^{-1} cm^{-2}, OCP was +0.14 V vs. RHE and the band alignment is deduced as Fig. 4.8d and the band bending was 0.8 V. The band bending was equal to the dark state. This is thought to be because the photogenerated carriers accumulated in the acceptor-like surface states and not in the depletion layer.

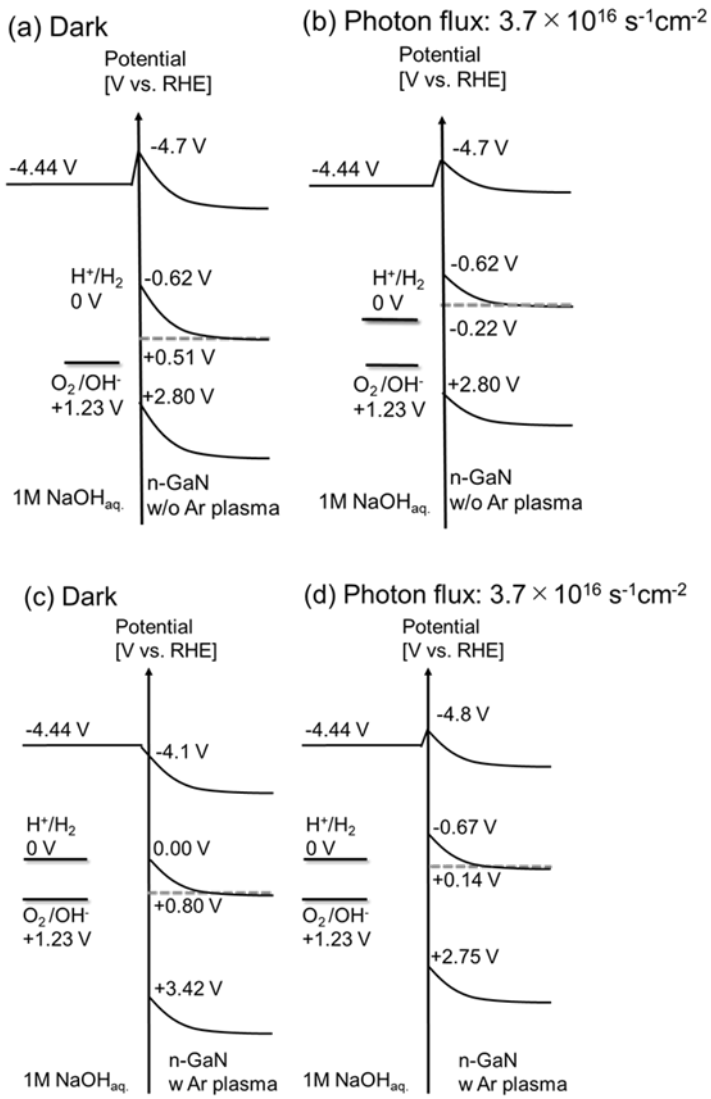

Figure 4.8 B Band alignment at the semiconductor/electrolyte interface under dark and light irradiation. (a) and (b) are for the n-GaN without Ar plasma treatment while (c) and (d) are for the n-

GaN with Ar plasma treatment. (a) and (c) are under dark while (b) and (d) are under the maximum illumination. The band edge potential is the value obtained from Mott-Schottky plot. For n-GaN with Ar plasma treatment, the potential shift by 0.67 eV due to activated acceptor-like surface states should be consideredwas observed. (a) and (b) are for the n-GaN without Ar plasma treatment while (c) and (d) are for the n-GaN with Ar plasma treatment. (a) and (c) are under dark while (b) and (d) are under the maximum illumination. Here, we used 4.44V as the difference between vacuum level and hydrogen redox.[42]

(iii) Origin of pinning in n-GaN with and without Ar plasma treatment

For the n-GaN treated by Ar plasma, the the pinning position was 0.8 V below conduction band edge CBM and surface states derived from $V_{Ga}O_N$ (discussed in section 4.3.2) are considered to be origin of pinning. For n-GaN without Ar plasma treatment, the pinning position was 1.1 V below conduction band edge. As mentioned in Section 3, for pristine n-GaN surfaces, it has been suggested that Fermi level is pinned at surface states related to V_N or O_N after water adsorption. As shown in the previous study [41], the defect states seem to originate from $V_{Ga}O_N$ are located at 1.24 eV- 2.1 eV, and it is possible that the sample without Ar plasma irradiation were also pinned to these defects.

Furthermore, although theoretical calculation in previous report [43] mentioned that quantitative considerations showed that a surface states density of 10^{13} cm^{-2} is required for complete Fermi level pinning to occur, our measurement for n-GaN without Ar plasma treatment clarified Fermi level was pinned at the surface states, the density of which is less than 10^{12} cm^{-2} as in Fig. 4.6.

The difference between the photon flux density at which Fermi level is free from pinning can be attributed to the large difference in the surface state density. The surface states function as the recombination centers for electrons and their negative contribution

to the accumulation of photo-generated carriers depends on the effective density of surface states.

4.4 Conclusion

Observation of OCP for a semiconductor photoelectrode as a function of the logarithm of irradiation light intensity provides us an insight into the behavior of photo-generated carriers in the surface vicinity of the photoelectrode. From the pinning position, the band bending with and without Ar plasma treatment were 0.8 V and 1.1 V , respectively, under dark condition. Regardless of the Ar plasma treatment, the surface state derived from $V_{Ga}O_N$ is considered to be the origin of the Fermi level pinning at n-GaN/1M NaOH interface. The difference in the flux density at which the Fermi level becomes unpinned is due to the large difference in the density of the surface states. The surface states act as electron recombination centers, and the negative contribution to the accumulation of photogenerated carriers depends on the effective density of the surface states. Furthermore, although theoretical calculation in previous reports have quantitatively shown that a surface states density of 10^{13} cm^{-2} is required for complete Fermi level pinning to occur, our measurement for the GaN without Ar plasma treatment revealed that the Fermi level is pinned at the surface state with a density of less than 10^{12} cm^{-2}. The difference in the flux density at which the Fermi level becomes unpinned is due to the large difference in the density of the surface states. The surface states act as electron recombination centers, and the negative contribution to the accumulation of photogenerated carriers depends on the effective density of the surface states. Ionic species in the electrolyte or adsorbed on the surface should terminate the electric force lines and be involved in the Fermi level pinning.

The above-mentioned behavior of photo-generated carriers and resultant dependence of OCP on irradiation light intensity was demonstrated for an n-GaN photoelectrode in NaOH electrolyte, and Ar plasma irradiation on the GaN surface was found to have detrimental impact on the accumulation of photo-generated carriers in the GaN electrode.

REFERENCES

[1] Fujishima, A.; Honda, K. Electrochemical Photolysis of Water at a Semiconductor Electrode. *Nature* **1972**, *238*, 37–38.

[2] Nellist, M. R.; Laskowski, F. A. L.; Lin, F.; Mills, T. J.; Boettcher, S. W. Semiconductor-Electrocatalyst Interfaces: Theory, Experiment, and Applications in Photoelectrochemical Water Splitting. *Acc. Chem. Res.* **2016**, *49* (4), 733–740.

[3] Kang, D.; Kim, T. W.; Kubota, S. R.; Cardiel, A. C.; Cha, H. G.; Choi, K. S. Electrochemical Synthesis of Photoelectrodes and Catalysts for Use in Solar Water Splitting. *Chem. Rev.* **2015**, *115* (23), 12839–12887.

[4] Verlage, E.; Hu, S.; Liu, R.; Jones, R. J. R.; Sun, K.; Xiang, C.; Lewis, N. S.; Atwater, H. A. A Monolithically Integrated, Intrinsically Safe, 10% Efficient, Solar-Driven Water-Splitting System Based on Active, Stable Earth-Abundant Electrocatalysts in Conjunction with Tandem III-V Light Absorbers Protected by Amorphous TiO_2films. *Energy Environ. Sci.* **2015**, *8* (11), 3166–3172.

[5] Hu, S.; Shaner, M. R.; Beardslee, J. A.; Lichterman, M.; Brunschwig, B. S.; Lewis, N. S. Amorphous TiO_2 Coatings Stabilize Si, GaAs, and GaP Photoanodes for Efficient Water Oxidation. *Science* **2014**, *344* (6187), 1005–1009.

[6] Sachsenhauser, M.; Sharp, I. D.; Stutzmann, M.; Garrido, J. A. Surface State Mediated

Electron Transfer Across the n-Type SiC/Electrolyte Interface. *J. Phys. Chem. C* **2016**, *120* (12), 6524–6533.

[7] Huygens, I. M.; Theuwis, A.; Gomes, W. P.; Strubbe, K. A (Photo-) Electrochemical Study on n-GaN in Aqueous Solutions. *Phys. Status Solidi C* **2002**, *0* (1), 448–452.

[8] Huygens, I. M.; Theuwis, A.; Gomes, W. P.; Strubbe, K. Photoelectrochemical Reactions at the n-GaN Electrode in 1 M H_2SO_4 and in Acidic Solutions Containing Cl- Ions. *Phys. Chem. Chem. Phys.* **2002**, *4* (11), 2301–2306.

[9] Hasegawa, H.; He, L.; Ohno, H.; Sawada, T.; Haga, T.; Abe, Y.; Takahashi, H. Electronic and Microstructural Properties of Disorder-Induced Gap States at Compound Semiconductor–insulator Interfaces. *J. Vac. Sci. Technol. B Microelectron. Process. Phenomina* **1987**, *5* (4), 1097–1107.

[10] Spicer, W. E.; Chye, P. W.; Skeath, P. R.; Su, C. Y.; Lindau, I. New and Unified Model for Schottky Barrier and III–V Insulator Interface States Formation. *J. Vac. Sci. Technol.* **1979**, *16* (5), 1422–1433.

[11] Caccamo, L.; Fàbrega, C.; Marschewski, M.; Fündling, S.; Gad, A.; Casals, O.; Lilienkamp, G.; Höfft, O.; Prades, J. D.; Daum, W.; et al. Charge Transfer Characteristics of n-Type $In_{0.1}Ga_{0.9}N$ Photoanode across Semiconductor-Liquid Interface. *J. Phys. Chem. C* **2016**, *120* (51), 28917–28923.

[12] Barroso, M.; Mesa, C. A.; Pendlebury, S. R.; Cowan, A. J.; Hisatomi, T.; Sivula, K. Dynamics of Photogenerated Holes in Surface Modified α - Fe_2O_3 Photoanodes for Solar Water Splitting. *Proc. Natl. Acad. Sci.* **2012**, *109* (39), 15640–15645.

[13] Pendlebury, S. R.; Wang, X.; Le Formal, F.; Cornuz, M.; Kafizas, A.; Tilley, S. D.; Grätzel, M.; Durrant, J. R. Ultrafast Charge Carrier Recombination and Trapping in Hematite Photoanodes under Applied Bias. *J. Am. Chem. Soc.* **2014**, *136* (28), 9854–9857.

[14] Liu, R.; Zheng, Z.; Spurgeon, J.; Yang, X. Enhanced Photoelectrochemical Water-Splitting Performance of Semiconductors by Surface Passivation Layers. *Energy Environ. Sci.* **2014**, *7* (8), 2504–2517.

[15] Matys, M.; Adamowicz, B.; Domanowska, A.; Michalewicz, A.; Stoklas, R.; Akazawa, M.; Yatabe, Z.; Hashizume, T. On the Origin of Interface States at Oxide/III-Nitride Heterojunction Interfaces. *J. Appl. Phys.* **2016**, *120* (22), 225305-1-225305-12.

[16] Zhong, D. K.; Choi, S.; Gamelin, D. R. Near-Complete Suppression of Surface Recombination in Solar Photoelectrolysis by "Co-Pi" Catalyst-Modified W:$BiVO_4$. *J. Am. Chem. Soc.* **2011**, *133* (45), 18370–18377.

[17] Le Formal, F.; Pendlebury, S. R.; Cornuz, M.; Tilley, S. D.; Grätzel, M.; Durrant, J. R. Back Electron-Hole Recombination in Hematite Photoanodes for Water Splitting. *J. Am. Chem. Soc.* **2014**, *136* (6), 2564–2574.

[18] Chakrapani, V.; Pendyala, C.; Kash, K.; Anderson, A. B.; Sunkara, M. K.; Angus, J. C. Electrochemical Pinning of the Fermi Level : Mediation of Photoluminescence from Gallium Nitride and Zinc Oxide Electrochemical Pinning of the Fermi Level : Mediation of Photoluminescence from Gallium Nitride and Zinc Oxide. *J. Am. Chem. Soc.* **2008**, *130* (39), 12944–12952.

[19] Bard, A. J.; Bocarsly, A. B.; Fan, F.-R. F.; Walton, E. G.; Wrighton, M. S. The Concept of Fermi Level Pinning at Semiconductor/Liquid Junctions. Consequences for Energy Conversion Efficiency and Selection of Useful Solution Redox Couples in Solar Devices. *J. Am. Chem. Soc.* **1980**, *102* (11), 3671–3677.

[20] Gerischer, H. The Role of Semiconductor Structure and Surface Properties in Photoelectrochemical Processes. *J. Electroanal. Chem.* **1983**, *150* (1–2), 553–569.

[21] Winnerl, A.; Pereira, R. N.; Stutzmann, M. Kinetics of Optically Excited Charge

Carriers at the GaN Surface. *Phys. Rev. B* **2015**, *91* (7), 075316-1-075316-11.

[22] Winnerl, A.; Garrido, J. A.; Stutzmann, M. GaN Surface States Investigated by Electrochemical Studies. *Appl. Phys. Lett.* **2017**, *110* (10), 101602-1-101602-4.

[23] lahr, B.; Gimenez, S.; Fabregat-Santiago, F.; Bisquert, J.; Hamann, T. W. Photoelectrochemical and Impedance Spectroscopic Investigation of Water Oxidation with "Co–Pi"-Coated Hematite Electrodes. *J. Am. Chem. Soc.* **2012**, *134* (40), 16693–16700.

[24] Klahr, B.; Gimenez, S.; Fabregat-santiago, F.; Hamann, T.; Bisquert, J. Water Oxidation at Hematite Photoelectrodes: The Role of Surface States. *J. Am. Chem. Soc.* **2012, *134* (9), 4294-4302**.

[25] Ponomarev, E. A.; Peter, L. M. A Kinetic Study of CdS Photocorrosion by Intensity Modulated Photocurrent and Photoelectrochemical Impedance Spectroscopy. *J. Electroanal. Chem.* **1999,** *473*, 192–203**.**.

[26] Lorenz, P.; Gutt, R.; Haensel, T.; Himmerlich, M.; Schaefer, J. A.; Krischok, S. Interaction of GaN(0001)-2×2 Surfaces with H_2O. *Phys. Status Solidi C* **2010**, *7* (2), 169–172.

[27] Zhang, X.; Ptasinska, S. Electronic and Chemical Structure of the H_2O/GaN(0001) Interface under Ambient Conditions. *Sci. Rep.* **2016**, *6*, 1–6.

[28] Lichterman, M. F.; Hu, S.; Richter, M. H.; Crumlin, E. J.; Axnanda, S.; Favaro, M.; Drisdell, W.; Hussain, Z.; Mayer, T.; Brunschwig, B. S.; et al. Direct Observation of the Energetics at a Semiconductor/Liquid Junction by *Operando* X-Ray Photoelectron Spectroscopy. *Energy Environ. Sci.* **2015**, *8* (8), 2409–2416.

[29] Deutsch, T. G.; Koval, C. A.; Turner, J. A. III-V Nitride Epilayers for Photoelectrochemical Water Splitting: GaPN and GaAsPN. *J. Phys. Chem. B* **2006**, *110*

(50), 25297–25307.

[30] Memming, R. *Semiconductor Electrochemistry@ Wiley-Vch*, 1st ed.; Wiley-VCH, Weinheim, 2001., 88-89

[31] Barker, A.S., Ilegems, M., Infrared Lattice Vibrations and Free-Electron Dispersion in GaN, Phys. Rev. B 7 (1973) 743.

[32] A. Winnerl, J. A. Garrido, and Martin Stutzmann, Electrochemical characterization of GaN surface states, J. Appl. Phys. **122**, 045302 (2017)

[33] Beach, J. D.; Collins, R. T.; Turner, J. A. Band-Edge Potentials of n-Type and p-Type GaN. *J. Electrochem. Soc.* **2003**, *150* (7), A899–A904.

[34] S. R. Morrison, "Electrochemistry at Semiconductor and Oxidized Metal Electrodes," Plenum press (1980).

[35] W-J TSENG, Ph.D. thesis, KU Leuven, 2014.

[36] X. A. Cao, A. P. Zhang, G. T. Dang, F. Ren, S. J. Pearton, R. J. Shul, and L. Zhang, Schottky diode measurements of dry etch damage in n- and p-type GaN, Journal of Vacuum Science & Technology A 18, 1144 (2000)

[37] R. Cheung, R. J. Reeves, S. A. Brown, E. van der Drift, and M. Kamp, Effects of dry processing on the optical properties of GaN, Journal of Applied Physics 88, 7110 (2000)

[38] Bougrov V., Levinshtein M.E., Rumyantsev S.L., Zubrilov A., in Properties of Advanced SemiconductorMaterials GaN, AlN, InN, BN, SiC, SiGe . Eds. Levinshtein M.E., Rumyantsev S.L., Shur M.S., John Wiley & Sons, Inc., New York, 2001, 1-30.

[39] A. Goossens and J. Schoonman, An Impedance Study of Boron Phosphide Semiconductor Electrodes, J. Electrochem. Soc. 139, 893 (1992).

[40] Z. Hens and W. P. Gomes, On the electrochemical impedance of InP and GaAs

electrodes in indifferent electrolyte. Part 1. Analytical description of the frequency dispersion, Phys. Chem. Chem. Phys. 1, 3607 (1999).

[41] M. A. Reshchikov, Chapter Nine - Point Defects in GaN, Semiconductors and Semimetals,91, 2015, 315-367

[42] Trasatti, S.. "The absolute electrode potential: an explanatory note (Recommendations 1986)" Pure and Applied Chemistry, vol. 58, no. 7, 1986, pp. 955-966

[43] A. J. Bard, A. B. Bocarsly, F. R. F. Fan, E. G. Walton, and M. S. Wrighton, The concept of Fermi level pinning at semiconductor/liquid junctions. Consequences for energy conversion efficiency and selection of useful solution redox couples in solar devices, J. Am. Chem. Soc. 1980, 102, 11, 3671–3677

Chapter 5 Impact of ionic species on the band bending at n-GaN/ electrolytes interface

To clarify the effect of ionic species and pH on the band alignment at a semiconductor/electrolyte interface, including the conduction/valence band edges, quasi-Fermi levels and the band bending in the depletion region, light-induced drift of open-circuit potential (OCP) for an n-GaN was analyzed under photoanode operation. This evaluation clarified that the surface states derived from $V_{Ga}O_N$ may determine the band bending, regardless of electrolyte used in the experiment. In addition, for n-GaN in Na_2SO_4 and H_2SO_4, the radiative recombination was considered to be dominant recombination process. For n-GaN in HCl, the holes are removed by the reduction reaction of Cl^- to Cl_2 (+1.3 V vs. SHE), which facilitates the accumulation of electrons. After the potential reached at $H+/H_2$ redox level, electrons can be used by the reducing H^+ to H_2. When the quasi-Fermi level is over the H^+/H_2 redox level, electrons and holes start to be used for radiative recombination inside the n-GaN as well as the reduction reaction of H^+. For n-GaN in NaOH, similar mechanism of electron accumulation to n-GaN in HCl may occurred. The holes may be removed by the reduction reaction of OH^- to H_2O (+1.23 V vs. SHE), which facilitates the accumulation of electrons. However, the reaction rate of OH^-/H_2O, a four-electron reaction, is slower than that of Cl^-/Cl_2, a two-electron reaction, and the rate of hole removal is smaller. Therefore, the number of electrons accumulated in n-GaN facing to NaOH solution is less than that the case of HCl solution. Although the band bending is decided by the surface states derived from $V_{Ga}O_N$ in these electrolytes without illumination, it is affected by the redox pair, which is contained in electrolytes under illumination.

5.1 Introduction

Since the first photoelectrochemical water splitting [1], to implement photoelectrochemical solar to hydrogen conversion, the surface of semiconductor has been modified with electrocatalysts [2,3] and protective layers [4,5]. However, the activity of the catalyst and lifetime of semiconductor are affected by pH and redox pair contained in electrolytes as well as the surface modification.

In n-GaN, which is useful both as an electronic component [8,9] and as a photocatalyst/electrode material for hydrogen generation [10-14], its carrier transport has been studied [15], and it has been reported that its overvoltage and lifetime vary depending on the electrolyte.

In 1.0 mol/L KOH aqueous solution, a clear generation of hydrogen from the counter electrode due to n-GaN photoelectrochemical reaction was observed when +1.0 V counter electrode bias was applied to the working electrode [16]. In 1.0 mol /L NaCl, the overpotential for water reduction in neutral water electrolyte was higher than that in acidic 1.0 mol/L HCl and basic 1.0 mol/L KOH [17]. These situations were similar when acidic, neutral, and basic were 0.5 mol/L Na_2SO_4, 0.5 mol/L H_2SO_4, and 1.0 mol/L NaOH III-nitride photoelectrodes, respectively.

The electrolyte dependence was also evaluated and it was summarized that the NaOH aqueous electrolyte is relatively good except in the case of non-oxygen evolution reactions such as HCl aqueous electrolyte [18]. The overpotential evaluated from the comparison between the flat band potential obtained from the Mott-Schottky plot and the turn-on voltage of the photocurrent was found to be larger in the case of H_2SO_4 acidic aqueous solution than in the case of NaOH basic aqueous solution [18]. This may be due to the difference in photovoltage generated in n-GaN and slower reaction rate in oxidation of water (H_2O) molecule in HCl than OH^- in NaOH. Therefore, the effect of electrolytes

on the band bending, which determines carrier splitting, and photovoltage should be investigated.

In sections 2 to 4, it is suggested that the band bending at the interface between n-GaN and the electrolyte is determined by the pinning of the Fermi level to the sub-surface crystal defect, $V_{Ga}O_N$. Under light irradiation, the photogenerated carriers fill the surface levels and resolve the pinning. They then accumulate in the depletion layer and the band bending is reduced. However, when the redox reaction proceeds significantly, the accumulated photogenerated carriers are used for the reaction and the amount of band bending relaxation is expected to decrease. Therefore, the band alignment may be affected by the electrolyte used.

In this study, to evaluate the effect of redox species in electrolytes on the band alignment, we evaluated the band alignment of the n-GaN/electrolyte interface by measuring the open-circuit potential (OCP) under illumination [19] and Mott-Schottky analysis. Under dark and weak illumination, the quasi-Fermi level is fixed in the surface state, but under strong illumination, the quasi-Fermi level should approach the flat band potential because photogenerated carriers fill in the surface state and accumulate in the depletion layer. The effect of redox reactions on the band bending can be clarified by the OCP as a function of illumination intensity.

We try to demonstrate our proposed framework of analysis using a model system, n-GaN/ electrolytes interface. By analyzing the band alignment of the GaN interface with various electrolytes, we will clarify the effect of redox reactions on the band alignment.

5.2 Method

5.2.1 Sample preparation

In this research, the photoanode was (0001) n-GaN layer on a Si substrate grown by metal organic chemical vapor phase epitaxy (MOVPE), provided by NuFlare Technology. The carrier concentration of the undamaged n-GaN was approximately 4×10^{18} cm^{-3} as estimated by hall measurement. Before electrochemical measurement, to remove organic compounds on the surface, the electrode was cleaned with ultrasound in acetone and isopropanol for 2 min, respectively. Then, it was rinsed in ultra-pure water and dried with nitrogen blow. The ohmic contact was formed on the surface of n-GaN with indium.

5.2.2 Evaluation method

The GaN photoelectrodes were analyzed in the experimental system shown in Fig. 1. Each sample was fixed on an electrochemical cell made of UV-transparent quartz glass. The photoelectrode was contacted with 1 M NaOH solution (pH = 14) , 0.2M Na_2SO_4 (pH:6.3), 1M HCl solution (pH: 0.0) or 0.5M H_2SO_4 solution (pH: 0.0) via a circular hole (6 mm in diameter) opened on the wall of the cell. Before the measurement, the cell was purged by 0.11 MPa Ar gas to remove the dissolved gas. All measurements were done in three-electrodes configuration with a potentiostat. A platinum wire was used as counter electrode. For NaOH, Hg/HgO/1 M NaOH electrode (+0.11 V vs. standard hydrogen electrode (SHE) at 290 K) was used, but for the others, $Ag/AgCl/KCl_{sat.}$ electrode (+0.20 V vs. SHE) was used as reference electrode.

To measure light intensity dependence of OCP, 325 nm He-Cd laser was used as a light source. The laser light was TEM multimode and the beam diameter ($1/e^2$) was 1.78 mm. The photon energy (3.82 eV) is enough to induce the intra-band transition of

carriers (3.42 eV in bandgap for GaN). Laser spot size was optically expanded to 6.0 mm in diameter to cover the hole entirely. A blackout curtain was employed to define the dark condition. The irradiated light intensity was varied from 2.9×10^{-5} to 1.6×10^{2} mW/cm^2 with ND filters. The corresponding photon flux ranged from 10^{9} to 10^{17} s^{-1} cm^{-2}.

Using this setup, light intensity dependence of OCP was measured for the n-GaN photoelectrodes in 1 M NaOH solution (pH:14), 0.2M Na_2SO_4 (pH:6.3), 1M HCl solution (pH: 0.0) and 0.5M H_2SO_4 solution (pH: 0.0), respectively. Laser light at each setpoint intensity was irradiated and the value of OCP jumped from a value under the dark condition to a value under illumination as shown. Since the OCP value showed a slight drift after the onset of light irradiation, the value after stabilization was used as the value corresponding to the light intensity. To examine the variation of OCP by physical or chemical surface modification after illumination, the light-intensity dependence of OCP was measured with both increasing and decreasing light intensity.

Impedance measurement was also conducted to obtain Mott-Schottky plot under the dark condition after the OCP measurement. DC bias voltage in impedance measurement was increased from -0.2 V to +1.3 V vs. reversible hydrogen electrode (RHE). At each DC bias voltages, impedance was measured by applying a small AC signal with frequencies from 2.0×10^{4} and 1.0×10^{2} Hz.

5.3 Results and discussion

5.3.1 Band edge potential of n-GaN photoelectrode

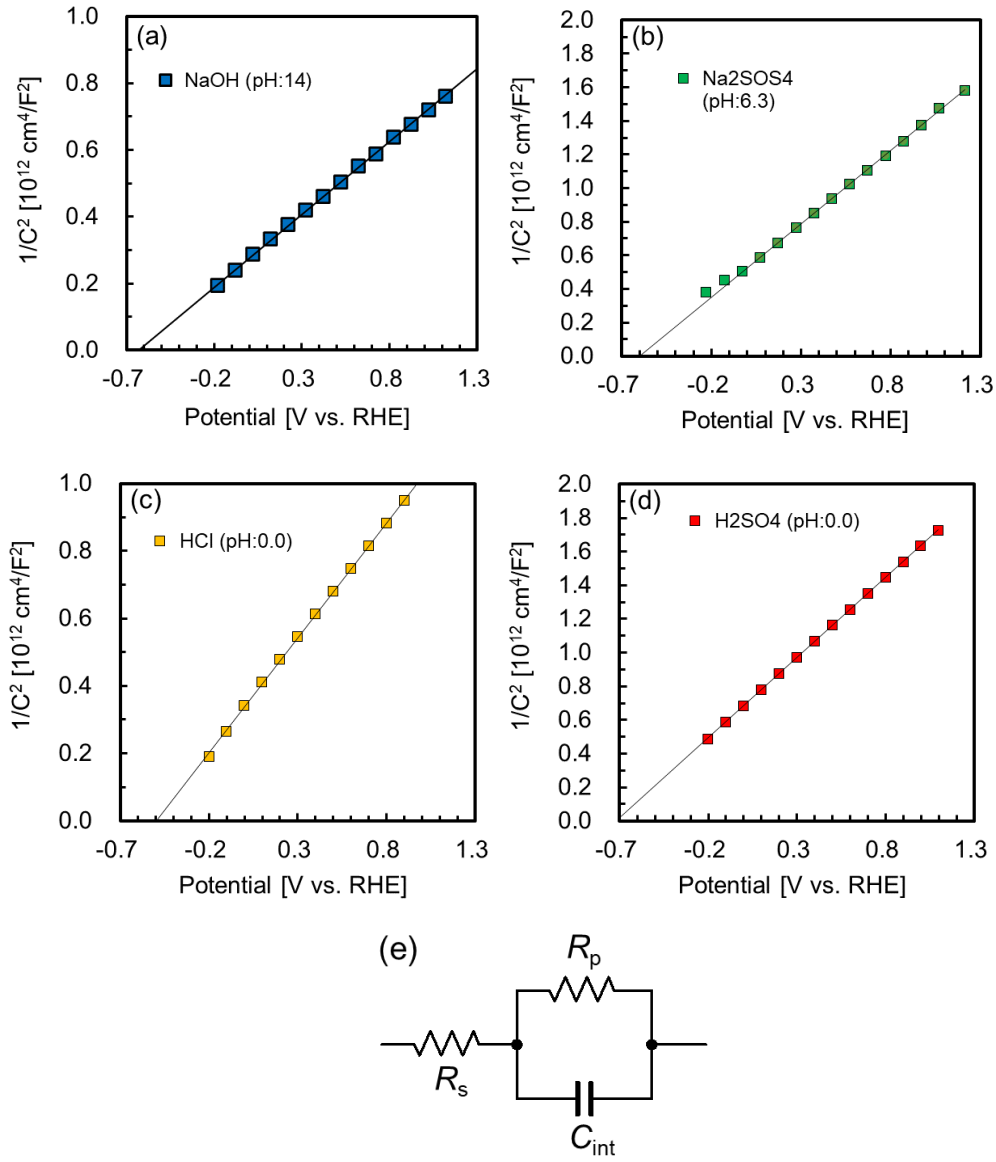

Figure 5.1 Mott-Schottky plot for an n-GaN photoelectrode in (a)$NaOH_{aq.}$, (b)$Na_2SO_{4aq.}$, (c)$HCl_{aq.}$ and (d) $H_2SO_{4aq.}$ The capacitance was obtained from fitting impedance data at each DC bias with the equivalent circuit shown in (e). C_{int} and R_p are capacitance and resistance in the semiconductor/electrolyte interface, respectively. R_s is the series resistance including the contribution of both the electrolyte and the semiconductor. The fitting was done in frequency range between 2.0×10^4 and 1.0×10^2 Hz. The solid line was analyzed by the Mott-Schottky equation in

Equation (5.1).

To obtain the band bending at the n-GaN/electrolytes interface without illumination, the conduction-band-edge potential, E_{Cs}, was evaluated by Mott-Schottky plot as the inverse square of the capacitance in the surface depletion region of n-GaN, C_{int}, as a function of applied bias in Fig. 5.1a, b, c and d. Flat-band potential, ϕ_{FB}, was estimated by fitting linear region with the following relationship, [20]

$$\frac{1}{C_{int}^2} = \frac{2}{\mathrm{e}\epsilon\epsilon_0 N_{\mathrm{D}}}\left(\phi - \phi_{\mathrm{FB}} - \frac{kT}{\mathrm{e}}\right), \tag{5.1}$$

where, e is the elemental charge, ϵ is the relative permittivity of 10.4 [21], ϵ_0 is the permittivity of vacuum, N_{D} is the donor density, ϕ is the applied potential, k is the Boltzmann constant and T is the absolute temperature.

To obtain, the experimental data C_{int} is fitted using the equivalent circuit models (Fig. 4.3c). The experimental data is represented by symbols and the lines show fits according to the Mott-Schottky equation. A linear dependence of the inverse square of the interface capacitance on the applied bias potential is expected [20]. For each condition, a linear dependence is observed. From this linear dependence, the flat band potentials were evaluated as -0.64 V vs. RHE in $NaOH_{aq.}$, -0.60 V vs. RHE in $Na_2SO_{4aq.}$, -0.50 V vs. RHE in $HCl_{aq.}$, -0.70 V vs. RHE in $H_2SO_{4aq.}$, respectively.

Using these values of flat-band potential, the conduction band edge potential of n-GaN was evaluated by the relationship,

$$E_{\mathrm{Cs}} = \phi_{\mathrm{FB}} - \frac{kT}{\mathrm{e}}\ln\left(\frac{N_{\mathrm{c}}^*}{n}\right), \tag{5.2}$$

where, E_{Cs} is the potential of conduction band edge at the surface, N_{c}^* is the effective density of states in the conduction band and n is the net carrier concentration, which was evaluated as 4×10^{18} cm^{-3} by hall measurement. Therefore, the conduction band edge potential at the surface of n-GaN were evaluated as -0.62 V *vs*. RHE in $NaOH_{aq.}$, -0.58 V

vs. RHE in $Na_2SO_{4aq.}$, -0.48 V vs. RHE in $HCl_{aq.}$, -0.68 V vs. RHE in $H_2SO_{4aq.}$, respectively, with N_c^* calculated as 2.13×10^{18} cm^{-3} from effective mass for the electron of $0.20m_0$,[21] where m_0 is the rest mass of the electron. Using this value and the bandgap of GaN (3.42 eV), the valence-band-edge potential E_{Vs} at the surface of an n-GaN photoelectrode were deduced to be + 2.80 V *vs*. RHE in $NaOH_{aq.}$, +2.84 V vs. RHE in $Na_2SO_{4aq.}$, +2.92 V vs. RHE in $HCl_{aq.}$, +2.72 V vs. RHE in $H_2SO_{4aq.}$, respectively. Also, the vacuum level at the surface were -4.7 V vs. RHE in $NaOH_{aq.}$ and $Na_2SO_{4aq.}$, -4.6 V vs. RHE in $HCl_{aq.}$, -4.8 V vs. RHE in $H_2SO_{4aq.}$., with the electron affinity of 4.1 eV.

These values of band edge potential except in $HCl_{aq.}$ and $H_2SO_{4aq.}$ are in good agreement with previous reports. [11, 22, 23] In these reports, this variation in the band edge potential of 59 mV/pH was expected to be due to the adsorption of H^+ ions on the semiconductor surface [24]. In $HCl_{aq.}$, the value is -0.48 V vs. RHE, which is far from this pH dependence, but similar values were reported in previous studies. [25-27] This may be due to the effect of surface adsorption of Cl^- ions as well as H^+. In $H_2SO_{4aq.}$, the value is -0.68 V vs. RHE, which is slightly different from this pH dependence. The band edge potential reported by previous studies have large deviation between -0.6 V vs. RHE and > 1.1 V vs. RHE. [28-30]. This may be due to the effect of surface adsorption of SO_4^- ions as well as H^+. Furthermore, the fits according to the Mott-Schottky equation evaluates the donor density N_D as 3.1×10^{19} cm^{-3} in $NaOH_{aq.}$, 1.6×10^{19} in $Na_2SO_{4aq.}$, 2.0×10^{19} in $HCl_{aq.}$, 1.4×10^{19} vs. RHE in $H_2SO_{4aq.}$, respectively. There was no significant difference in the dope concentration among the solutions.

5.3.2 Fermi level pinning observed by OCP measurement

Since the electric contact is in equilibrium with n-GaN, OCP of n-GaN in NaOH electrolyte corresponds to E_F under the dark condition. The value shifted to the negative direction with increasing illumination intensity. The value of OCP is plotted in Fig. 5.2 with respect to the logarithm of illumination intensity.

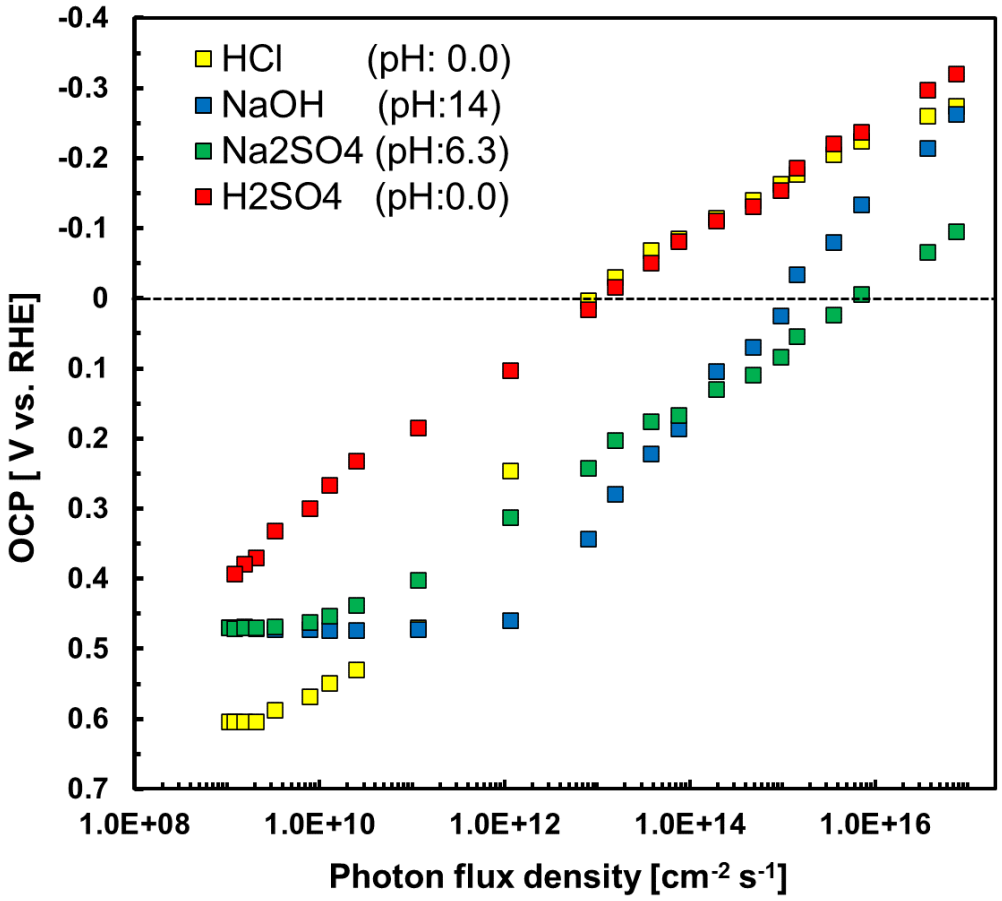

Figure 5.2 Open-Circuit potential (OCP) plotted with respect to logarithm of photon flux density. OCP was measured for the n-GaN photoelectrodes in (blue square) $NaOH_{aq.}$ (pH:14), (green square) Na_2SO_4 $_{aq.}$ (pH:6.3), $HCl_{aq.}$ (pH: 0.0) and H_2SO_4 $_{aq.}$ (pH: 0.0), respectively. Also, redox potentials of hydrogen evolution reactions are shown as broken lines at 0 V vs. RHE.

(i) n-GaN/ $NaOH_{aq.}$

For n-GaN/ $NaOH_{aq.}$, OCP was +0.51 V vs. RHE under the dark condition. The band alignment under the dark condition is deduced as in Fig. 5.3a and the band bending was 1.2 V. With increasing photon flux, OCP approached to the flat-band potential and band bending was reduced accordingly.

Upon light irradiation, OCP shifted to the negative direction. For the photon flux below 10^{12} s^{-1} cm^{-2}, OCP was constant at +0.51 V vs. RHE with increasing photon flux. Above a photon flux of $1.2 \times 10^{12}\ s^{-1}\ cm^{-2}$, the value of OCP drifted to the negative direction in an almost linear manner with the logarithm of light intensity, and the value approached to the flat-band potential of -0.62 V vs. RHE obtained by Mott-Schottky plot (Fig. 5.1a). Below a photon flux of $1.2 \times 10^{12}\ s^{-1}\ cm^{-2}$, the value of OCP seems to be affected significantly by the surface states. This pinning position was 1.1 V below CBM. Above a photon flux of $1.2 \times 10^{12}\ s^{-1}\ cm^{-2}$, the behavior of OCP is considered to be almost free from the impact of the surface states and the accumulation of photocarriers in the depletion region of n-GaN seems to be responsible for the reduction of band bending. The linear relationship between OCP and the logarithm of light intensity is often observed for open-circuit voltage in photovoltaic cells. The slope was ~150 mV/dec.

(ii) n-GaN/ $Na_2SO_{4\ aq.}$

For n-GaN/ $Na_2SO_{4\ aq.}$, OCP was +0.47 V vs. RHE under the dark condition. The band alignment under the dark condition is deduced as in Fig. 5.3b and the band bending was 1.1 V. With increasing photon flux, OCP approached to the flat-band potential and band bending was reduced accordingly.

Upon light irradiation, OCP shifted to the negative direction. For the photon flux

below 3.3 × 10^9 s^{-1} cm^{-2}, OCP was constant at +0.47 V vs. RHE with increasing photon flux. Above a photon flux of 3.3 × 10^9 s^{-1} cm^{-2}, the value of OCP drifted to the negative direction in an almost linear manner with the logarithm of light intensity, and the value approached to the flat-band potential of -0.60 V vs. RHE obtained by Mott-Schottky plot (Fig. 5.1b). Under a photon flux of 3.3 × 10^9 s^{-1} cm^{-2}, the value of OCP seems to be affected significantly by the surface states. This pinning position was 1.1 V below CBM. Above a photon flux of 3.3 × 10^9 s^{-1} cm^{-2}, the behavior of OCP is considered to be almost free from the impact of the surface states and the accumulation of photocarriers in the depletion region of n-GaN seems to be responsible for the reduction of band bending. The linear relationship between OCP and the logarithm of light intensity is often observed for open-circuit voltage in photovoltaic cells. The slope was ~80 mV/dec.

(iii) n-GaN/ $HCl_{aq.}$

For n-GaN/ $HCl_{aq.}$, OCP was +0.61 V vs. RHE under the dark condition. The band alignment under the dark condition is deduced as in Fig. 5.3c and the band bending was 1.1 V. With increasing photon flux, OCP approached to the flat-band potential and band bending was reduced accordingly.

Upon light irradiation, OCP shifted to the negative direction. For the photon flux below 2.0 × 10^9 s^{-1} cm^{-2}, OCP was constant at +0.61 V vs. RHE with increasing photon flux. Above a photon flux of 2.0 × 10^9 s^{-1} cm^{-2}, the value of OCP drifted to 0 V vs. RHE radically (250 mV/dec) in an almost linear manner with the logarithm of light intensity. After the OCP reached at 0V vs. RHE, the value approached gently (70 mV/dec) to the flat-band potential of -0.50 V vs. RHE obtained by Mott-Schottky plot (Fig. 5.1c). Under a photon flux of 2.0 × 10^9 s^{-1} cm^{-2}, the value of OCP seems to be affected

significantly by the surface states. This pinning position was 1.1 V below CBM. Above a photon flux of $2.0 \times 10^{9}\ s^{-1}\ cm^{-2}$, the behavior of OCP is considered to be almost free from the impact of the surface states and the accumulation of photocarriers in the depletion region of n-GaN seems to be responsible for the reduction of band bending. The slope were ~250 mV/dec (photon flux: $1.2 \times 10^{11}\ s^{-1}\ cm^{-2}$ - $8.0 \times 10^{12}\ s^{-1}\ cm^{-2}$) and ~70 mV/dec(photon flux: $8.0 \times 10^{12}\ s^{-1}\ cm^{-2}$ - $7.5 \times 10^{16}\ s^{-1}\ cm^{-2}$).

(iv) n-GaN/ $H_2SO_{4\ aq.}$

For n-GaN/ $H_2SO_{4\ aq.}$, OCP was +0.40 V vs. RHE under the dark condition. The band alignment under the dark condition is deduced as in Fig. 5.3d and the band bending was 1.1 V. The Fermi level was also positioned at 1.1 V below CBM. With increasing photon flux, OCP approached to the flat-band potential and band bending was reduced accordingly.

Upon light irradiation, the value of OCP drifted to the negative direction in an almost linear manner with the logarithm of light intensity, and the value approached to the flat-band potential of -0.70 V vs. RHE obtained by Mott-Schottky plot (Fig. 5.1d). Unlike the other electrolytes, no pinning was observed. The linear relationship between OCP and the logarithm of light intensity is often observed for open-circuit voltage in photovoltaic cells. The slope was ~80 mV/dec.

(v) Origin of pinning in n-GaN

The Fermi level of n-GaN was located at 1.1 eV below CBM in all solutions used in the experiments. As shown in the previous study [31-33], the defect states derived from $V_{Ga}O_N$ are located at ~1.1 eV. Therefore, the surface states originated from $V_{Ga}O_N$ are

considered to be origin of pinning. However, the density of surface states is not enough

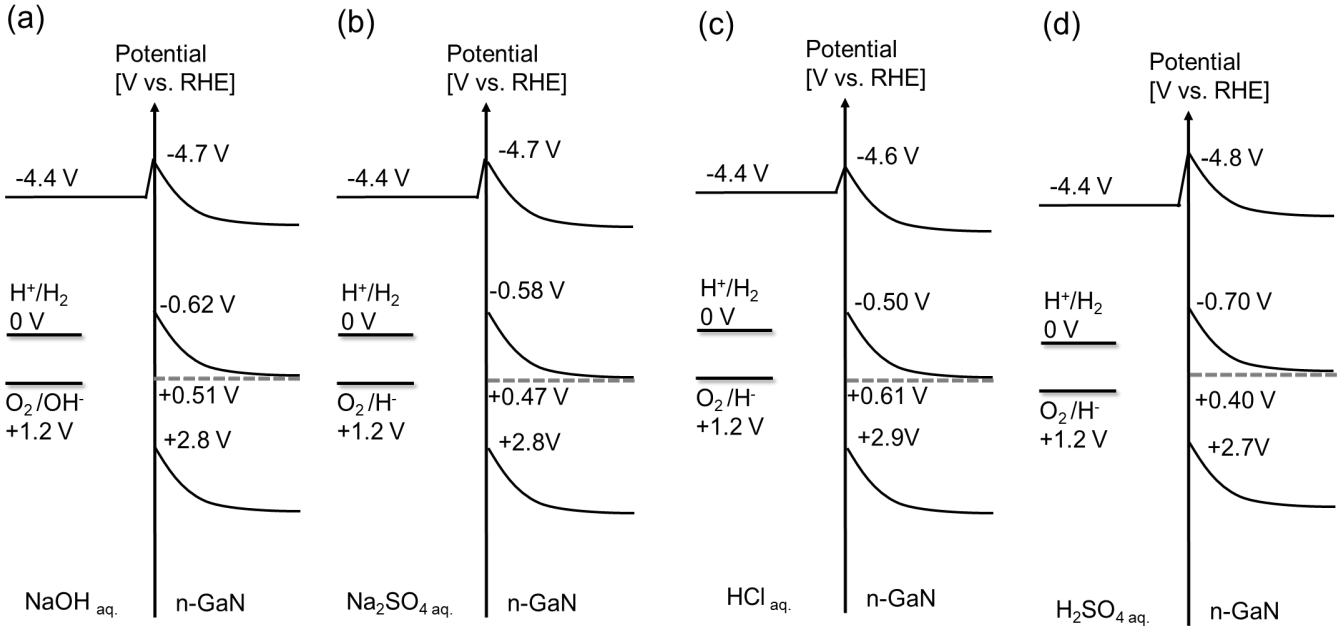

to cause Fermi level pinning at 1.1 eV below conduction band edge. Therefore, the negative charge present in the electrolyte is considered to contribute to the pinning. In fig. 5.2, the unpinning light intensity is positively correlated with increasing pH, except in HCl. This result suggests that OH^- ions in electrolyte terminate electric flux lines from donor in the depletion layer in n-GaN. In HCl, the Cl^- ions terminate them, instead of OH^-. Therefore, the reactive anion species should be the origin of carrier annihilation via redox reactions. Since these reactions are likely to be triggered by specifically adsorbed OH- and Cl-, the unpinning light intensity is thought to correspond to the amount of specifically adsorbed OH^- and Cl^-. In a previous study [34], the pH dependence of Ga-H_2O, Ga-OH, and N-H coverage on the GaN (10-10) was discussed theoretically. The coverage of Ga-OH changed by less than one order of magnitude between pH 14 and 7, while the unpinning light intensity changed by two orders of magnitude. Therefore, it is possible that the coverage on the GaN (0001) surface differs by several orders of magnitude from that on GaN (10-10), or that N-H and Ga-H_2O, which vary by orders of magnitude with respect to pH, affect the elemental reactions involving OH.

Figure 5.3 Band alignment at the n-GaN/ $NaOH_{aq.}$ (a), $Na_2SO_{4aq.}$(b), $HCl_{aq.}$ (c) and in $H_2SO_{4aq.}$ (d) interface under dark condition. The band edge potential is the value obtained from Mott-Schottky plot. Here, we used 4.44V as the difference between vacuum level and hydrogen redox.

5.3.3 OCP under light irradiation and carrier recombination mechanism

When the Fermi level was free from pinning, the value of OCP drifted to the negative direction in an almost linear manner with the logarithm of light intensity. Since the light intensity dependence of OCP has similar characteristics to the open-circuit voltage of solid-state solar cells, the same theory can be applied. However, there is a need to note that the difference in OCP with and without illumination (difference between quasi-Fermi level for majority carrier with and without illumination) is different from the open-circuit voltage in photovoltaic (difference between quasi-Fermi level for electrons and holes). Therefore, the model for surface photovoltage, V_{spv} (V_{spv} = OCP (illumination) – OCP (dark)), analysis should be used.

According to the model which has been proposed by Reshchikov et al., [35] V_{spv} can be described as

$$V_{\mathrm{spv}} = \frac{\mathrm{nkT}}{e} \ln\left(\frac{\mathrm{cP_0}}{R_0} + 1\right), \tag{5.3}$$

where

$$c = 1 - \mathrm{e}^{-\alpha W}, \tag{5.4}$$

$$R_0 = C_{\mathrm{n1}} N_{\mathrm{ss}}{}' N_c^* \exp\left(-\frac{|\phi_{\mathrm{FB}} - \mathrm{OCP(dark)}|}{kT}\right). \tag{5.5}$$

Here, n is ideality factor, P_0 is photon flux density, α is light absorption coefficient, W is length of depletion layer, R_0 is the bulk-to-surface flow rate of free electrons under

dark conditions, C_{n1} is effective electron capture cross section,N_{ss}' is the density of unoccupied surface states, N_c^* is the effective density of states in the conduction band. R_0 stands for the rate of thermionic transitions of electrons between the surface states and bulk without illumination, where such transitions obey Boltzmann statistics. Free electrons from the bulk region can overcome the barrier height and be trapped by surface states. Under high photon flux ($cP_0/R_0 >> 1$), eq. (5.3) can be approximated to be

$$V_{spv} \approx \frac{nkT}{e}\{\ln(P_0) + \ln(c) - \ln(R_0)\} . \quad (5.6)$$

Therefore, the ideality factor can be evaluated by using eq. (5.6) in linear region in Fig 5.2 under high photon flux density. In the curves in Fig. 5.2, the slopes of (dV_{spv}) / (dlog P_0) are 150 mV/dec (NaOH), 80 mV/dec (Na_2SO_4), 250 meV/dec and 70 mV/dec (HCl) and 80 mV (H_2SO_4), respectively, which are 2.5, 1.2, 4.2 and 1.3, 1.3 times higher than kT/e of 60 mV/dec. For n-GaN (HCl), the slope of ~250 mV/dec and ~70 mV/dec correspond to the radical shift (photon flux between 1.2×10^{11} s^{-1} cm^{-2} and 8.0×10^{12} s^{-1} cm^{-2}) and the linear behavior (photon flux between 8.0×10^{12} s^{-1} cm^{-2} and 7.5×10^{16} s^{-1} cm^{-2}), respectively. When Shockley-Read-Hall (SRH) recombination or radiative recombination in the depletion region are dominant, the ideality factor is close to 2 or 1, respectively [36]. Therefore, for n-GaN in Na_2SO_4 and H_2SO_4, the radiative recombination was considered to be dominant recombination process. For n-GaN in HCl, under photon flux between 1.2×10^{11} s^{-1} $cm^{-2}$and 8.0×10^{12} s^{-1} cm^{-2}, the ideality factor of 4.2 is much higher than 2. It means more photogenerated electrons can accumulate in the depletion layer. It is thought that the holes are removed by the reducing Cl^- to Cl_2 (+1.3 V vs. SHE), which facilitates the accumulation of electrons. Then, the quasi-Fermi level for electron, OCP, drifted to negative potential and reached at H^+/H_2 redox potential of 0 V vs. RHE. After the potential reached at H^+/H_2 redox level, electrons can be used by t reduction reaction of H^+ to H_2. When the quasi-Fermi level is over the H^+/H_2 redox level,

the ideality factor is 1.3. It means electrons and holes start to be used for radiative recombination and redox reaction above photon flux of $8.0 \times 10^{12}\ s^{-1}\ cm^{-2}$. This hypothesis is supported by the no observation of radical shift in other electrolytes which do not contain hole scavenger such as Cl^-. For n-GaN in NaOH, the ideality factor of 2.5 is also over 2. In this case, similar mechanism of accumulation to n-GaN in HCl may occurred. The holes may be removed by reducing OH^- to H_2O (+1.23 V vs. SHE), which facilitates the accumulation of electrons. However, the reaction rate of OH^-/H_2O, a four-electron reaction, is slower than that of Cl^-/Cl_2, a two-electron reaction, and the number of removed holes is smaller. Therefore, the number of electrons accumulated in NaOH is less than that in HCl, and its ideality factor is considered to be 2.5, which is smaller than that in HCl.

5.4 Conclusion

Effect of electrolytes on the band bending of n-GaN is analyzed by Mott-Schottky plot and OCP as a function of the logarithm of irradiation light intensity. The variation in band edge potentials except in $HCl_{aq.}$ and $H_2SO_{4aq.}$ are in good agreement with 59 mV/pH was expected to be due to the adsorption of H^+ ions on the semiconductor surface. In $HCl_{aq.}$, the value is -0.5 V vs. RHE, which is far from this pH dependence due to the effect of surface adsorption of Cl^- ions as well as H^+. In $H_2SO_{4aq.}$, the value is -0.5 V vs. RHE, which is far from this pH dependence due to the effect of surface adsorption of SO_4^- ions as well as H^+. Although the band edge potential was different, the Fermi level of n-GaN was located at 1.1 eV below CBM in all solutions used in the experiments. Regardless of electrolyte in the experiment, the surface states derived from $V_{Ga}O_N$ are considered to be origin of pinning. In addition, no pinning was observed in sulfuric acid. Sulfuric acid removes more O from the surface than hydrochloric acid, which may have reduced the

amount of $V_{Ga}O_N$.

When the Fermi level was free from pinning, the value of OCP drifted to the negative direction in an almost linear manner with the logarithm of light intensity. For n-GaN in Na_2SO_4 and H_2SO_4, the radiative recombination was considered to be dominant recombination process. For n-GaN in HCl, the holes are removed by the reducing Cl^- to Cl_2 (+1.3 V vs. SHE), which facilitates the accumulation of electrons. Then, the quasi-Fermi level for electron, OCP, drifted to negative potential and reached at H^+/H_2 redox potential of 0 V vs. RHE. After the potential reached at H^+/H_2 redox level, electrons can be used by the reducing H^+ to H_2. When the quasi-Fermi level is over the H^+/H_2 redox level, electrons and holes start to be used for radiative recombination and redox reaction. For n-GaN in NaOH, a mechanism for the electron accumulation in n-GaN may take place similarly to the case in HCl. The holes may be removed by reducing OH^- to H_2O (+1.23 V vs. SHE), which facilitates the accumulation of electrons. However, the reaction rate of OH^-/H_2O, a four-electron reaction, is slower than that of Cl^-/Cl_2, a two-electron reaction, and the amount of holes removed is smaller. Therefore, the number of electrons accumulated in NaOH is less than that in HCl. Although the band bending is decided by the surface states derived from $V_{Ga}O_N$ in these electrolytes without illumination, it is affected by the redox pair, which is contained in electrolytes under illumination. To enhance the carrier transport in n-type semiconductor, amount of the reactive anion which is contained in the electrolyte should be reduced.

REFERENCES

[1] Fujishima, A.; Honda, K. Electrochemical Photolysis of Water at a Semiconductor Electrode. *Nature* **1972**, *238*, 37–38.

[2] Nellist, M. R.; Laskowski, F. A. L.; Lin, F.; Mills, T. J.; Boettcher, S. W.

Semiconductor-Electrocatalyst Interfaces: Theory, Experiment, and Applications in Photoelectrochemical Water Splitting. *Acc. Chem. Res.* **2016**, *49* (4), 733–740.

[3] Kang, D.; Kim, T. W.; Kubota, S. R.; Cardiel, A. C.; Cha, H. G.; Choi, K. S. Electrochemical Synthesis of Photoelectrodes and Catalysts for Use in Solar Water Splitting. *Chem. Rev.* **2015**, *115* (23), 12839–12887.

[4] Zhong, D. K.; Choi, S.; Gamelin, D. R. Near-Complete Suppression of Surface Recombination in Solar Photoelectrolysis by "Co-Pi" Catalyst-Modified W:$BiVO_4$. *J. Am. Chem. Soc.* **2011**, *133* (45), 18370–18377.

[5] Verlage, E.; Hu, S.; Liu, R.; Jones, R. J. R.; Sun, K.; Xiang, C.; Lewis, N. S.; Atwater, H. A. A Monolithically Integrated, Intrinsically Safe, 10% Efficient, Solar-Driven Water-Splitting System Based on Active, Stable Earth-Abundant Electrocatalysts in Conjunction with Tandem III-V Light Absorbers Protected by Amorphous TiO_2films. *Energy Environ. Sci.* **2015**, *8* (11), 3166–3172.

[6] Liu, R.; Zheng, Z.; Spurgeon, J.; Yang, X. Enhanced Photoelectrochemical Water-Splitting Performance of Semiconductors by Surface Passivation Layers. *Energy Environ. Sci.* **2014**, *7* (8), 2504–2517.

[7] Hu, S.; Shaner, M. R.; Beardslee, J. A.; Lichterman, M.; Brunschwig, B. S.; Lewis, N. S. Amorphous TiO_2 Coatings Stabilize Si, GaAs, and GaP Photoanodes for Efficient Water Oxidation. *Science* **2014**, *344* (6187), 1005–1009.

[8] Ponce, F. A.; Bour, D. P. Nitride-Based Semiconductors for Blue and Green Light-Emitting Devices. *Nature*. **1997**, 351–359.

[9] Shur, M. S. GaN Based Transistors for High Power Applications. *Solid. State. Electron.* **1998**, *42* (12), 2131–2138.

[10] Chichibu, S.; Azuhata, T.; Sota, T.; Nakamura, S. Excitonic Emissions from

Hexagonal GaN Epitaxial Layers. *J. Appl. Phys.* **1996**, *79* (5), 2784–2786.

[11] Beach, J. D.; Collins, R. T.; Turner, J. A. Band-Edge Potentials of n-Type and p-Type GaN. *J. Electrochem. Soc.* **2003**, *150* (7), A899–A904.

[12] Fujii, K.; Ohkawa, K. Photoelectrochemical Properties of P-Type GaN in Comparison with n-Type GaN. *Jpn. J. Appl. Phys.* **2005**, *44* (28), L909–L911.

[13] Howgate, J.; Schoell, S. J.; Hoeb, M.; Steins, W.; Baur, B.; Henrich, S.; Nickel, B.; Sharp, I. D.; Stutzmann, M.; Eickhoff, M. Photocatalytic Cleavage of Self-Assembled Organic Monolayers by UV-Induced Charge Transfer from GaN Substrates. *Adv. Mater.* **2010**, *22* (24), 2632–2636.

[14] Wang, D.; Pierre, A.; Kibria, M. G.; Cui, K.; Han, X.; Bevan, K. H.; Guo, H.; Paradis, S.; Hakima, A. R.; Mi, Z. Wafer-Level Photocatalytic Water Splitting on Gan Nanowire Arrays Grown by Molecular Beam Epitaxy. *Nano Lett.* **2011**, *11* (6), 2353–2357.

[15] Schäfer, S.; Wyrzgol, S. A.; Lercher, J. A.; Stutzmann, M.; Sharp, I. D. Charge Transfer across the GaN/Pt Nanoparticle Interface in an Electrolyte. *ChemCatChem* **2013**, *5* (11), 3224–3227.

[16] K. Fujii, T. Karasawa and K. Ohkawa, Hydrogen gas generation by splitting aqueous water using n-type GaN photoelectrode with anodic oxidation, Jpn. J. Appl. Phys., 44 (2005), p. L543

[17] K. Fujii and K. Ohkawa, Hydrogen generation from aqueous water using n-GaN by photoassisted electrolysis, Phys. Status Solidi C, 3 (2006), pp. 2270-2273

[18] K. Koike, A. Nakamura, M. Sugiyama, Y. Nakano and K. Fujii, Surface stability of n-type GaN depending on carrier concentration and electrolytes under photoelectrochemical reactions Phys. Status Solidi C, 11 (2014), pp. 821-823

[19] Deutsch, T. G.; Koval, C. A.; Turner, J. A. III-V Nitride Epilayers for

Photoelectrochemical Water Splitting: GaPN and GaAsPN. *J. Phys. Chem. B* **2006**, *110* (50), 25297–25307.

[20] Memming, R. *Semiconductor Electrochemistry@ Wiley-Vch*, 1st ed.; Wiley-VCH, Weinheim, 2001., 88-89

[21] Barker, A.S., Ilegems, M., Infrared Lattice Vibrations and Free-Electron Dispersion in GaN, Phys. Rev. B 7 (1973) 743.

[22] S. S. Kocha, M. W. Peterson, D. J. Arent, J. M. Redwing, M. A. Tischler, and J. A.Turner, Electrochemical Investigation of the Gallium Nitride-Aqueous Electrolyte Interface, J. Electrochem. Soc., 142, L238 (1995).

[23] I. M. Huygens, K. Strubbe, and W. P. Gomes, Electrochemistry and Photoetching of n-GaN, J. Electrochem. Soc., 147, 1797 (2000).

[24] S. R. Morrison, Electrochemistry at Semiconductor and Oxidized Metal Electrodes, Chap. 2, Plenum Press, New York (1980).

[25] M. ono, K. Fujii, T. Ito, Y. Iwaki, A. Hirako, T. Yao, K. Ohkawa, Photoelectrochemical reaction and H2 generation at zero bias optimized by carrier concentration of n-type GaN, J. Chem. Phys. 126, 054708 (2007)

[26] K. Fujii, Y. Iwaki, H. Masui, T. J. Baker, M. Iza, H. Sato, J. Kaeding, T. Yao, J. S. Speck,

S. P. Denbaars, S. Nakamura and K. Ohkawa, Photoelectrochemical Properties of Nonpolar and Semipolar GaN, Jpn. J. Appl. Phys. 46 6573

[27] A. M. Basilio, Y.-K. Hsu, W.-H. Tu, C.-H. Yen, G.-M. Hsu, O. Chyan, Y. Chyan, J.-S. Hwang, Y.-T. Chen, L.-C. Chen and K.-H. Chen, Enhancement of the energy photoconversion efficiency through crystallographic etching of a c-plane GaN thin film, J. Mater. Chem., 2010,20, 8118-8125

[28] H. Bae, E. Kim, J.-B. Park, S.-J. Kang, K. Fujii, S. H. Lee, H.-J. Lee and J.-S. Ha, Effect of Polarity on Photoelectrochemical Properties of Polar and Semipolar GaN Photoanode, J. Electrochem. Soc. 163 H213

[29] Koike, K., Nakamura, A., Sugiyama, M., Nakano, Y. and Fujii, K. (2014), Surface stability of n-type GaN depending on carrier concentration and electrolytes under photoelectrochemical reactions. Phys. Status Solidi C, 11: 821-823.

[30] D. R. Baker and C. A. Lundgren, Electrochemical determination of the galliumnitride photocorrosion potential in acidic media, J. Mater. Chem. A, 2017, 5, 20978

[31] D. Bisi, M. Meneghini, C. de Santi, A. Chini, M. Dammann, P. Brückner, M. Mikulla, G.Meneghesso and E. Zanoni, "Deep-Level Characterization in GaN HEMTs-Part I: Advantages and Limitations of Drain Current Transient Measurements," in IEEE Transactions on Electron Devices, vol. 60, no. 10, pp. 3166-3175

[32] L. Stuchlíková, J. Šebok, J. Rybár, M. Petrus, M. Nemec, L. Harmatha, J. Benkovská, J. Ková, J. Škriniarová, T. Lalinský, R. Paskiewicz, and M. Tlaczala, “Investigation of deep energy levels in heterostructures based on GaN by DLTS,” in Proc. 8th Int. Conf. ASDAM, Oct. 2010, pp. 135–138.

[33] M. A. Reshchikov, Chapter Nine - Point Defects in GaN, Semiconductors and Semimetals,

91, 2015, 315-367

[34] Z. Guo, F. Ambrosio, and . Pasquarello, Evaluation of Photocatalysts for Water Splitting through Combined Analysis of Surface Coverage and Energy-Level Alignment, ACS Catal. 10, 13186−13195 (2020)

[35] M. A. Reshchikov, M. Foussekis, and A. A. Baski, Surface photovoltage in undoped

-type GaN, J. Appl. Phys. 107, 113535 (2010)

[36] 24S. M. Sze, Physics of Semiconductor Devices, 2nd ed. Wiley, New York, 1981.

Chapter 6 Conclusions

6.1 Overview of the dissertation

In this dissertation entitled “Elucidation of Electronic Structure at n-GaN and Electrolyte Interface”, n-GaN(0001)/electrolyte was used as the model case of semiconductor/electrolyte interface for water splitting to clarify the determinant of the band bending. n-GaN(0001) surface was chosen because of its defined surface of +c plane, chemical stability and band edge potential that straddles the redox potentials of water oxidation and reduction reactions. To suppress the effect of redox reaction and analyze the effect of surface adsorption, the band bending under ultra-high vacuum (UHV) and water vapor was compared. Then, the effect of surface states and redox reaction was evaluated at n-GaN/electrolyte interface.

In chapter 2, band bending for GaN(0001) was investigated under UHV and ambient H_2O. The energy difference $\Delta E_{\mathrm{VBM\text{-}3d}}$ for GaN should be between 17.36 and 17.55 eV. $\Delta E_{\mathrm{VBM\text{-}3d}}$ = 17.5 eV, which was evaluated by bulk sensitive SXE, is recommended instead of the conventionally used 17.76 eV. With this constant, the band bending was estimated to be 0.5 eV under UHV and 0.1 eV under a relative humidity of 46%. For the latter condition, a SPV of 20 meV was observed upon Xe-lamp irradiation with a photon flux density (above a photon energy of 3.4 eV) of 1.3×10^{16} s^{-1} cm^{-2}. By re-evaluating the band bending for the previous reports using $\Delta E_{\mathrm{VBM\text{-}3d}}$ = 17.5 eV and reported Ga 3d peak locations, it appears that the band bending for GaN(0001) after passivation of Ga dangling bonds is between 0.1 eV and 0.3 eV regardless of the growth method of GaN (MOVPE or molecular beam epitaxy) or the surface preparation of GaN. Upon H_2O adsorption, Ga dangling bonds on the GaN surface are considered to be passivated with the dissociative absorption of H_2O, but sub-surface states in the vicinity of GaN(0001) surface, such as V_N or a complex defect related to O_N decorated along dislocation, may still pin the Fermi

level.

In chapter 3, it was evidenced that the dependence of OCP of a semiconductor photoelectrode on the irradiated light intensity gives us an insight on how the defects, especially those on the surface of a semiconductor, affect the photocatalytic activity in an electrolyte. The quantum states at the electrolyte/semiconductor interface seem to suppress the increase of quasi-Fermi-level splitting with light intensity, which is the driving force of photoelectrochemical reactions. According to this fining, a guiding principle for high-efficiency photocatalysts is deduced: a good surface modification for boosting photocatalytic activity, such as the introduction of co-catalyst and surface coating, should never lock the OCP at a certain value with an increase in light intensity. The proposed method of observing OCP under light irradiation is a concise and effective method for screening good photoelectrodes with appropriate surface modification.

In chapter 4, the influence of the surface states at the electrolyte/semiconductor interface was further investigated by introducing crystal defects on the GaN surface by the irradiation of Ar ions. From the pinning position, the band bending with and without Ar plasma treatment were 1.2 V and 1.5 V, respectively, under dark condition. Regardless of the Ar plasma treatment, the surface state derived from $V_{Ga}O_N$ is considered to be the origin of the Fermi level pinning at n-GaN/1M NaOH interface. Furthermore, although previous reports have quantitatively shown that a density of ~10^{13} cm^{-2} is necessary for the surface state to pin the Fermi level, our measurement revealed that the Fermi level is pinned at the surface state with a density of less than 10^{12} cm^{-2}. The difference in the flux density at which the Fermi level becomes unpinned is due to the large difference in the density of the surface states. The surface states act as electron recombination centers, and the negative contribution to the accumulation of photogenerated carriers depends on the effective density of the surface states. Ionic species in the electrolyte or adsorbed on the surface should terminate the electric force lines and be involved in the Fermi level pinning.

In chapter 5, Effect of ionic species in electrolytes on the band bending of n-GaN was analyzed by Mott-Schottky plot and OCP as a function of the logarithm of irradiation light intensity. The variation in band edge potentials with pH, 59 mV/pH, was expected to be due to the adsorption of H^+ ions on the semiconductor surface. Except in HCl and H_2SO_4 solutions, the obtained band-edge energy in each electrolyte followed this tendency. In $HCl_{aq.}$, the value is -0.5 V vs. RHE, which is far from this pH dependence due to the effect of surface adsorption of Cl^- ions as well as H^+. In $H_2SO_{4aq.}$, the value is -0.5 V vs. RHE, which is far from this pH dependence due to the effect of surface adsorption of SO_4^- ions as well as H^+. Although the band edge potential was different, the Fermi level of n-GaN was located at 1.1 eV below CBM in all the solutions used in the experiments. Regardless of electrolyte in the experiment, the surface states derived from $V_{Ga}O_N$ are considered to be the origin of pinning. In addition, no pinning was observed in sulfuric acid. Sulfuric acid removes more O from the surface than hydrochloric acid, which may have reduced the amount of $V_{Ga}O_N$. When the Fermi level was free from pinning, the value of OCP drifted to the negative direction in an almost linear manner with the logarithm of light intensity. For n-GaN in Na_2SO_4 and H_2SO_4, the radiative recombination was considered to be the dominant recombination process. For n-GaN in HCl, the holes are removed by the reduction reaction of Cl^- to Cl_2 (+1.3 V vs. SHE), which facilitates the accumulation of electrons. Then, the quasi-Fermi level for electrons, i.e., OCP, drifted to negative potential with an abrupt slope with respect to the logarithm of light intensity and reached at H^+/H_2 redox potential of 0 V vs. RHE. After the potential reached at H^+/H_2 redox level, electrons can be used by the reduction reaction of H^+ to H_2. When the quasi-Fermi level is over the H^+/H_2 redox level, electrons and holes are started to be used for radiative recombination and redox reaction. For n-GaN in NaOH, a similar mechanism of electron accumulation in n-GaN in HCl was suggested by the behavior of OCP under light irradiation. The holes may be removed by the reduction reaction of OH^-

to H_2O (+1.23 V vs. SHE), which facilitates the accumulation of electrons. However, the reaction rate of OH^-/H_2O, a four-electron reaction, is slower than that of Cl^-/Cl_2, a two-electron reaction, and the rate of holes removal is smaller. Therefore, the number of electrons accumulated in NaOH is less than that in HCl. Although the band bending is decided by the surface states derived from $V_{Ga}O_N$ in these electrolytes without illumination, it is affected by the redox pair in electrolytes under illumination.

6.2 A general conclusion

Band alignment, which governs carrier separation and transport, is essential for improving the efficiency of water splitting based on photoelectrochemistry. However, there are still many unknowns about the determinants of band bending and the relationship between redox and quasi-Fermi level. In this study, our XPS experiments at the GaN/water molecule adsorption interface revealed that the sub-surface states, which is derived from V_N or O_N related defects, is the origin of pinning at GaN/water molecule adsorption interface. In addition, we show that the Fermi level is determined by the presence of 10^{12} cm^{-2} sub-surface states, which originate from $V_{Ga}O_N$, at the interface between n-GaN and the electrolyte. It was also shown that the redox pair in the electrolyte was affected by the amount of change in the quasi-Fermi level under light irradiation. These results indicate that the electric force line from the donors in n-GaN must be terminated by anions in electrolyte, and that recombination can be suppressed by increasing the activity of the reaction using minority carriers.

6.3 Recommendation for future research

For further elucidation of the carrier transport efficiency in GaN based PEC devices, the effect pf polarity and doping on the band bending should be investigated by using the evaluation technique. Due to the lower polarization field in semi-polar GaN,

band bending is poor and most carrier electrons in semi-polar GaN do not flow easily, so electron-hole recombination occurs more efficiently in semi-polar GaN than in polar GaN. In addition, the

To simulate the carrier transport in n-GaN photoelectrode system, the carrier injection into reactive anion species should be considered. It can be evaluated by the cross section of carriers by reactive anion.

To improve quantum efficiency for achieving STH of 10%, the material, which has narrower band gap for further utilization of solar spectrum, should be investigated by using the evaluation technique which is applied in this dissertation. With this evaluation technique, the origin of Fermi level pinning and recombination center will be clarified. Based on the clarified origin, a design principle to improve the quantum efficiency will be derived. In addition, to enhance the carrier transportation to reactants from semiconductor electrodes, co-catalyst or protective layer has been loaded. Different bonding states should appear when the n-GaN surface atoms are not in direct contact with the electrolyte but in contact with the catalyst/protective film. As a result, the interfacial state distribution changes, and the pinning origin is also expected to change. With the surface modification, the interface state and recombination mechanism are possibly modulated. For the system, the origin will be elucidated and the strategy for ideal contact with co-catalyst/protective layer will be clarified.

Appendix A Band bending at n-GaN/H_2O interface

A.1 Surface preparation

The sample was n-GaN with a Ga-polar (0001) surface (thickness of n-GaN: 2.5 mm/u-GaN:2.0 mm/AlGaN 450 nm/AlN 250 nm), grown on a Si substrate by metal organic vapor phase epitaxy (MOVPE). The clean surface of n-GaN was prepared by cycles of 0.5 keV nitrogen ion bombardment followed by annealing at 1100 K in N_2 (1.0×10^{-6} mbar). After cleaning, the (1×1) surface was confirmed by low energy electron diffraction (LEED) (Figure A1).

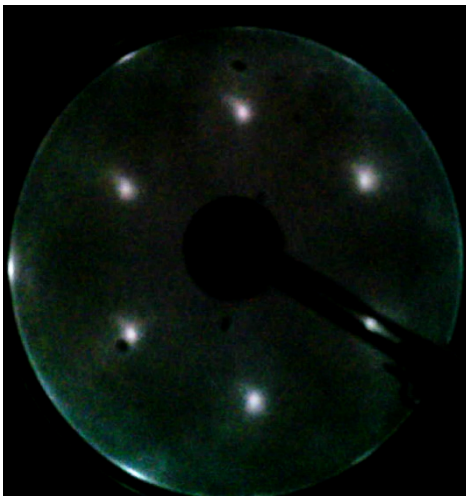

Figure A1 The low energy electron diffraction (LEED) pattern for a n-GaN(0001) surface confirming (1×1) reconstruction after a cleaning process of nitrogen ion bombardment followed by annealing. The incident electron energy was 73 eV.

A.2 Verifying reduction in the surface band bending under ambient H2O vapor by N 1s

To verify the fitting of Ga 3d, the difference of the band bending between UHV and ambient H_2O vapor was confirmed by the shift of peak of N 1s in Figure A2a, b. As we showed in Figure 2.3a, b, the shift of Ga 3d from UHV to ambient H_2O vapor was 0.402 ± 0.007 eV for Ga 3d. The shift of N 1s was 0.41 ± 0.005 eV. They are consistent with each other, indicating that the shift of the band bending occurs due to the H_2O adsorption on the surface of GaN(0001).

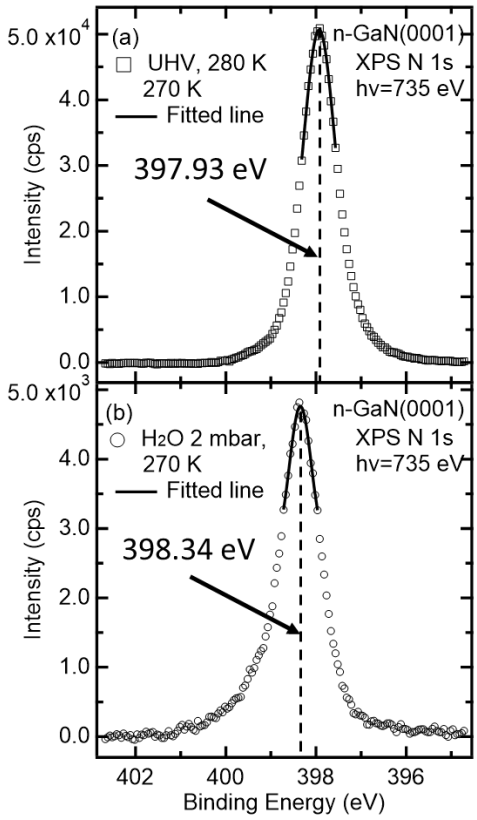

Figure A2 XPS spectra for N 1s on n-GaN(0001) surface under (a) UHV at 280 K (the black squares and line) and under (b) 2 mbar ambient H_2O vapor at 270 K (the black circles and line). lines are the result of peak fitting for XPS spectra. These peaks were normalized for comparison. The peak locations were evaluated as 397.93 ± 0.001 eV under UHV and 398.34 ± 0.004 eV under ambient H_2O vapor, respectively.

A.3 SPV under ambient H2O vapor in N 1s spectra

To verify the SPV in Ga 3d spectra under Xe lamp irradiation, the spectra shift was confirmed by the N 1s peak shift in Figure A3a, b. The peak location of N 1s shifted by +20 meV under Xe lamp irradiation in binding energy scale. The amplitude of shift by SPV is consistent with the SPV evaluated in the shift of the peak location of Ga 3d.

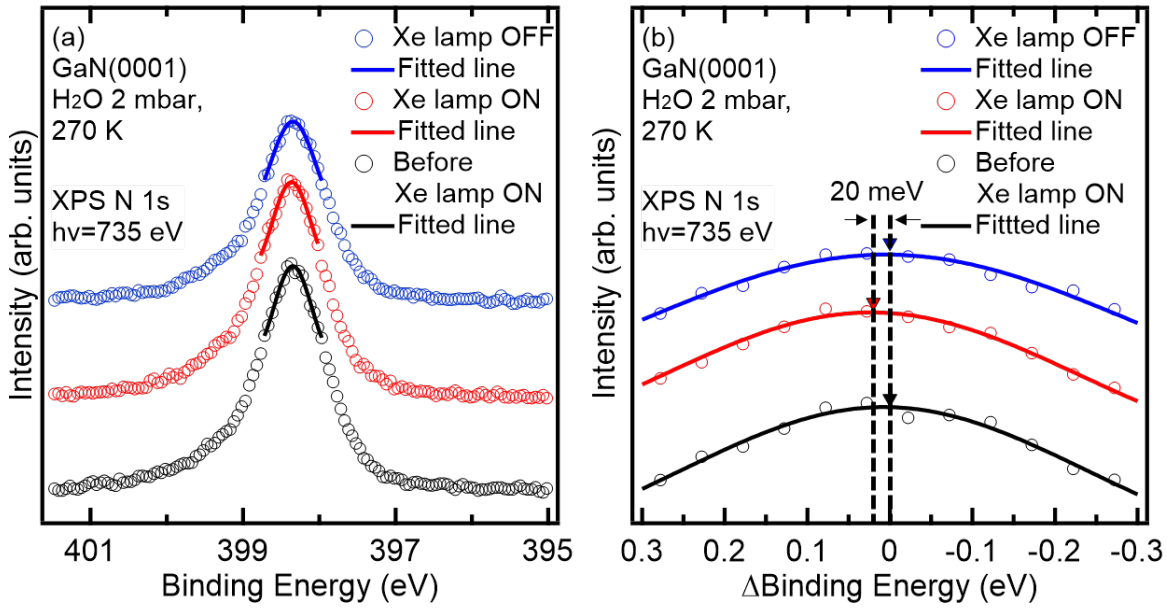

Figure A3 (a) XPS spectra for N 1s on the n-GaN(0001) surface under 2 mbar ambient H_2O vapor at 270 K before Xe lamp irradiation (the black circles and line denoted by "Before Xe lamp ON"), with irradiation ("Xe lamp ON": red circles and line) and after shutting off Xe lamp ("Xe lamp OFF": blue circles and line). Circles and lines are experimental data and result of peak fitting, respectively. The energy and flux of probe X-rays were 735 eV and 1.2×10^{15} s^{-1} cm^{-2}. The photon flux density (which has higher energy than GaN band gap, 3.4 eV) of the pump Xe lamp was 1.3×10^{16} s^{-1} cm^{-2}. (b) The enlarged view around the peak maximum is indicated by a triangle. The peak location before Xe lamp irradiation is set to zero. The peak location is shifted by +20 meV under Xe lamp irradiation in binding energy scale. After shutting off the Xe lamp, the peak location approached zero.

A.4 Dissociative adsorption confirmed by increase of OH groups in O 1s spectra

Dissociative adsorption of water molecules produces OH groups on the GaN (0001) surface. OH groups in O 1s spectra are shown in Figure A4a under UHV and Figure A4b under 2 mbar ambient H_2O vapor. According to our previous report[1], O 1s spectra were deconvoluted to five peaks including that originating from the water vapor. Under UHV condition, the peaks at 531.88 eV, 532.96 eV and 533.84 eV can be assigned to adsorbed O atom, OH groups and intact water molecules. The peak at 530.74 eV (labeled Ox) is probably attributed to O atoms adsorbed on Ga adatoms. As we discussed in our previous report[1], the presence of water (presumably present in the background) is seen in a trace amount even under UHV conditions because the GaN surface is highly active for water adsorption. Under and H_2O vapor, 531.08 eV, 532.22 eV, 533.30 eV, 534.18 eV and 536.03 eV can be assigned to Ox, adsorbed O atom, OH groups, intact water molecules and H_2O vapor. Area Ratio of OH groups to O atoms were 0.29 under UHV and 1.3 under 2 mbar ambient H_2O vapor, respectively. This increase in the ratio of OH groups to O atoms experimentally confirm the dissociative adsorption of water molecules in the GaN surface.

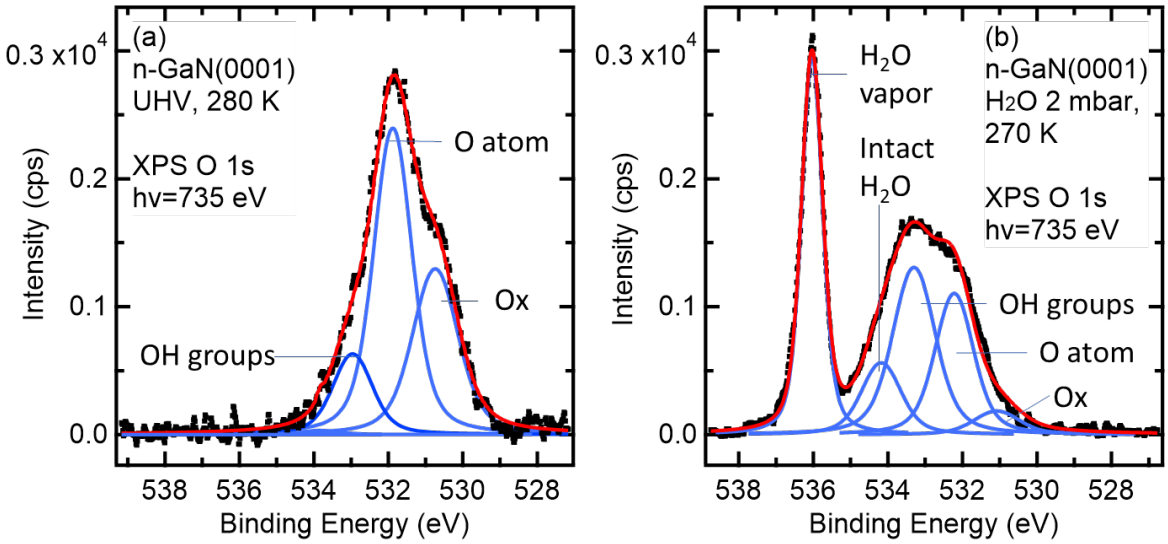

Figure A4 O 1s spectra under (a) UHV conditions and (b) 2 mbar ambient H_2O vapor conditions. The incident photon energy was 735 eV. Black dots, blue lines, and red lines are experimental data, fitting peaks with Voigt function, and the sum of the fitting peaks, respectively. The scales of the vertical axes are the same. No corrections are made for the attenuation of the signal due to the water vapor**.**

(1) Sato, M.; Imazeki, Y.; Takeda, T.; Kobayashi, M.; Yamamoto, S.; Matsuda, I.; Yoshinobu, J.; Nakano, Y.; Sugiyama, M. Atomistic-Level Description of GaN/Water Interface by a Combined Spectroscopic and First-Principles Computational Approach. *J. Phys. Chem. C* **2020,** *124,* 12466-12475.

Appendix B Surface states and band bending at n-GaN/1M NaOH interface

B.1 XPS spectrum without and with Ar plasma treatment

Figure B1 shows the XPS of n-GaN with and without Ar plasma treatment, where B1a, B2b, and B2c are Ga 3d, N 1s, and O 1s, respectively. a and b show that the N/Ga peak area ratio was 68% before Ar plasma irradiation, but became 9.6% after irradiation, indicating that the nitrogen was removed. In addition, the peak area ratio of O/Ga increased from 29% to 102%, indicating that the oxygen content increased. The peak separation results show that the O atom (Ga-O) has increased, especially Ga-O, indicating the formation of O_N. Due to the dissolution of gallium oxide on the surface by chemical or electrochemical reaction, gallium vacancies are created, which combine with adjacent anti-site defects caused by oxygen atoms occupying nitrogen sites[1].

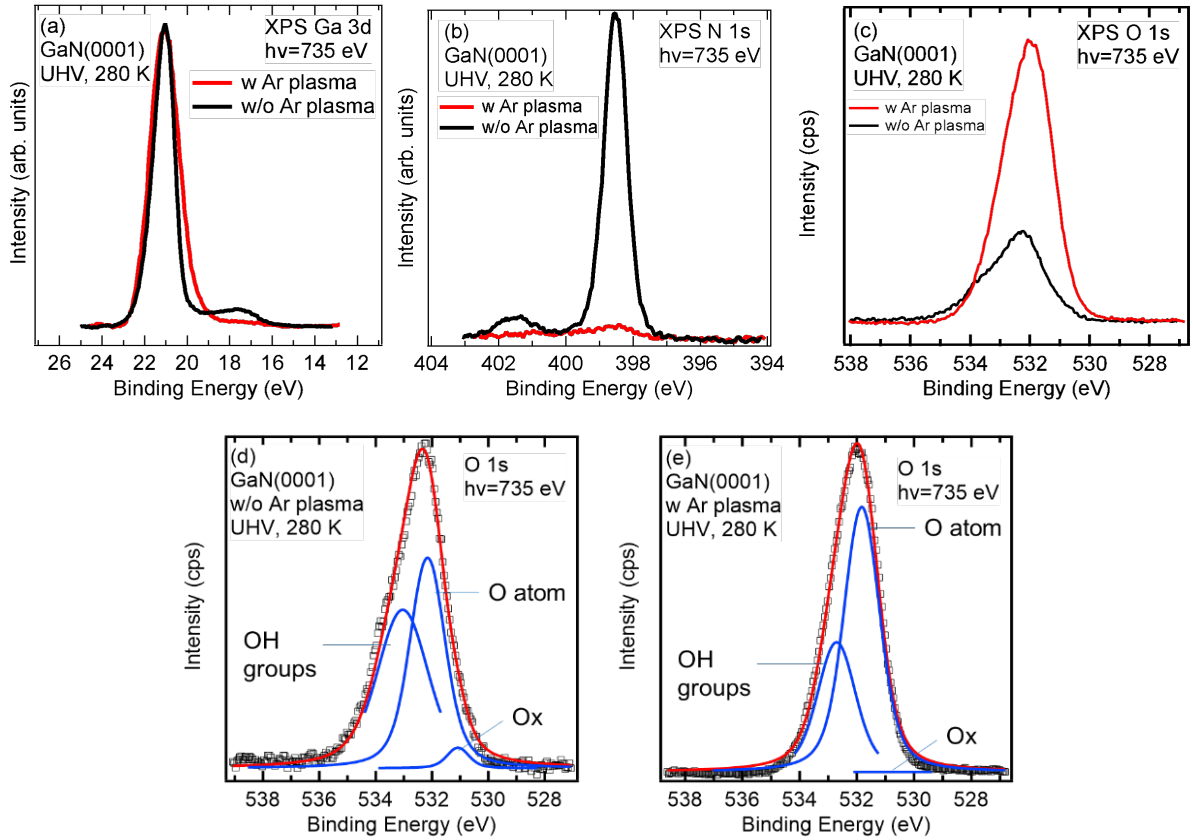

Figure B1 (a) Ga 3d, (b)N 1s, (c)O 1s spectra for GaN without (black line) and with Ar plasma treatment (red line). The incident photon energy was 735 eV. (d) Peak fitting of O 1s for GaN without Ar plasma and (e) with it. Black dots, blue lines, and red lines are experimental data, fitting peaks with Voigt function, and the sum of the fitting peaks, respectively.

(1) J. M. Hwang, J. T. Hsieh, H. L. Hwang and W. H. Hung, A damage-reduced process revealed by photoluminescence in photoelectrochemical etching GaN, *Materials Research Society Internet Journal of Nitride Semiconductor Research* 5 , **2000** , pp. 873 - 879

List of publication

1. Journal paper

1) Yuuki Imazeki, Yohei Iwai, Akihiro Nakamura, Kayo Koike, Shin-ichiro Sato, Takeshi Ohshima, Katsushi Fujii, Masakazu Sugiyama and Yoshiaki Nakano, "Band Circuit Potential for Efficient Water Splitting", ECS Transactions, 77 (4) 25-30 (2017)

2) Masahiro Sato, Yuki Imazeki, Katsushi Fujii, Yoshiaki Nakano, and Masakazu Sugiyama, “First-principles modeling of GaN(0001)/water interface: Effect of surface charging”, J. Chem. Phys. 150, 154703 (2019)

3) Masahiro Sato, Yuki Imazeki, Takahito Takeda, Masaki Kobayashi, Susumu Yamamoto, Iwao Matsuda, Jun Yoshinobu, Yoshiaki Nakano, and Masakazu Sugiyama, “Atomistic-Level Description of GaN/Water Interface by a Combined Spectroscopic and First-Principles Computational Approach”, J. Phys. Chem. C, 124, 23, 12466–12475 (2020)

4) Yuki Imazeki, Masahiro Sato, Takahito Takeda, Masaki Kobayashi, Susumu Yamamoto, Iwao Matsuda, Jun Yoshinobu, Masakazu Sugiyama, and Yoshiaki Nakano “Band Bending of n-GaN under Ambient H_2O Vapor Studied by X-ray Photoelectron Spectroscopy”, J. Phys. Chem. C, 125, 17, 9011–9019 (2021)

2.International conference

1) Yuki Imazeki, Yohei Iwai, Akihiro Nakamura, Kayo Koike, Kentaroh Watanabe, Katsushi. Fujii, Masakazu Sugiyama and Yosiaki Nakano, “Photo-Induced Gain of Open-Circuit-Potential (OCP) in GaN Photoelectrodes for Characterizing Defects and Photoelectrochemical Activity”, 2017 Material Research Society Spring Meeting & Exhibit, Apr. 17-21, 2017, Phoenix, USA, ES7.9.03

2) Yuuki Imazeki, Yohei Iwai, Akihiro Nakamura, Kayo Koike, Shin-ichiro Sato, Takeshi Ohshima, Katsushi Fujii, Masakazu Sugiyama and Yoshiaki Nakano, “Band Alignment at n-GaN/electrolyte Interface Explored by Photo-Induced Offset of Open-Circuit Potential for Efficient Water Splitting”, 231st Electrochemical society Meeting, May 28 - June 1, 2017, New Orleans, USA, G01: Processes at the Semiconductor Solution Interface 7 Water Splitting and Solar Fuel 1 1203

3) Yuki Imazeki, Masahiro Sato, Katsushi Fujii, Masakazu Sugiyama, Yoshiaki Nakano, “Evaluation of Surface States in GaN Photoelectrodes by Open-Circuit-Potential (OCP) spectroscopy under illumination”, 2018 Material Research Society Spring Meeting & Exhibit, Apr.2-6, 2018, Phoenix, USA, EN18.03.04

4) Masahiro Sato, Yuki Imazeki, Katsushi Fujii, Yoshiaki Nakano, Masakazu Sugiyama, “First Principles Modeling of GaN(0001)/Water Interface—Effect of Surface Charging,” 2018 Material Research Society Spring Meeting & Exhibit, Apr.2-6, 2018, Phoenix, USA, EN18.03.04 EN18.04.02

5) Masahiro Sato, Yuki Imazeki, Katsushi Fujii, Yoshiaki Nakano, Masakazu Sugiyama, "The Effect of Illumination on the Geometric Structure of Water Molecules on GaN(0001) Surface," MRS 2018 Fall Meeting, Nov. 25-30, 2018, Boston, USA, CM03.09.

6) Yuki Imazeki, Supawan Ngamprapawat, Masahiro Sato, Katsushi Fujii, Tsutomu Minegishi, Masakazu Sugiyama and Yoshiaki Nakano, "Effect of Dissolved O2 on Band Alignment at n-GaN/NaOH Interface", 2019 Material Research Society Fall Meeting & Exhibit, Dec. 1-6, 2019, Boston, USA, EN07.03.10

7) Supawan Ngamprapawat, Yuki Imazeki, Tsutomu Minegishi, Masahiro Sato, Katsushi Fujii, Masakazu Sugiyama, "Comparison of Light-Intensity-Dependent Open-Circuit Potential among TiO2, SrTiO3 and GaN Single-Crystalline Photoanodes," 2019 Material Research Society Fall Meeting & Exhibit, Dec. 1-6, 2019, Boston, USA, EN07.08.04

8) Masahiro Sato, Yuki Imazeki, Takahito Takeda, Masaki Kobayashi, Susumu Yamamoto, Iwao Matsuda, Jun Yoshinobu, Yoshiaki Nakano and Masakazu Sugiyama, "A Combined Spectroscopic and First-Principles Approach for the Atomistic-Level Description of Semiconductor/Electrolyte Interface," 2019 Material Research Society Fall Meeting & Exhibit, Dec. 1-6, 2019, Boston, USA, EN07.06.04

4.Domestic conference

1)今関裕貴, 佐藤正寛, 渡辺健太郎, 藤井克司, 杉山正和, 中野義昭, 「光電気化学反応の理解に向けた n-GaN エピタキシャル結晶の評価」, 応用物理学会結晶工学分科会 第 6 回結晶工学未来塾 研究ポスター発表会, 東京大学, 2017 年 11 月 2 日 (2017).

2)今関裕貴, 佐藤正寛, 藤井克司, 杉山正和, 中野義昭, 「光誘起 OCP 法による半導体・電解液界面バンドアライメントの解析」, 第 65 回応用物理学会春季学術講演会, 19p-F102-7, 早稲田大学, 2018 年 3 月 19 日 (2018)

3)佐藤 正寛, 今関 裕貴, 藤井 克司, 中野 義昭, 杉山 正和, 「GaN(0001)/水界面の構造への表面帯電の影響」, 第 65 回応用物理学会春季学術講演会,19p-F102-6, 早稲田大学, 2018 年 3 月 19 日 (2018)

4)今関 裕貴, ナーンプラパーワット スパワン, 佐藤 正寛, 藤井 克司, 嶺岸 耕, 杉山 正和, 中野 義昭, 「n-GaN 光電極/電解液界面バンドアライメントに及ぼす溶存酸素の影響」, 第 80 回応用物理学会秋季学術講演会, 19p-E216-5, 北海道大

学，2019 年 9 月 19 日（2019）

5) Supawan Ngamprapawat, Yuki Imazeki, Tsutomu Minegishi, Katsushi Fujii, Masakazu Sugiyama, “Material-dependent Photoresponse of quasi-Fermi Level in Single-crystalline Photoanodes”, The 80st JSAP Autumn Meeting, 19p-E216-6, Hokkaido University, Sep. 19th (2019)

Acknowledgement

本論文は多くの方々のご協力なしでは成立しえないものであり、この場をお借りしてご協力頂いた皆様へのお礼を述べさせて頂きます.

指導教官である中野義昭教授には, 研究に関してより大局的な観点からのアドバイスをいただくと共に,研究室での生活をあらゆる面で支えていただきました．このように快適な研究環境を整備していただいたため、５年間の研究を滞りなく遂行することが出来ました．杉山正和教授には，実験方針や結果に関して数多くの有益なご助言を頂くと共に, 学会での発表や論文執筆に際しても的確なご指導をいただきました.種村拓夫准教授には主にミーティングを通じて, 鋭いご意見を多く頂きました. 異なる分野の視点からの質問やコメントは自身では気付かなかった点について考え直すきっかけとなりました.嶺岸耕特任准教授には，実験を遂行する上での技術的な補佐や，実験方針や結果に関する数多くの助言をいただきました．佐藤正寛助教には，実験方針や結果に関して，計算科学の知見に基づく有益なご助言を数多く頂くと共に, 学会での発表や論文執筆に際しても的確なご指導をいただきました.理化学研究所の藤井克司研究員には，多くの議論や資料の添削を通して数々のご助言をいただきました．また, 田畑仁教授,岡田至崇教授には本論文の審査員を務めていただくとともに有意義なご助言を数多くいただきました.東京大学物性研究所の吉信淳教授，松田巌准教授，東北大学の山本達准教授，電気系工学専攻の小林正起准教授，武田崇広氏らには，Spring-8でのAP-XPS測定を進める際に大変お世話になりました.渡辺健太郎特任講師, ハサネットソダーバンル特任助教，研究室配属当初より様々な装置の使用法を教えていただくと共に, 各種実験を進める際に多くご協力をいただきました.日々の実験を進めるうえで，PECグループ(ユーリピホシュ博士，中村亮裕博士, 小池佳代博士,カーンファハド博士,羽柴寛博士, 小沼 賢二郎氏，バトプレフモンゴル氏，グラディスルーカス氏，謝玉洪氏，ナーンプラ

パーワットスパワン氏，沈旻哉氏，遠藤達郎氏，岩井耀平氏, 丸山裕晃氏, 地主真由子氏)に所属する方々とは各種のメンテナンスや実験結果に関する議論など, 研究室生活を通して大いにお世話になりました.

研究活動の他にも様々な活動に携わる機会がありました.おかげさまで日々の生活を有意義なものとすることができ, また多くの経験を得たと感じています. 最後に改めて，中野・杉山・種村研の一員として過ごした 5 年間で関わった全ての方々に感謝の意を述べさせていただきます.

2020 年 12 月 1 日

今関　裕貴